TRC0903

The Marked Tree Site:

Evaluation of Geosynthetic Reinforcements in Flexible Pavements

Brady R. Cox, Taylor M. Goldman, John S. McCartney

Final Report

2011

THE MARKED TREE SITE: EVALUATION OF GEOSYNTHETIC
REINFORCEMENTS IN FLEXIBLE PAVEMENTS

Final Report for project TRC 0903:
Evaluation of Basal Reinforcement of Flexible Pavements with Geosynthetics

Submitted to the Arkansas State Highway and Transportation Department by:

Brady R. Cox, Ph.D., P.E.
and
Taylor M. Goldman,
The University of Arkansas
and
John S. McCartney, Ph.D., P.E.,
The University of Colorado, Boulder

ABSTRACT

This document presents findings from a three-year, full-scale, field research project aimed at determining the benefits of using geosynthetic reinforcements to improve the performance of flexible pavements constructed over poor subgrade soils. The test site, known as the Marked Tree site, is an 850-ft (258-m) long segment of low-volume frontage road along Highway 63 in the town of Marked Tree, Arkansas. The site, constructed in 2005, consists of seventeen 50-ft (15.2-m) long flexible pavement test sections with various types of geosynthetic reinforcements (woven and nonwoven geotextiles, and geogrids), which were all positioned at the base-subgrade interface, and two different nominal base course thicknesses [6-in (15.2-cm) and 10-in (25.4-cm)]. One section in each nominal base course sector was left unreinforced to allow for monitoring of the relative performance between reinforced and unreinforced sections of like basal thicknesses.

The different sections were evaluated in this study using deflection-based, surficial testing conducted between 2008 and 2011, as well as subsurface forensic investigations conducted in October 2010. Signs of serious pavement distress appeared in some of the test sections in the Spring of 2010. Distress surveys revealed that all of the "failed" sections [defined herein as sections with average rut depths > 0.5 in (1.3 cm)] had nominal base thicknesses of 6-in (15.2-cm) and were reinforced with various geosynthetics. None of the sections with 10-in (25.4-cm) nominal base thicknesses had "failed" despite receiving more than twice the number of ESALs as the 6-in (15.2-cm) sections.

The impact of base course thickness was easily observed in the deflection-based test results and rutting measurements. However, it was difficult to discern a consistent, clear trend of better pavement performance relative to the various geosynthetic types in each nominal base

course thickness. Irrespective of geosynthetic reinforcement type (or lack thereof) all of the sections that "failed" with respect to excessive rutting were the sections with the least combined total pavement thickness (i.e., combined asphalt and base course thickness).

TABLE OF CONTENTS

LIST OF FIGURES

LIST OF TABLES

LIST OF FIGURES

LIST OF TABLES

Chapter 1

1.0 Introduction

1.1 Overview

In late 2004, the Arkansas Highway and Transportation Department (AHTD) began construction of a low-volume frontage road (Frontage Road 3) along US Highway 63 in the town of Marked Tree, Arkansas at the intersection of Arkansas Highway 75. An 850-ft (258-m) long segment of this frontage road was utilized for a research project (AHTD TRC-0406) aimed at determining the benefits, if any, of using geosynthetics to improve the performance of flexible pavements on state funded roadway projects where poor subgrade soils were encountered. This full-scale field study consisted of seventeen different 50-ft (15.2-m) long flexible pavement sections constructed over poor subgrade soils (CH or A-7-6). Eight of these sections were constructed with a 10-in (25.4-cm) nominal base course thickness and eight were constructed with a 6-in (15.2-cm) nominal base thickness. The section in the middle served as a transition between the two sectors with different nominal base course thicknesses. Seven of the eight sections in each nominal base course sector were reinforced with various geosynthetics (woven and nonwoven geotextiles, and geogrids), which were all positioned at the base-subgrade interface of the roadway. One section in each nominal base course sector was left unreinforced to allow for monitoring of the relative performance between reinforced and unreinforced sections of like basal thicknesses.

The sixteen test sections were instrumented with earth pressure cells and strain gauges applied to the geosynthetics and the asphalt. The transition section was instrumented with earth pressure cells, control strain gauges (geosynthetics and asphalt) for environmental calibration,

moisture content probes, thermocouples, and piezometers. However, this instrumentation was only monitored for a limited period of time (approximately 6 months) between September 2005 and March 2006 under normal and accelerated traffic loading. Limited conclusions were drawn from this monitoring (Howard 2006, Warren and Howard 2007a & 2007b) and the project was abandoned until July 2008. At this time, the Marked Tree project was re-started as research project AHTD TRC-0903, with the goal of continuing to monitor the instrumented sections. Unfortunately, all of the instrumentation, with exception of the asphalt strain gauges, had failed during the two-plus year gap in monitoring. Detailed information on the history of the Marked Tree site is found in Chapter 3.

Since the original instrumentation was no longer functioning, the new research group decided to monitor the relative performance of the test sections through a combination of surficial and subsurface testing. The surficial testing techniques consisted primarily of deflection-based tests such as the Falling Weight Deflectometer (FWD), static Plate Load Test (PLT), Accelerated Dynamic Deflectometer (ADD), and Light Weight Deflectometer (LWD). Results from these tests were used to infer relative pavement performance between test sections. These tests and results are described in great detail in Chapter 5.

Signs of serious pavement distress (primarily deep rutting with some alligator cracking) appeared in some of the test sections in the spring of 2010, leading AHTD to document the pavement performance with manual distress surveys in June of 2010 and April of 2011. These distress surveys revealed that a few sections of the roadway, especially in the westbound lane, were performing poorly. All of the "failed" sections [defined herein as sections with average rut depths > 0.5 in (1.3 cm)] were located in the sector with 6-in (15.2-cm) nominal base thickness. Furthermore, traffic surveys conducted during this time frame indicated that the 10-in (25.4-cm)

2

nominal base course sections had received more than twice the number of ESALs over the life of the pavement than the 6-in (15.2-cm) nominal base course sections. Detailed information about the traffic and distress surveys conducted at the Marked Tree site is provided in Chapter 4.

The research team was tasked with trying to figure out why certain 6-in (15.2-cm) nominal base course sections had "failed", while others had not. A subsurface forensic investigation was completed on each test section during a site visit in October 2010. The subsurface investigation was conducted so the research group could gather information concerning subsurface layer properties (i.e., in-situ dry density, in-situ moisture content, plasticity index, etc.), as well as subsurface relative strength/stiffness values (in-situ CBR, DCP penetration resistance, laboratory resilient modulus and undrained shear strength), to determine what properties, or combinations of properties, were causing some sections to fail while the rest of the sections performed substantially better. Results from the subsurface forensic excavation are presented in Chapter 6.

1.2 Objectives

The main objective of this work was to quantify the performance benefits, if any, from using geosynthetic reinforcements in flexible pavements on state funded roadway projects where soft subgrade soils were encountered. The findings presented herein were derived from an extensive investigation of a full-scale reinforced pavement with a current life of over 6 years. Absolute and relative pavement performance has been quantified through cracking and rut depth data collected during distress surveys conducted in June 2010 and April 2011. Surficial deflection-based tests conducted between September 2005 and May 2011 have been analyzed to determine which test(s) and data analysis method(s) can best be used to best infer the observed pavement performance. Additionally, subsurface investigations within the pavement test sections

have been conducted to determine if differences in the base and subgrade properties across the site significantly influenced the observed pavement performance.

A ranking system (from 1 through 16) has been used throughout this work to distinguish the "best" sections from the "worst" sections based on every test conducted at the site. The surficial deflection-based tests and subsurface layer properties have been synthesized in terms of these rankings to arrive at a final evaluation of the sections relative to the observed pavement rutting measurements. While the data is not perfect, and at times perplexing for any individual test, the one thing that seems to stand out is that irrespective of geosynthetic reinforcement type (or lack thereof) all of the sections that have "failed" via rutting are also the sections with the least combined total pavement thickness (i.e., asphalt plus base thickness). Therefore, a clear benefit from utilizing geosynthetic reinforcements at the Marked Tree site was not observed either through the deflection-based testing program or through the observed pavement rutting.

1.3 Scope

The following is an outline of the subsequent chapters, as well as a brief description of each chapter:

- Chapter 2 outlines the literature review on geosynthetic reinforcements installed in flexible pavement structures.

- Chapter 3 presents site information (i.e., geographic location and site construction), as well as results from soil testing prior to construction.

- Chapter 4 contains information about the testing history of research projects TRC-0406 and TRC-0903, project objectives, estimated traffic loading derived from traffic count data collected from January to August of 2011, and the pavement condition as of April 2011.

- Chapter 5 presents the methods of conducting and analyzing the surficial deflection-based tests conducted throughout the life of the roadway.

- Chapter 6 presents information gathered during the subsurface forensic investigation in October 2010, as well as testing methods and results from samples collected during the subsurface investigation.

- Chapter 7 contains conclusions drawn from the data presented in the previous chapters and recommendations for future studies on the Marked Tree site and other similar geosynthetic reinforced pavements.

Chapter 2

2.0 Literature Review

2.1 Overview

The focus of this chapter is to discuss and summarize information collected through researching technical literature associated with flexible pavement structures reinforced with geosynthetic materials. More specifically, this review will closely examine studies involving the construction and testing of pavement structures with and without geosynthetic reinforcements. There have been many projects geared toward quantifying the beneficial effects of geosynthetic reinforcements installed in flexible pavement structures. However, many of these projects have differed in both their approach (in-situ vs. laboratory testing) and materials used (various types of soils, geosynthetics, configurations, etc.). The goal of this review is to analyze the findings from the researched literature to develop a sense of how and under what circumstances geosynthetic reinforcement benefit flexible pavement structures. The types of tests previously used to analyze the benefits from geosynthetic reinforcements in pavement structures will be investigated to conclude which of the testing methods most accurately detects and describes the reinforcement potential. However, discrepancies from one study to the next, as well as the lack of a universally accepted design standard, provide uncertainties in design and application.

2.2 Introduction

Flexible pavements usually consist of a bituminous surface underlain with a layer of granular material and a layer of a suitable mixture of coarse and fine materials. These structures are designed so that traffic loads are transferred by the wearing surface (asphalt layer) to the underlying supporting materials through the interlocking of aggregates, the frictional effect of

the granular materials, and the cohesion of the fine materials (Garber and Hoel 2002). With the assumptions of these materials transferring the loads as anticipated, the pavement structure is expected to support a designed amount of traffic over the desired life of the structure. Most premature pavement failures are structural in nature, meaning that one or more of the materials in the system have reached a mechanical failure state. Structural failures in pavement structures occur due to unexpected variables or variations in design factors that change the pavement materials such as: unexpected loadings, environmental interaction, drainage problems, and other factors such as cyclic degradation, frost heave, and subgrade settlement. In order to counter some of these adverse effects, engineers, owners, and contractors commonly incorporate practices such as thick structural pavement sections to account for weak subgrade soil conditions (Archer 2008). However, the practice of constructing thicker base layers to accommodate for poor subgrade soils can accrue excessive costs in many situations.

The implementation of geosynthetic reinforcements in the pavement structure can be an advantageous alternative by increasing the pavement service life and reducing the cost in lieu of more expensive natural materials (Brandon et al. 1996). Geosynthetic materials have been proven to be effective as reinforcement materials in slope stability applications and retaining walls, and for over 30 years, geosynthetics have been applied to experimental pavement structures due to the expected potential to improve pavement performance. In slopes and retaining walls, the soil transfers shear stresses to the geosynthetic reinforcements, which resist these imposed stresses through mobilized tensile resistance. Numerous field and lab studies have illustrated that geosynthetic reinforcements applied in the base course of pavement structures have the capability to improve bearing capacity, extend the service life, reduce the necessary fill thickness, reduce differential settlement, and delay rut formation (Hufenus et al. 2005).

7

2.3 Geosynthetic Materials

Geosynthetic materials are fabric-like materials made from polymers such as polyvinyl chloride (PVC), polyethylene, polypropylene, and polyester (Das 2006). The term geosynthetics represents many types of construction materials that serve several purposes, but the two forms of geosynthetics that are most widely used in pavement systems are geogrids and geotextiles (Al-Qadi et al. 1994). Although both of these reinforcements may contribute to pavement performance, Al-Qadi et al. (1994) found that the mechanisms by which the two types reinforced the pavement are different.

2.3.1 Geogrid

A geogrid is a geosynthetic material constructed of longitudinal and transverse ribs that create openings referred to as apertures. These apertures are of sufficient size to allow strike-through of surrounding soil, stone, or other geotechnical material (Koerner 2000). The interlocking potential of geogrids allows them to be ideal reinforcement in granular layers, such as the base course of a pavement structure. When the surface of a pavement structure reinforced with a geogrid is vertically loaded, the granular materials will become interlocked with the geogrid. The interlocking effect restrains the aggregate laterally and transmits tensile forces from the aggregate to the geogrid (Maubeuge 2011). By laterally restraining the soil, the geogrid contributes in preventing lateral spreading of the base aggregate, increasing the strength of the base in the vicinity of the reinforcement, improving vertical stress distribution on the subgrade, and reducing shear stress in the subgrade (Berg et al. 2000). In this mechanism, the geogrid does not likely go into tension unless higher strains are observed in the system (Giroud and Noiray 1981).

2.3.2 Geotextile

The geotextiles typically used for reinforcement applications are woven filament sheets (Koerner 2000), however, nonwoven geotextiles have also been used. The main reinforcement mechanism provided by woven geotextiles is separation. A geosynthetic placed at the interface between the aggregate base course and the subgrade functions as a separator to prevent two dissimilar materials (subgrade soils and aggregates) from intermixing (Berg et al. 2000). Separation allows a stiff material placed on a soft subgrade to maintain its full thickness throughout the life of the pavement. In order to mobilize tensile resistance, it is possible that the geosynthetics have to be subjected to strains close to those prompted by failure induced loading, similar to geogrid tensile mobilization. Cuelho and Perkins (2009) suggested that the puncture resistance of the geotextile should be taken into account, as penetration of particles through the geotextile will reduce its strength and stiffness (Cuelho and Perkins 2009).

2.4 Testing Methods

Geosynthetic-reinforced pavement test sections have been constructed and evaluated over the past 30 years and, as a whole, have demonstrated positive and significant benefits provided by reinforcement (Perkins and Cortez 2005). Though the general consensus from past research efforts describe that pavement structures have been improved through the installation of geosynthetic reinforcements, there are too many discrepancies between test methods attempting to quantify the performance benefits of incorporating geosynthetic reinforcements in flexible pavement structures. There are basically three methods for testing the contributions of geosynthetic reinforcements in pavement structures as follows: (1) cyclic loading of laboratory contained test sections (box tests), (2) controlled-traffic track tests that apply loads with standard trucks and moving wheel loads (MWL) single wheel load applicators, and (3) full-scale field test

sections (Perkins and Cortez 2005). The majority of these tests quantify the presence or lack of benefits from the reinforcements through dynamic and permanent surface deformations. However, a few researchers have instrumented pavement structures and geosynthetic reinforcements to attempt to quantify the performance and contributions provided by each layer of the structure. The instrumented full scale pavement tests are expected to be the most representative of the actual field conditions because they are loaded in the same manner as actually present in the field. The majority of testing, however, is done in controlled environments due to the possibility of environmental conditions, such as temperature and moisture contents throughout the base and subgrade, varying over time in full-scale field tests, which would cause inconsistencies in results. Unfortunately, the results provided from a test conducted in a completely controlled environment can only represent the estimated performance without climate and environmental factors that always play a strong role in pavement performance. Variations of uncontrollable conditions, such as climate, best represent how the structures would perform when the same design was applied to practice.

2.4.1 Laboratory Testing

Testing conducted to quantify the benefits of geosynthetic reinforcements in pavement structures is often executed in a laboratory setting. Laboratory studies can be conducted more quickly and usually include more parametric alternatives (Cuelho and Perkins 2009). The two most common types of laboratory tests conducted are cyclic plate load tests on fabricated sections in laboratory tanks (box tests), as shown in Figure 2.1 (Al-Qadi et al. 1994, Montanelli et al. 1997, Maubeuge and Klompmaker 2011, and Ling and Liu 2001), and track testing with heavy vehicle simulators (HVS), as shown in Figure 2.2 (Perkins and Cortez 2005, Henry et al. 2011, and Kinney et. Al 1998).

Cyclic plate load testing in laboratory tanks (box tests) cannot be considered exactly representative of full-scale pavements due to boundary and scaling effects. Specifically, the size of the test section and layer thicknesses are reduced; however, the distribution of soil particle sizes (gradation curve) or geosynthetic properties are not scaled down in the same manner as the section sizes. When analyzing results from 'box tests' it must be considered that there is only a small section of pavement structure being tested that is enclosed by much superior materials, often concrete walls. The test results may be influenced by stress waves passing through the soils and rebounding off of the boundaries and back into the structure. The constraints of the boundaries help prevent lateral displacement which would simulate a response from the structure different than that if the section being tested was surrounded by a much larger area of like materials.

Montanelli et al. (1997) performed cyclic plate load tests on sections reinforced with geogrid. This test was performed by applying 300,000 sinusoidal loading cycles through a 12-in (300-mm) diameter circular loading plate providing 0 to 9 kips (0 - 40 kN) [maximum applied pressure of 82 psi (570 kPa)] at frequencies of 5 and 10 Hz (Montanelli et al. 1997). Al-Qadi et al. (1994) performed a similar test, except the loading frequency was 0.5 Hz, and presented a goal of testing until at least one inch (25 mm) of displacement had occurred (Al-Qadi et al. 1994). Al-Qadi et al. (1994) also tested geotextiles as well as a geogrid in comparison to a control section. The typical presentation of data collected from these tests is a comparison of surface deformation at a given location versus number of loading cycles of the applied load, as well as a cross-sectional profile of surface deformation at a specified number of loading cycles. Figures 2.3 and 2.4 are examples of the latter mentioned data presentation methods, respectively, via Al-Qadi et al. (1994). As observed in Figure 2.4, the control was the poorest performing

11
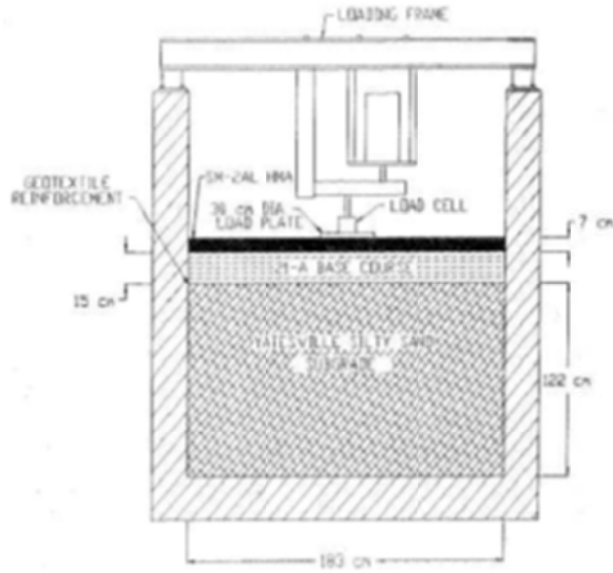
Figure 2.1. Cyclic Plate Load Test in laboratory tank (Al-Qadi et al. 1994).

Figure 2.2. Heavy Vehicle Simulator (HVS) (Perkins and Cortez 2005).
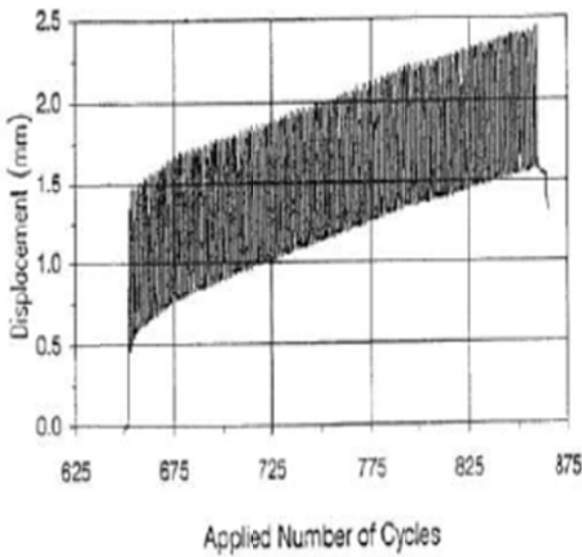
Figure 2.3. Typical relationship between displacement and loading cycles (Al-Qadi et al. 1994).
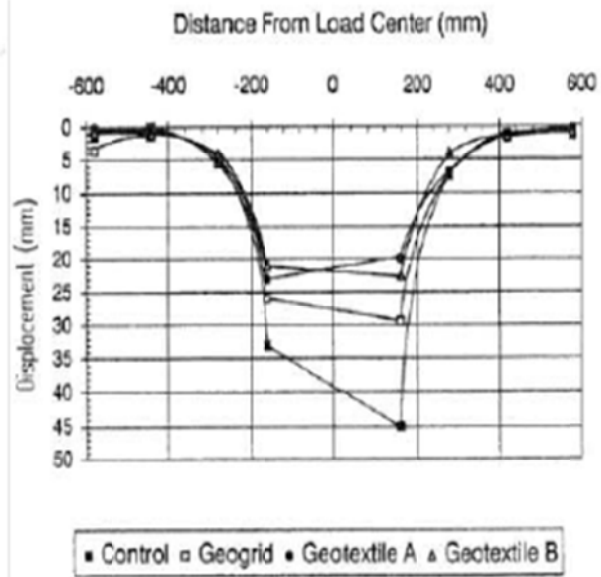
Figure 2.4. Permanent displacement profile at 800 cycles (Al-Qadi et al. 1994).

12

section after 800 loading cycles were applied, but the geotextiles unexpectedly outperformed the geogrid.

Other studies involve laboratory testing using heavy vehicle simulators (HVS) (Perkins and Cortez 2005, Henry et al. 2011, and Kinney et al. 1998). The use of HVS systems are more representative of actual pavement loading because larger test sections are constructed and rolling wheel loads are used; however, the construction and testing of these test sections are often time consuming and expensive. This is especially the case if site-specific soils need to be transported to the HVS location. The testing facilities are normally constructed indoors in long rectangular pits (Perkins and Cortez 2005 and Henry et al. 2011) or outdoor test tracks constructed of more representative boundaries, such as plywood surrounded by gravel and sand rather than concrete walls (Kinney et al. 1998). The sections are loaded using a load frame with a wheel attached that travels unidirectionally along the longitudinal axes of the text sections (Perkins and Cortez 2005). The test sections are typically loaded to a finite number of Equivalent Single Axle Loads (ESALs), which are equivalent to 18 kip (80 kN), or until failure (Henry et al. 2011). Henry et al. (2011) presented testing results as average rut depth versus cumulative ESALs for all sections tested. This data presentation is displayed as Figure 2.5.

It can be observed in Figure 2.5 that the section with 6 inches (150 mm) of asphalt and 12 inches (300 mm) of base performed contradictory of what would be expected. The unreinforced section resulted with less rut depth than the geosynthetic reinforced section after equivalent ESALs were applied. However, it must be noted that the base course in the unreinforced section was significantly softer, with a base modulus from FWD back calculations of approximately 30.6 ksi (281 MPa) (Henry et al. 2011). It should also be noticed that the thickest overall section, asphalt and base layers combined, resulted in negligible differences in rutting between the
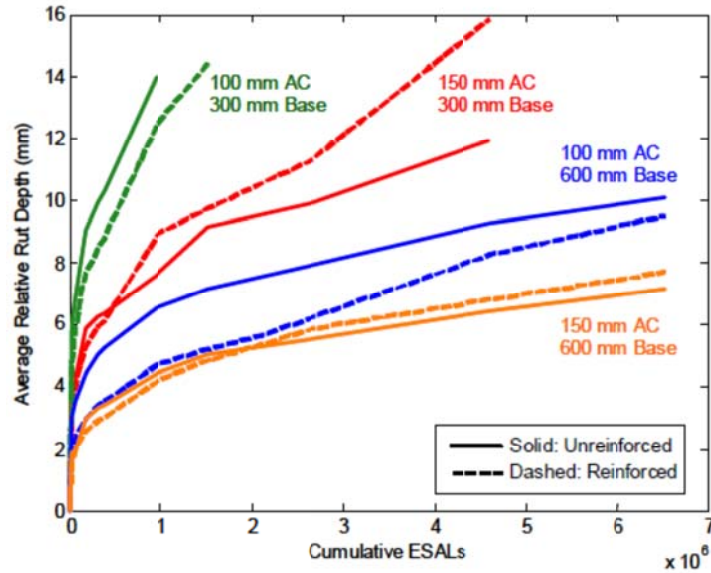
Figure 2.5. Average relative rut depth vs. cumulative ESALs (Henry et al. 2011).

reinforced and unreinforced sections. This could represent a point of diminishing returns with regard to grid reinforcement (Henry et al. 2011). It could be possible that once a certain amount of base course is applied, the mobilization of the geosynthetic reinforcement is not reached until the pavement structure has reached the point of failure.

2.4.2 Full Scale Field Testing

Full scale testing is typically performed to evaluate pavements under the actual traffic, environmental, and boundary conditions encountered in a given area, as shown in Figure 2.6. However, this can be inconvenient and uncertain as the environmental and loading conditions cannot be controlled. Field test sites also prevent control of uniform site conditions due to natural variations in the subgrade profile. Therefore, to be able to understand that contribution of the geosynthetic material in the pavement design, a uniform testing material must be used and often times a geosynthetic liner is used to eliminate migration of the natural subgrade into the test section during testing. Construction quality control and assurance must be monitored strictly as to prevent trafficking of the sections prior to traffic loads being applied. Performance of test

14

sections is usually quantified by comparing average rut depths or surface deflections versus type of section, such as Figure 2.7, (White et al. 2011, Cuelho et al. 2011, Tingle and Jersey 2009, and Hufenus et al. 2006). Other testing methods of full scale test sections have been performed to observe the quality of the structure after being trafficked. Joshi and Zornberg (2011) used falling weight deflectometer (FWD) data to quantify the relative performance of reinforced pavement sections . FWD tests were performed periodically throughout the life of the tested structure to analyze the deflection basins created by the FWD in each section to identify layer properties and to quantify relative damage to the pavement layers. Distress survey results were also compared to the deflection data (Joshi and Zornberg 2011). Cox et al. (2010a) presents a test method that uses a Vibroseis (shaker) truck to perform cyclic plate load (CPL) tests on geosynthetic reinforced flexible pavements. The results from the latter test presented definite improvements in pavement performance with increasing basal thickness, but the effects of the geosynthetic reinforcements were not clearly defined, possibly because more surface deflection was needed to mobilize the potential contributions from the geosynthetics (Cox et al. 2010a).

2.4.3 Instrumented Test Sections

Normally, both laboratory and full scale field tests only measure surface behavior of tested sections. However, many times the problematic area is not the surface, or cannot be observed from the surface. When moisture builds up in the pavement base and subgrade layer, the shear strength in these layers begins to decrease and weaken. The weakening of the subgrade soils can cause fatigue cracking and rutting in the pavement, but it is a result of wet conditions, causing the subgrade and base course to mix, the drainability of the materials to decrease, and a reduction in the initial design thickness of the pavement (Warren and Howard 2007a). While there is evidence from field experiments, laboratory investigations and numerical evaluations

15

Figure 2.6. Full-scale field testing (Cuelho and Perkins 2009).
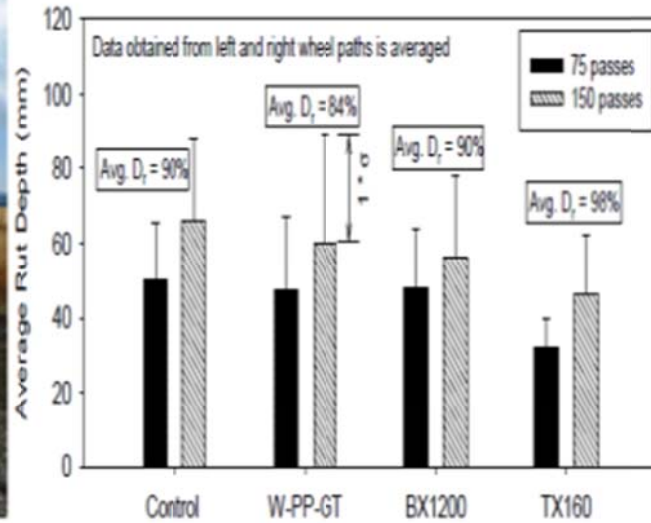
Figure 2.7. Average rut depth after 75 and 150 truck passes (White et al. 2011).

that supports the benefits of geosynthetic inclusions in a flexible pavement structure (Warren and Howard 2007a), there is a lack of knowledge and confidence as to how the geosynthetics actually benefit the structure and affect the other layers. Therefore, a testing method that measures strain within the test section is needed to determine what is happening as a function of depth during loading. Several studies have been done on instrumented test sections, such as Brandon et al. (1996), Warren and Howard (2007b) and Warren et al. (2008), but results have been limited. Issues in collecting valuable results from previously instrumented pavements are associated to a lack of information on proper instrument selection and installation. Therefore, the instrumentation in geosynthetic reinforced roadways historically does not last long enough to obtain valuable information (Brandon et al. 1996 and Warren and Howard 2007b). Table 2.1 is a table of instrument survivability after 8 months (Brandon et al. 1996). Though the table displays fairly decent survivability for the majority of the instruments, the rates are only after 8 months of instrumentation. The survivability could drastically go down over time, but Brandon et al. (1996)

16

only presents the data from one date. It is likely that the non-survived instruments were damaged at installation and would have survived if a proper installation process was available. Weak spots are also created in the pavement layers due to poor compaction around the instrumentation.

2.5 Previous Research

Numerous studies have been conducted to determine the performance of geogrid- and geotextile-reinforced flexible pavement structures. The research presented in Tables 2.2, 2.3, and 2.4 (Berg et al. 2000 and Cox et al. 2010b) are laboratory and full scale field tests that quantify the contribution of the geosynthetic reinforcements in pavement performance by examining surface deflections. Table 2.2 is a summarization of the properties of several tests conducted on the topic of geosynthetic reinforcements in flexible pavement structures. This includes soil classifications, test type, testing area dimensions, and layer thicknesses. Table 2.3 summarizes the loading properties of each test, such as loading type, applied load and frequency of loading. Table 2.4 is the summarization of the geosynthetic reinforcements' properties and the location in the pavement structure for each testing instance. Table 2.4 also contains information on the subbase thickness, the California Bearing Ratio (CBR) of the subgrade, surface deformations, and the benefit of the geosynthetic reinforcement in terms of the traffic benefit ratio (TBR). The TBR is the ratio of the number of loading cycles on the geosynthetic reinforced test section to reach a certain rut depth to the number of loading cycles it takes a non-reinforced test section to reach the same rut depth (Tencate 2010). All the studies examined in this section were conducted on paved roadways, and they all provide some insight into potential benefits of geosynthetics as reinforcement in flexible pavement structures (Berg et al. 2000). These studies also help summarize how many different variables can impact reinforced pavement structure performance. Each of these variables are very difficult to assess individually because they are interrelated, but

17

Table 2.1. Instrument survivability after 8 months (Brandon et al. 1996).

Gage Type	Number Installed	Number Survived	Percent Survived
Kulite earth pressure cells	6	3	50%
Carlson earth pressure cells	21	16	76%
HMA strain gages	35	26	74%
Geotextile strain gages	18	1	6%
Geogrid strain gages	18	5	28%
Soil strain gages	6	5	83%
Thermocouples	17	15	88%
Gypsum blocks	18	18	100%

many have similar behaviors over a large range of different configurations. Trends found in these variables developed from previous tests have been summarized in Tables 2.2, 2.3, and 2.4 (Cox et al. 2010b).

2.5.1 Evaluation of the Impact of Subgrade Strength

The relevance of the different reinforcement mechanisms may depend on the subgrade soil atop which the pavement rests. With a high quality subgrade beneath the pavement structure, the reinforcement may never reach the stain level needed to be mobilized. Softer subgrade soils will allow for much greater deformations, which will then begin to reach the strain levels required to mobilize the geosynthetic reinforcement. California Bearing Ratio (CBR) is a measure of the mechanical strength of a subgrade and is a design criterion for pavement structures when choosing a suitable subgrade soil. The greater the CBR value, the stiffer the subgrade is. Subgrades with CBR values less than 8 see the most benefit from geosynthetic reinforcement (Tencate 2010). The reinforcement can be viewed as improving the bearing capacity of the subgrade as it aids in supporting construction traffic, and the reinforcement can help prevent differential settlements by bridging over weaker areas and transferring load to the stronger areas if subgrade turns out to be heterogeneous (Perkins et al. 2005).

Table 2.2. Summary of previous research test section properties (Cox et al. 2010b).

Author	Testing Facility	Facility Dimension (ft)	Layer Thickness (in)		Soil Classification	
			Asphalt	Base	Base	Subgrade
Al-Qadi (1994)	Soil Tank	10.2 L x 5.9 W x 6.9 D	2.7	5.9 / 7.8	GW-GM	SM
Al-Qadi (1997)	Public Road	443 L x 49 W	3.5	3.9 / 5.9	GW	ML
Barker (1987)	Test Track	68.8 L x 15 W x 3.6 D	2.9	5.9	GP	Sandy Silt
Barksdale (1989)	Test Track	16 L x 7.8 W x 4.9 D	1.5	7.8	GP-GM	CL
Cancelli (1996)	Soil Tank	2.9 L x 2.9 W x 2.9 D	2.9	11.8	GW	SP
Cancelli (1999)	Test Track	689 L x 13.1 W x 3.9 D	2.9	11.8 / 15.7 / 19.6	Gravel	CL
Collin (1996)	Test Track	47.9 L x 14.4 W x 3.9 D	1.9	7.1 / 11.8	GW	CL
Cuelho (2009)	Full-Scale	49.2 L x 13.1 W	None	7.8 / 7.8	GW-GM	SC
Haas (1988)	Soil Tank	14.7 L x 5.9 W x 2.9 D	2.9	7.8 / 11.8 / 7.8	GW	SP
Perkins (1997)	Soil Tank	6.6 L x 6.6 W x 4.9 D	2.9	11.8 / 14.7	GW	SM
Tingle (2005)	Soil Tank	6 L x 6W x 4.5 D	None	13.8 / 13.3	SW-SM	CH
Webster (1993)	Test Track	144.4 L x 12.5 W x 2.3 D	1.9	5.9 / 9.8 / 11.8 / 13.7 / 17.7	SM-SC	CH

Table 2.3. Summary of previous research loading properties (Cox et al. 2010b).

Author	Loading Type	Applied Load (lb)	Load Frequency or Speed
Al-Qadi (1994)	11.8" circular plate	8,768	0.5 Hz
Al-Qadi (1997)	Traffic	Traffic	Traffic
Barker (1987)	Moving Wheel	26,978	Unknown
Barksdale (1989)	Moving Wheel	1,484	2.9 mph
Cancelli (1996)	11.8" circular plate	8,992	5 Hz, 10 Hz
Cancelli (1999)	Single wheel front axle	5,058 per wheel	12.5 mph
Collin (1996)	Moving Wheel	4,496	2.7 mph
Cuelho (2009)	Three Axle Dump Truck	45,988	9.32 mph
Haas (1988)	11.8" circular plate	8,992	8 Hz
Perkins (1997)	11.8" circular plate	8,992	0.67 Hz
Tingle (2005)	12" ciruclar plate	8,992	1 Hz
Webster (1993)	Moving Wheel	29,225	Unknown

Table 2.4. Summary of previous research geosynthetic properties and test results (Cox et al. 2010b).

Author	Geosynthetic Reinforcement	Secant Modulus in Machine Direction at 5% Strain (lb/ft)	Reinforcement Location	Subbase Thickness (in)	Subgrade CBR	Rut Depth (in)	TBR
Al-Qadi (1994)	Woven Geotextile	13700	Interface	5.9	2	1	1.7
	Woven Geotextile	15600	Interface	7.8	4	1	3
Al-Qadi (1997)	Woven Geotextile	13700	Interface	3.9	7	0.7	1.6
	Punched Geogrid	13700	Interface	3.9	7	0.8	1.4
Barker (1987)	Punched Geogrid	15100	Middle of Base Course	5.9	2.7	1	1.2
Barksdale (1989)	Woven Geotextile	Unknown	Middle of Base Course	7.8	2.7	0.5	4.7
	Woven Geotextile	Unknown	Interface	7.8	2.7	0.5	1
	Punched Geogrid	8200	Middle of Base Course	7.8	3.2	0.5	2.8
	Punched Geogrid	8200	Interface	7.8	2.5	0.5	1
Cancelli (1996)	Woven Geotextile	13400	Interface	11.8	3	1	1.7
	Punched Geogrid	8200	Interface	11.8	3	1	1.7
	PVC Coated Polyester Geogrid	16900	Interface	11.8	3	1	1.7
	Multilayer Biaxial Geogrid	12300	Interface	11.8	1	0.5	15
	Multilayer Biaxial Geogrid	12300	Interface	11.8	3	1	5.2
	Multilayer Biaxial Geogrid	12300	Interface	11.8	8	1	3.2
	Biaxial Geogrid	13700	Interface	11.8	1	1	7
	Biaxial Geogrid	13700	Interface	11.8	3	1	7.1

Table 2.4 (continued). Summary of previous research geosynthetic properties and test results (Cox et al. 2010b).

Author	Geosynthetic Reinforcement	Secant Modulus in Machine Direction at 5% Strain (lb/ft)	Reinforcement Location	Subbase Thickness (in)	Subgrade CBR	Rut Depth (in)	TBR
Cancelli (1999)	Woven Geotextile	13400	Interface	15.7	3	0.4	220
	Punched Geogrid	8200	Interface	11.8	3	0.8	220
	Punched Geogrid	8200	Interface	15.7	3	0.3	340
	Punched Geogrid	8200	Interface	19.6	3	0.5	8.4
	Punched Geogrid	8200	Interface	11.8	8	0.3	1.2
	Multilayer Biaxial Geogrid	12300	Interface	11.8	3	0.6	300
	Multilayer Biaxial Geogrid	12300	Interface	15.7	3	0.3	330
	Multilayer Biaxial Geogrid	12300	Interface	19.6	3	0.4	13
	Multilayer Biaxial Geogrid	12300	Interface	11.8	8	0.3	1.6
Collin (1996)	Punched Geogrid	8200	Interface	7.1	1.9	1	2
	Punched Geogrid	15100	Interface	11.8	1.9	1	3.3
Cuelho (2009)	Woven Geotextile	1100	Interface	7.2	1.75	1	1.7
	PVC Coated Polyester Geogrid	400	Interface	6.7	2	1	2.6
Haas (1988)	Punched Geogrid	13700	Middle of Base Course	7.8	8	0.8	3.3
	Punched Geogrid	13700	Interface	7.8	8	0.8	3.1
Perkins (1997)	Woven Geotextile	13700	Interface	11.8	1.5	0.9	-
	Punched Geogrid	8200	Interface	11.8	1.5	0.9	17
	Punched Geogrid	8200	Interface	14.7	1.5	0.7	17
Tingle (2005)	Non-woven Geotextile	Unknown	Interface	13.8	22	1	28.9
	Punched Geogrid	800	Interface	13.3	13.7	1	1.5
Webster (1993)	Punched Geogrid	13700	Interface	13.7	3	1	2.7
	Punched Geogrid	15100	Interface	5.9	8	1	22
	Punched Geogrid	15100	Interface	9.8	8	1	6.7
	Punched Geogrid	15100	Interface	11.8	3	1	3.1
	Punched Geogrid	15100	Interface	13.7	3	1	4.7
	Punched Geogrid	15100	Middle of Base Course	13.7	3	1	2.2
	Punched Geogrid	15100	Interface	17.7	3	1	1.3
	Woven Geogrid	15600	Interface	13.7	3	1	0.9
	Knitted Geogrid	14900	Interface	13.7	3	1	1.6

2.5.2 Evaluation of the Impact of Base Course Layer Thickness

Geosynthetic reinforcements have been shown to increase structural performance of pavements; therefore, geosynthetic reinforcements are sometimes used to reduce the thickness of the base course while maintaining an equivalent service life (Perkins et al. 2005). Pavements reinforced with geosynthetics on weaker subgrades, CBR=1, cannot reduce the base course layer and maintain the same structural integrity (Haas et al. 1988). However, on subgrades with adequate strength, CBR=8, the base course layer can be reduced by as much as 50% (Webster 1993). There is no definitive relationship between geosynthetic reinforcement and equivalent base course thickness that can be replaced.

2.5.3 Evaluation of Geosynthetic Location

The ideal location of the geosynthetic reinforcement within the pavement layer is dependent on the magnitude of the applied load and the quality and thickness of the pavement structure being reinforced (Berg et al. 2000, Barksdale et al. 1989, and Haas et al. 1988). Even though there are many parameters, such as subgrade quality, layer thicknesses, geosynthetic type, and predicted loading, that can affect the "correct" placement of the geosynthetic reinforcement in the flexible pavement structure; the most effective placement of the geotextile is always at a layer interface, acting as a separator to keep one layer from mixing with another. Barksdale et al. (1989) showed that the most effective location of a geogrid is somewhere within the base course, not at the layer interface. However, the thickness of the base course does effect the position of the geogrid. For a thin base layer, the geogrid should be located near the bottom of the layer, but for a base course thickness greater than 9 inches, the geogrid performs better near the midpoint of the layer (Hass et al. 1988). However, the geogrid should not be placed too high in the base

course, or the geogrid will not be able to mobilize in time to prevent lateral spreading of the base course, resulting in rutting.

2.5.4 Evaluation of Geosynthetic Properties

It is understood that adequate junction strength and rib flexural stiffness is essential for a biaxial geogrid in order to transfer the load between longitudinal and transverse ribs effectively in base reinforcement applications (Hatami 2011). The aperture size of a geogrid should also be considered in comparison to the gradation of the base course to insure that lateral restraint can occur. The thickness of the geogrid should also be considered when looking to provide lateral restraint because it would seem that the thicker the grid, the more it would laterally withstand. Pullout resistance should be considered because geogrids placed in an aggregate base layer can be subjected to significant stresses from compaction equipment during construction. The pullout capacity will also affect the strain distributions along the reinforcement anchorage length outside the pressure zone under the wheel load at relatively low confining pressures (Hatami 2011). When choosing a type of geosynthetic to apply to a flexible pavement structure, the level of service of the structure should be considered because different geosynthetics have different strain levels that must be met before being mobilized. Barksdale et al. (1989) suggests that geotextile materials require significantly more deformation of the pavement to mobilize the same amount of reinforcement as a geogrid due to the interlocking ability of the geogrid (Barksdale et al. 1989). Stiff geosynthetic materials work well on soft subgrades, but the influence of the geosynthetic stiffness decreases as the stiffness of the subgrade increases. It is important to develop just enough rutting to mobilize the geosynthetic to prolong the service life of the pavement without failing the pavement (Hufenus et al. 2006). Without quantitative guidelines for

design, a review of research projects with similar properties and acceptable results should be conducted to help determine the correct geosynthetic reinforcement type.

2.6 Evaluation of Reinforcement Mechanisms

The reinforcement mechanisms that will be discussed are those factors that affect the performance of geosynthetic reinforced pavement structures. This section will describe what allows or forces the geosynthetic reinforcements to perform these mechanisms and improve the pavement structure performance.

2.6.1 Lateral Restraint

Lateral restraint describes the ability of the aperture geometry of a grid to confine aggregate particles within the plane of the material (Archer 2008). A vertical load induces lateral forces, which spread the aggregate particles and lead to local deformations of the fill. Due to the frictional interaction and interlocking between the fill material and the geosynthetic, the aggregate particles are restrained at the interface between the subgrade and the fill (Hufenus et al. 2006). The interlocking transmits tensile forces from the aggregate to the geogrid. The lateral restraint mechanism has also been referred to as shear resisting interface (Maubeuge and Klompmaker 2011). This feature yields a stiffening effect to the reinforced granular material, both above and below the geogrid (in the case of the material being installed within the base course), that results in an increase in modulus of the reinforced layer (Archer 2008). The reinforcement mechanisms achieved by laterally restraining soil particles are illustrated in Figure 2.8. This mechanism increases base course stiffness while reducing horizontal strain in the base course. Vertical stresses and strains in the base course are reduced, improving load distribution. Vertical stress and strain, as well as shear stress, in the subgrade are also reduced through lateral restraint (Maubeuge and Klompmaker 2011). The confining mechanism does not imply the need

24
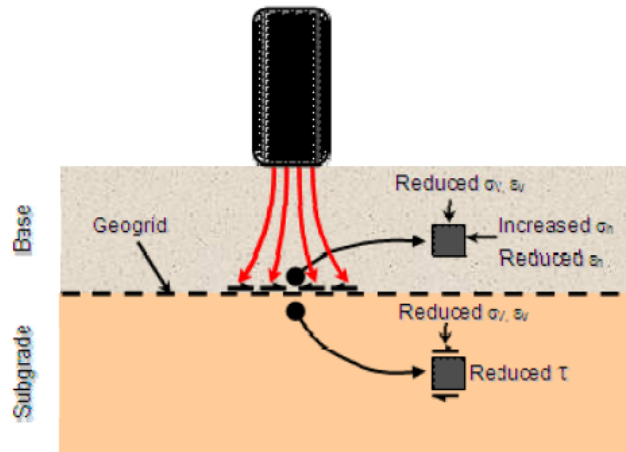
Figure 2.8. Lateral base course restraint (Maubeuge and Klompmaker 2011).

for significant rut depths to form and therefore is also of interest for permanent paved roads (Hufenus et al. 2006).

2.6.2 Separation

Normally in roadways, a stiff material is placed over a soft material and when these two materials intermix, the stiff material layer may decrease in thickness, creating a larger layer of weak soil beneath a thin layer of stiff soil, as illustrated in Figure 2.9. This mixing of the layers is known as fines migration. When this condition is present, separation is the most important mechanism of the geosynthetic material. Al-Qadi et al. (1994) discovered that the separation mechanism is more important in strengthening reinforced pavement sections than had been reported previously in literature after excavating through test sections at the end of testing (Al-Qadi et al. 1994). Studies performed on pavement reinforcement with geotextiles tend to show that separation and filtration are the most important mechanisms for thin base course aggregate thicknesses and weak subgrade conditions which are susceptible to fines migration (Fannin and Sigurdsson 1996). Geotextiles are more effective at separation than geogrids.
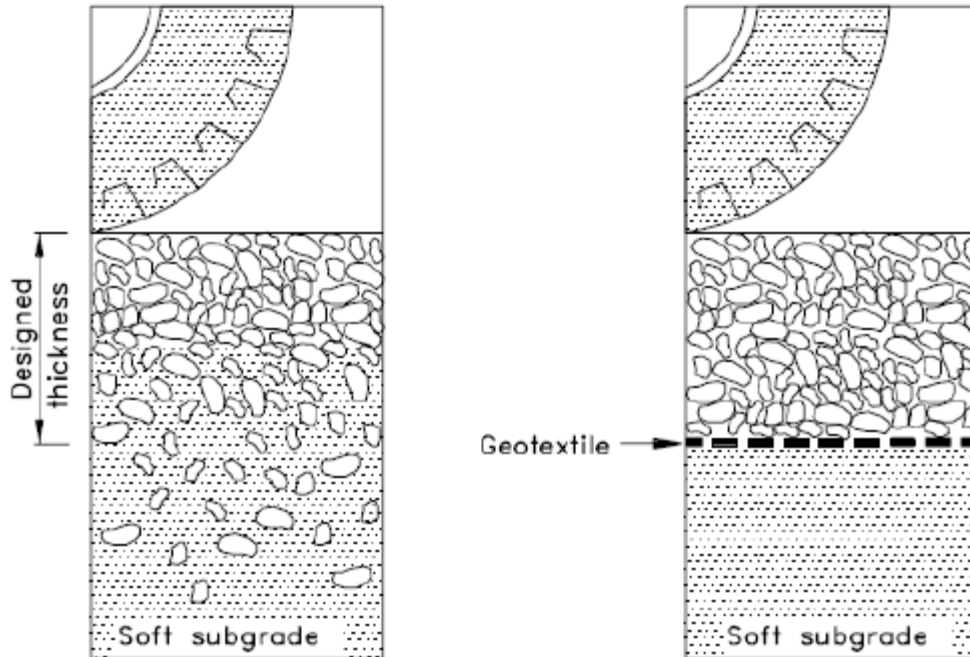
Figure 2.9. Contribution of geotextile separation in pavements to prevent intermixing of layers (Berg et al. 2000).

2.6.3 Tensioned-Membrane Effect

If heavy traffic loads are applied to the base course surface and/or the subgrade is extremely soft, significant deformations on the base course surface as well as on the subgrade surface occur (Maubeuge and Klompmaker 2011). When geosynthetics are placed in heavily trafficked roadways, predominantly unpaved roadways, the soil along the geosynthetic reinforcement is able to deform enough to transfer enough stress to the geosynthetic to mobilize tension, although this may require significant rutting (Giroud and Noiray 1981). The configuration of the geogrid in such cases can be assumed as shown in Figure 2.10 (Maubeuge and Klompmaker 2011). The geosynthetic reinforcement is stressed due to depression basin created by the wheel path causing the geosynthetic to act as tensile support in the vertical direction, reducing stresses applied to the subgrade and increasing bearing capacity. However, high stiffness geosynthetic reinforcements along with large enough deformations to mobilize the
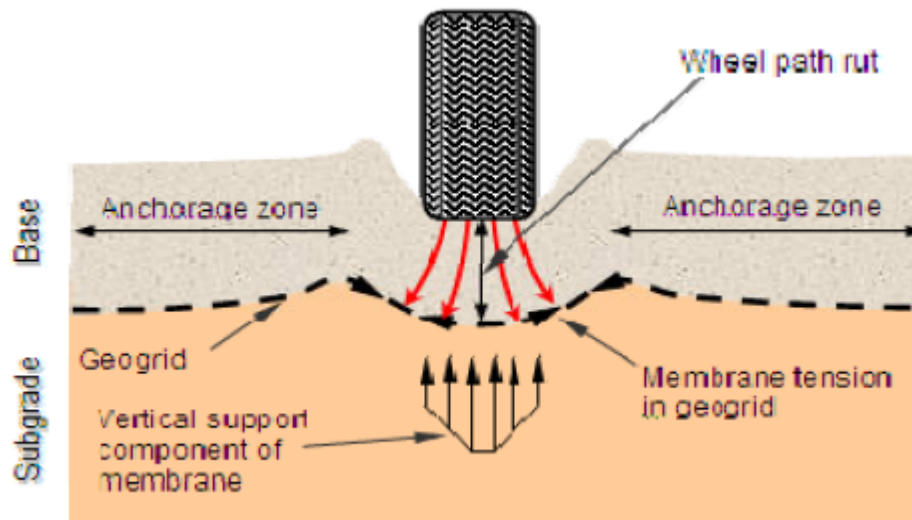
Figure 2.10. Tensioned membrane effect (Maubeuge and Klompmaker 2011).

geosynthetic are needed for the tensioned-membrane mechanism to be effective. Although, punched and drawn geogrids are manufactured by "pre-straining" the polymer yielding an effective stress transfer of vertical and horizontal stresses, mobilizing tensile resistance in both woven and non-woven geotextiles requires strain to be induced after the product is installed, which leads to rut accumulation in the base and subgrade layers before the geosynthetic actually responds (Archer 2008).

2.7 Design Methods

Design methods for geosynthetic-reinforced pavements have been developed, but most do not include many of the variables that impact pavement performance. The results gathered through empirical studies are mixed; with some showing geosynthetics provide benefits to pavement structures while some show there is no benefit. There are discrepancies between the empirical studies that report there is a benefit because some claim geogrids perform better than geotextiles, some claim they perform equally, and others claim that geotextiles outperform geogrids. The empirical studies, therefore, reduce to gathering enough data to form an empirical

27

design method (Kinney et al. 1998). Empirical design methods are unable to account for variations in the pavement configuration and geosynthetic type and placement. Due to the variations in input parameters in flexible pavements, finite element design methods have been created, but it is difficult to model the behavior of different soil types, geosynthetic behavior, and the interactions between the two. These models are also limited to a response of the pavement under a single load. Giroud and Han (2004) published a design method that combines bearing capacity theory with empirical data from full-scale test sections and monitored unpaved roads (Archer 2008). The Giroud and Han (2004) method considers: (1) the effects of variation in base course strength, (2) the number and size of load cycles and the desired roadway performance, (3) how the load distribution angle within the base course changes over time, and (4) recognition that geogrids and geotextiles perform differently in roads and differently even from like materials (Archer 2008). Giroud and Han (2004) state that the advanced design is theoretically based and experimentally calibrated. Therefore, it more accurately predicts performance for both geogrid and geotextile reinforced unpaved roads, and the new method supersedes the previous methods from Giroud and Noiray (1981) and Giroud et al. (1985) (Giroud and Han 2004). However, there is no specified and accepted design method even though geosynthetic materials have been used to reinforce pavements for over 30 years. The lack of a standard design method limits the growth of geosynthetic reinforcements being applied in flexible pavement structures.

2.8 Conclusion from Literature Evaluation

Many geosynthetic reinforced flexible pavement evaluations have been conducted. This literature has referenced some of this work, but is not inclusive. There have been a number of research efforts that display significant benefits to pavement performance brought by the inclusion of geosynthetic reinforcements, such as Perkins and Cortez (2005), Al-Qadi et al.

(1994), and Cuelho et al. (2011). However, the amount and type of benefit are not typically consistent from one study to the next. A few studies have shown little improvement from including geosynthetic reinforcements in pavements, such as Cox et al. (2010a) and Henry et al. (2011). These discrepancies seem to indicate that the problem is complex and many variables need to be considered before simply assuming that placing geosynthetics in all pavement structures will provide a cost-effective performance benefit. Henry et al. (2011) stated and illustrated through data presentation that there could be a diminishing effect on the benefit returns from the geosynthetic reinforcements as base course thickness increases. Geosynthetic reinforcements have the potential to be greatly beneficial in flexible pavement structures with poor subgrade soils or thin base course layers, but until there is consistency in research results there will continue to be uncertainties in whether or not including geosynthetic reinforcements will benefit specific flexible pavement structures and ultimately save money while improving the service life of the road.

Chapter 3

3.0 Site History

3.1 Overview

In 2004, the Arkansas Highway and Transportation Department (AHTD) began construction of a frontage road (Frontage Road 3) along US Highway 63 in the town of Marked Tree, Arkansas at the intersection of Arkansas Highway 75. This frontage road was constructed for a research project (AHTD TRC-0406). This field study was aimed at determining the benefits, if any, of using geosynthetics for flexible pavement reinforcement on state funded roadway projects. Typically, when poor subgrade soils are encountered, AHTD will over-excavate and replace the poor material with quarried materials such as large crushed stone (B-Stone) or standard road base (AHTD SB2-Class 7), depending on availability (Brooks 2009). However, in many areas of the state with poor native soils, there are very few sources of quality fill material within a reasonable distance, resulting in long hauling and costly pavements. The native silt and clay subgrade soils in Northeast Arkansas have particularly poor engineering qualities; therefore, it was hypothesized that the resulting benefits from geosynthetic materials installed at the base and subgrade interface in a flexible pavement structure in this area would be evident if these materials do, in fact, substantially enhance performance.

The initial objectives of TRC-0406 (referred to as the Marked Tree Project) were to: (1) construct a full-scale flexible pavement with various configurations (i.e., base course thicknesses, geosynthetic types, control sections, etc.), (2) instrument the pavement with strain gauges, pressure cells, climate sensors, etc., (3) collect data from the instrumentation to infer the mechanism(s) that most influence pavement performance, and (4) develop a finite element model

that could be used to predict critical structural responses of flexible pavements reinforced with geosynthetics (Howard 2006). A profile view of the configuration of the pavement sections, including type and location of instrumentation, is presented in Figure 3.1.

The original pavement configuration for the research consisted of 13, 50-ft (15-m) long, 10-ft (3.05-m) wide test sections (numbered 1 through 13 from east to west; refer to Figure 3.1). Section 7 was constructed as a transition section that separated Sections 1-6, with 10-in (25-cm) thick base layers, and Sections 8-13, with 6-in (15-cm) thick base layers. Sections 1 and 13 were left unreinforced to act as control sections for each base thickness. Prior to construction, two Mirafi geosynthetics (a geotextile and a geogrid) that were not initially planned were added to the study. These two products were installed at each end of the pavement and were identified as Sections 1A, 1B, 13A, and 13B (Warren and Howard 2007b). The geosynthetic configuration for the first eight sections (Sections 1B – 6) is a mirror image of the configuration in the last eight test sections (Sections 8 –13B) about Section 7. The specific types and manufacturers of the geosynthetics installed in each section are provided in Figure 3.2. It must be noted that all geosynthetics (including geogrids) were installed at the interface between the compacted subgrade and the base course. No products were installed within the base. Furthermore, two sections (Section 5 and Section 12) contained both a geogrid and a geotextile atop one another.

The soil properties and construction methods employed to create the Marked Tree geosynthetic-reinforced pavement test sections will be explored in this chapter. The initial conclusions drawn from the instrumentation and data processing involved with the original research project (TRC 0406) will also be briefly summarized.
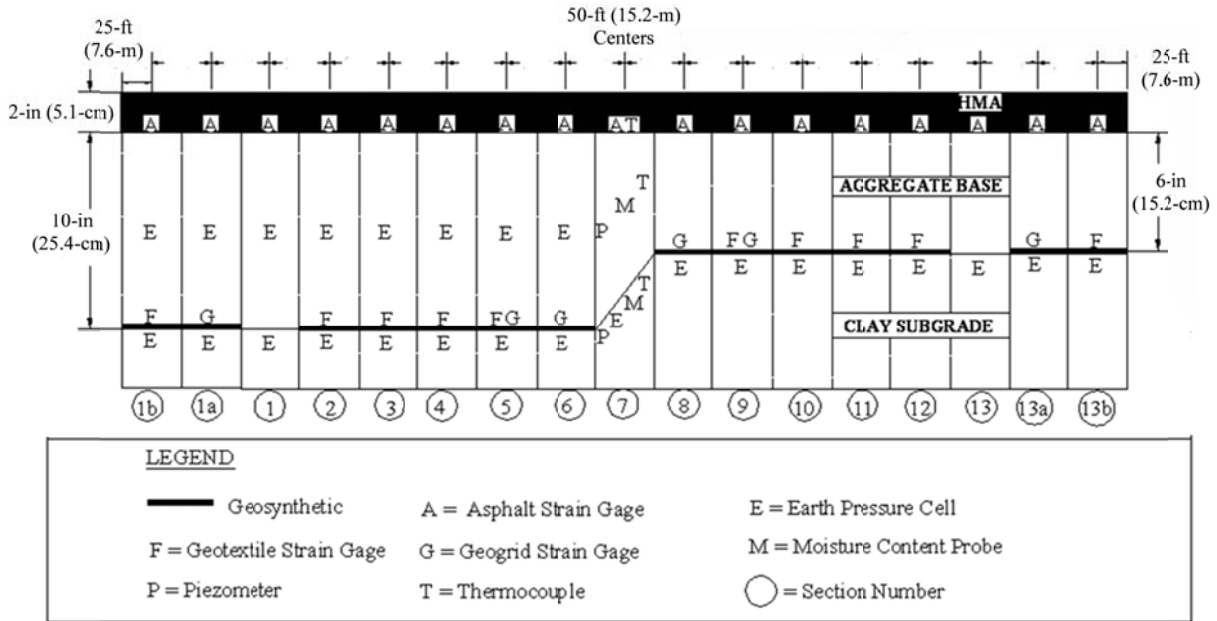
Figure 3.1. Profile view of instrumentation configuration (Warren and Howard 2007).
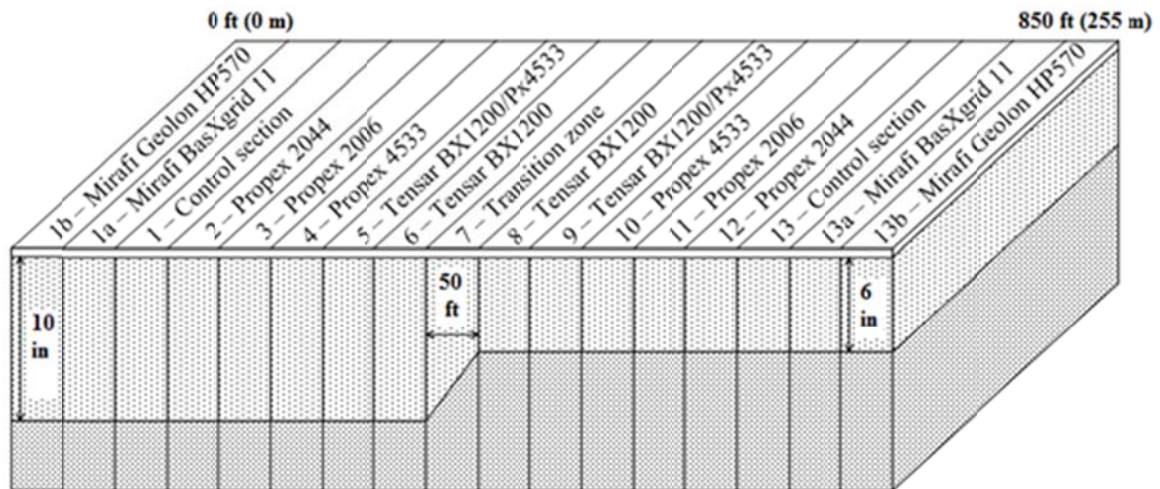
Figure 3.2. Schematic of geosynthetic reinforced test sections in Marked Tree, Arkansas (Cox et al. 2010b).

3.2 Site Description

The Marked Tree site consists of characteristically weak soils, which was the primary reason for its initial selection for the geosynthetic reinforcement in flexible pavements project. Weak subgrade soils plague the eastern side of Arkansas, making building efficient roadways difficult. Geosynthetics can potentially improve the performance of low volume pavements in such conditions by providing lateral restraint to the base course layer.

3.2.1 Site Location

The roadway under investigation is located in Marked Tree, Arkansas. Marked Tree is in the northeastern portion of the state, approximately 33 miles south from Jonesboro, Arkansas and 38 miles north from Memphis, Tennessee. Figure 3.3 is a state map of Arkansas, which highlights the county in which construction took place (Poinsett County). The test site is located on Frontage Road 3, which serves to connect US Highway 63 and Arkansas Highway 75. Figure 3.4 is a vicinity map on which the test section has been denoted in red. At the time of construction, Highway 63 was being converted into a controlled access roadway with interstate-type on and off ramps as the only access points.

The sixteen test sections and the transition section are located between STA. 136+50 and STA. 145+00 (850-ft [255-m] long) in the east-bound lane of Frontage Road 3 (the west-bound lane was not part of the special instrumentation/construction plan). It should be noted that the frontage road dead ends west of the testing site since it affects the traffic pattern of the roadway.

The topography of the test site is relatively flat. The majority of the land in the adjacent areas is used for produce farming. Figure 3.5 is a picture of the test site prior to construction. Marked Tree is a relatively small town located in an agricultural area with a population of approximately 2,600. At the time of construction the majority of the traffic on Frontage Road 3

Figure 3.3. Arkansas state map featuring the project location.
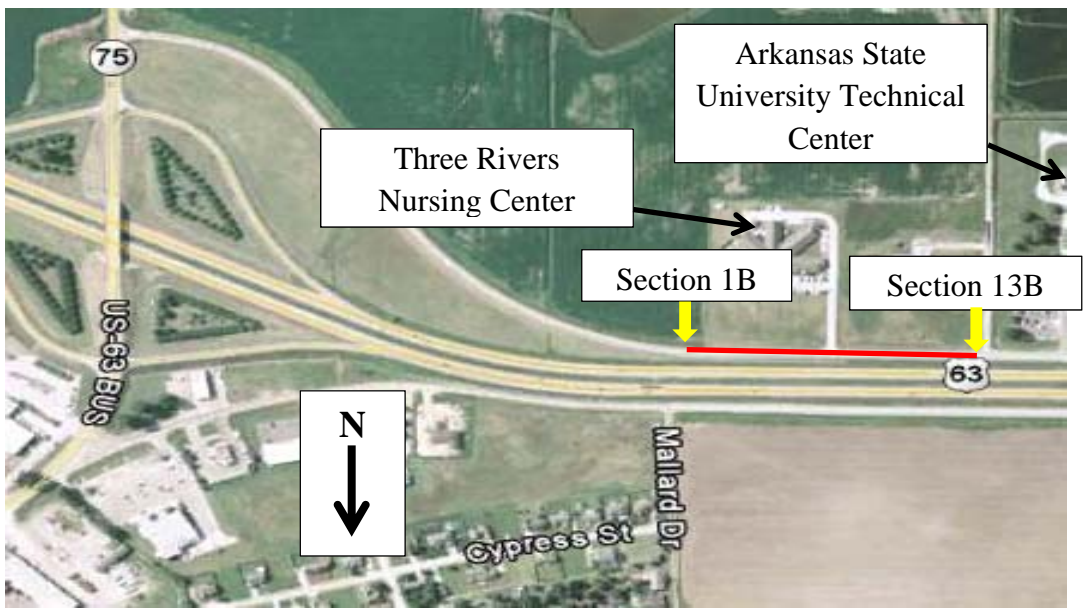
Figure 3.4. Vicinity map of test site denoting approximate extent of test sections.

was anticipated from vehicles associated with the Arkansas State University Technical Center located west of Section 13B (refer to Figure 3.4). However, a nursing home (Three Rivers Nursing Center) was constructed just after completion of the road whose driveway intersects the

Figure 3.5. Test site prior to construction (Howard 2006).

testing area between Sections 7 and 8. This ultimately resulted in slightly different trafficking of the 10-in (25-cm) thick base course sections (Sections 1B – 6) than the 6-in (15-cm) thick base course sections (Sections 8 – 13B) refer to Chapter 4, Section 4.5.1).

3.2.2 Site Characterization

There were two distinct phases in the characterization of the onsite soils. The first phase was initial sampling and testing that was done as part of the design process. The second round of sampling and testing took place during the first attempt to construct the roadway. This round of testing was used to conduct index and strength testing to fully characterize the materials (Brooks 2009).

3.2.2.1 Sampling and Laboratory Testing

Prior to the roadway design and construction, a subsurface exploration was conducted by AHTD. This exploration occurred between September 8 and September 10, 2003, during which time a series of twelve borings were completed. These twelve borings each terminated at a depth

of 10-feet (3.05m) below existing grade, which varies from 2- to 4-feet (0.61- to 1.22-m) below final top of subgrade for the completed roadway embankment. Each boring was located along the centerline of the proposed road and spaced on approximately 50-feet (15.2-m) centers. Samples collected during this exploration included both split spoon (disturbed) and Shelby tube (undisturbed) samples (Brooks 2009).

A second set of borings was completed between October 5 and October 7, 2004. This set of borings consisted of three holes within each planned test section: one for disturbed samples (split spoon), one for undisturbed samples (Shelby tube), and one for bulk samples (auger cuttings). There were 13 locations drilled at 50 feet (15.2 m) intervals along the centerline of the road. These borings were drilled to a depth of 10 feet (3.05 m) below the rough finished grade of the roadway earthwork after all necessary fill had been placed prior to blue-topping and final fine grading of the roadway in preparation for the placement of geosynthetics and aggregate base course (Brooks 2009). AHTD compiled final boring logs and extruded the Shelby tube samples before transferring the packaged samples to the University of Arkansas in Fayetteville for storage and subsequent testing. All extruded samples were carefully packaged and stored to ensure preservation of moisture content. In-situ moisture contents were taken from the bag samples. A composite soil profile based on all of the boring logs is presented in Figure 3.6. The elevations in Figure 3.6 are in feet. Note that several more feet of compacted fill subgrade was placed below the 6-in (15.2-cm) base course sections (Sections 8 – 13B) than below the 10-in (25.4-cm) sections (Sections 1B – 6).

Laboratory testing was conducted on the samples to classify the soils as well as to determine the strength and stiffness characteristics of the soils at each test section. Before testing, the soil was processed to ensure all particles could pass through a #4 sieve. For classification

36
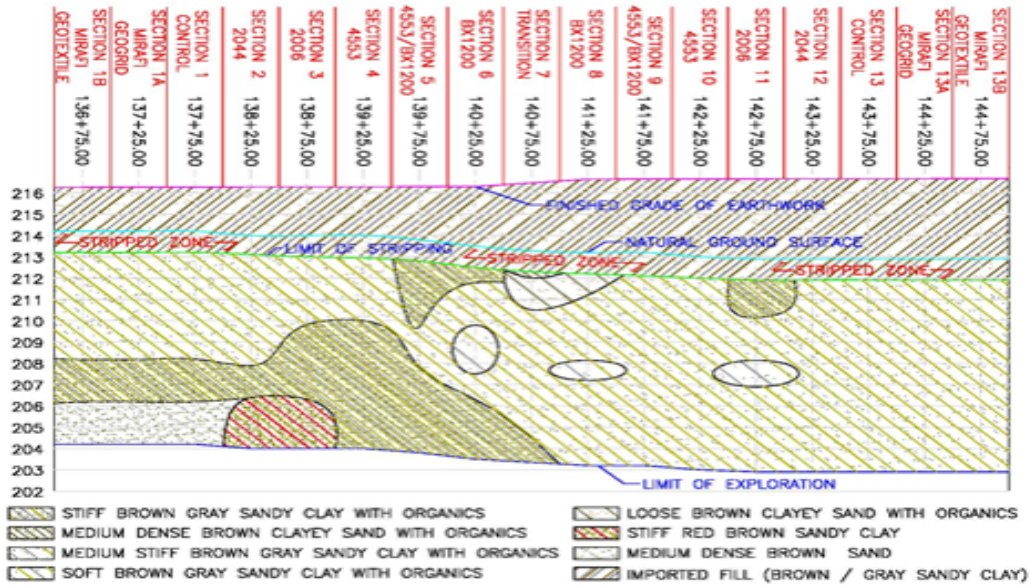
Figure 3.6. Subgrade soil profile based on Geotechnical exploration (Brooks 2009).

purposes, the soils were subjected to the following tests: Atterberg limits (ASTM D 4318-00),Specific Gravity (ASTM D 854-02), and Particle Size Distribution (ASTM D 442-63). The soils were classified according to both the USCS (ASTM D 2487) and AASHTO classification systems. The index testing results and the soil classifications for Sections 1 – 13, excluding Section 7, are provided in Tables 3.1 and 3.2 for USCS and AASHTO, respectively. Note that classification information is not available for Sections 1B, 1A, 13A and 13B since those sections were not planned at the time of site investigation. It can be seen that the site is very uniform in terms of its soil classification (CH or A-7-6). Only Section 8 (station 141+25) classifies as CL. Fines contents across these sections range from 67 – 90% and PI ranges from 35 – 53. The plastic limit values are graphically presented in Figure 3.7. Nearly all sections had subgrade PI ranging from 40 – 50, with only Sections 8 and 9 (slightly lower) and Section 13 (slightly higher) falling outside this range.

37

Table 3.1. USCS soil classification of bulk samples from 2.5' to 12.5' (Brooks 2009).

Section	LL	PL	PI	Specific Gravity	% Passing 3/4"	% Passing #4	% Passing #200	% Gravel	% Sand	Group Symbol	Group Name
1	67	20	47	2.72	100	100	89.4	0	10.6	CH	Fat Clay
2	63	22	41	2.69	100	100	87.7	0	12.3	CH	Fat Clay
3	66	22	44	2.69	100	100	90.2	0	9.8	CH	Fat Clay
4	66	20	46	2.68	100	100	85.3	0	14.7	CH	Fat Clay
5	65	19	46	2.69	100	100	83.9	0	16.1	CH	Fat Clay w/ Sand
6	63	17	46	2.69	100	100	83.0	0	17.0	CH	Fat Clay w/ Sand
8	49	14	35	2.71	100	100	67.3	0	32.7	CL	Sandy Lean Clay
9	55	17	38	2.68	100	100	76.8	0	23.2	CH	Fat Clay w/ Sand
10	60	17	43	2.67	100	100	83.6	0	16.4	CH	Fat Clay w/ Sand
11	61	18	43	2.71	100	100	85.7	0	14.3	CH	Fat Clay
12	62	17	45	2.71	100	100	87.8	0	12.2	CH	Fat Clay
13	73	20	53	2.71	100	100	89.0	0	11.0	CH	Fat Clay

Table 3.2. AASHTO soil classification (Brooks 2009).

Section	Depth (ft)	Samply Type	LL	PL	PI	Specific Gravity	% Passing #10	% Passing #40	% Passing #200	Group Class.	Group Index
1	2.5-12.5	Bulk	67	20	47	2.72	99.7	99.2	89.4	A-7-6	46
2	2.5-12.5	Bulk	63	22	41	2.69	99.9	99.4	87.7	A-7-6	39
3	2.5-12.5	Bulk	66	22	44	2.69	99.8	99.4	90.2	A-7-6	43
4	2.5-12.5	Bulk	66	20	46	2.68	99.9	99.2	85.3	A-7-6	43
5	2.5-12.5	Bulk	65	19	46	2.69	100	99.3	83.9	A-7-6	41
6	2.5-12.5	Bulk	63	17	46	2.69	100	99.1	83	A-7-6	40
8	2.5-12.5	Bulk	49	14	35	2.71	99.8	91	67.3	A-7-6	21
9	3.5-13.5	Bulk	55	17	38	2.68	99.9	99.6	76.8	A-7-6	29
10	3.5-13.5	Bulk	60	17	43	2.67	100	99.6	83.6	A-7-6	37
11	3.5-13.5	Bulk	61	18	43	2.71	100	99.5	85.7	A-7-6	39
12	3.5-13.5	Bulk	62	17	45	2.71	99.9	99.5	87.8	A-7-6	42
13	3.5-13.5	Bulk	73	20	53	2.71	100	99.4	89	A-7-6	52

The Shelby tube specimens from Sections 1 and 13 were divided into different zones as a function of depth to represent the compacted subgrade, the upper natural ground, and the lower natural ground. The in-situ dry density (unit weight) of the upper natural ground was 85 pcf (1362 kg/m^3), the lower natural ground was 95 pcf (1522 kg/m^3), and the compacted subgrade was 101 pcf (1618 kg/m^3) (Howard 2006). The bulk samples collected during the second subsurface investigation were used in Proctor testing to determine the maximum dry density and optimum moisture content of the re-compacted subgrade soil at each section. The proctor tests
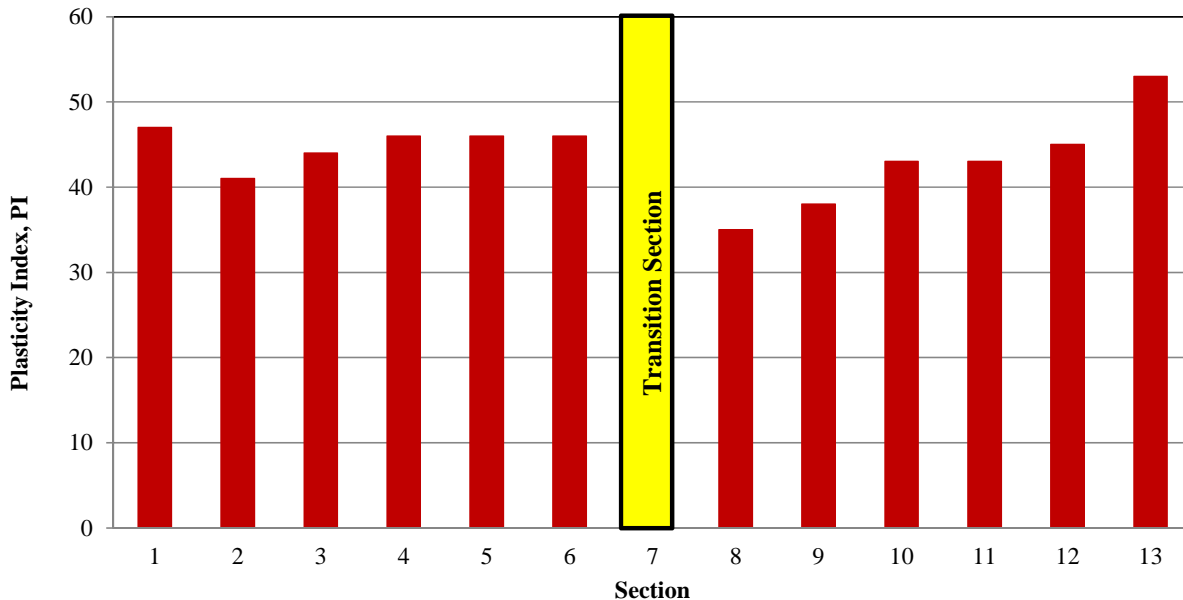
Figure 3.7. Plasticity index values of the subgrade from each section of the Marked Tree site from tests conducted in October 2004.

followed ASTM D 698-00 Method C. After a set of standard proctor tests were run on the soils, it was determined that the maximum dry density was approximately 106 pcf (1698 kg/m^3) and the optimum moisture content was approximately 16.8% (Brooks 2009).

Additional laboratory tests were conducted on the compacted subgrade at Sections 1 and 13, such as California Bearing Ratio (CBR), resilient modulus (Mr) and unconsolidated undrained (UU) triaxial tests. All these tests were, however, conducted on Proctor samples rather than undisturbed samples that would more accurately represent the soil stiffness/strength in the field. Mr values for Sections 1 and 13 ranged from approximately 11.0 – 15.8 ksi (75.8 – 108.9 MPa), undrained shear strengths (Su) ranged from approximately 2.91 – 5.36 ksi (18.9 – 37.0 MPa), and CBR values ranged from 1.38 to 1.66, but could be expected to reach a minimum of 0.8 (Brooks 2009). The processes for conducting these tests, as well as the results, can be found in greater detail in Howard (2006) and Brooks (2009).

3.3 Site Construction

The research team for the initial Marked Tree project (TRC 0406) originally traveled to the site and installed earth pressure cells in the finished subgrade in October of 2004. Unfortunately, harsh winter weather prevented completion of the roadway, forcing all subgrade sensors to be removed to allow the subgrade surface to be re-worked in June of 2005.

The following subsections discuss the construction techniques for completing the geosynthetic-reinforced and instrumented eastbound lane of Frontage Road 3. Unfortunately, the original work described in Howard (2006) did not mention the geosynthetics that were installed in the westbound lane. It was known from construction photographs that a single type of geosynthetic was installed at the interface of the compacted subgrade and base in the westbound lane, however, the type of geosynthetic was not known. It was discovered in an October 2010 forensic exploration of the westbound lane adjacent to Sections 13 and 13B that the westbound lane was reinforced with a Carthage Mills woven, slit film geotextile (FX-66). This geotextile was installed over the entire width of the westbound lane and overlapped into the eastbound lane approximately 3 feet (0.91 m). Figures 3.8 and 3.9 are construction pictures displaying the overlapping of the Carthage Mills geosynthetics from the westbound lane to the eastbound lane. This overlap only left approximately 9 feet (2.74 m) of the eastbound lane from the south edge of the roadway (the right wheel path) to observe the effects of the geosynthetics installed in the 16 different eastbound lane test sections.

3.3.1 Subgrade

As previously noted, the subgrade was prepared in October of 2004, but winter weather prevented completion of the roadway and the subgrade had to be reworked in June of 2005. The re-work consisted of removal of the top few centimeters of the subgrade and re-compacting new
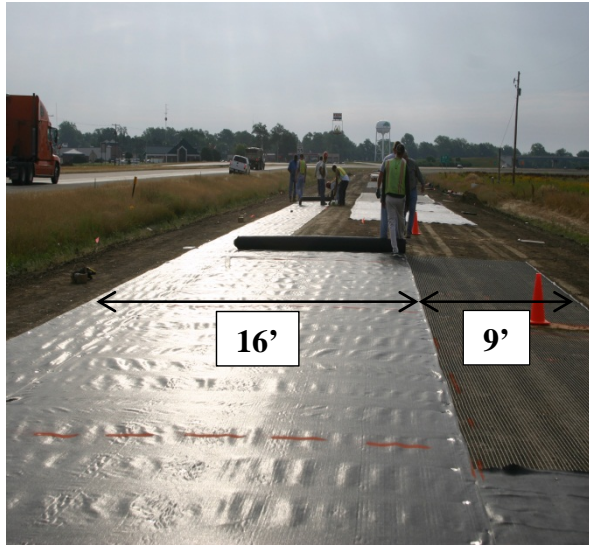
Figure 3.8. East facing view of geosynthetic overlap.
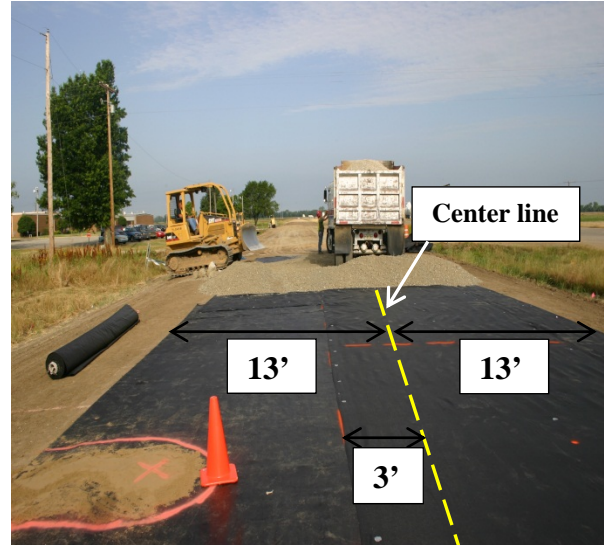
Figure 3.9. West facing view of geosynthetics in both lanes.

material in its place (Howard 2006). A picture of the finished subgrade can be found in Figure 3.10. There were no new proctor tests conducted to discover the maximum dry density or optimum moisture content of the new fill material that was placed on top of the reworked subgrade. However, it was assumed that the new fill material was equivalent to the original subgrade fill material, so it could be assumed that the maximum dry density was considered to be 106 pcf (1697 kg/m^3) with an optimum moisture content of 16.8%. It should be noted that in the October 2004 construction, Sections 5, 6, 7, 9, 10, 11, and 12 were not compacted to at least 95% of the maximum dry density, while the average moisture content of each section was approximately 4.4% dry of the 16.8% optimum moisture content.. The few centimeters of reworked subgrade were compacted to an average dry density of 112 pcf (1789 kg/m^3). The moisture content of the reworked subgrade was on average approximately 2.1% dry of optimum, while a few sections (Sections 4, 5, and 6) had moisture content values wet of optimum. The density values used for comparison are from an average of three nuclear density gage readings at

41

Figure 3.10. Finished cut subgrade (Howard 2006).

each section. The density values from both dates are provided in Table 3.3 and graphically displayed versus Section in Figure 3.11.

3.3.2 Geosynthetics

The geosynthetics were installed at the subgrade and base course interface. There was not a strong justification for putting the geosynthetics at this depth. Woven geotextiles will provide a separation effect when placed between two layers, but the interaction between the geogrids and the base course may not be sufficient to obtain a benefit (Berg et al. 2001).

Instrumentation was attached to the geosynthetics to infer the strains induced by traffic loading. The goal of this instrumentation was to infer the level of improvement gained by using the geosynthetics in the pavement structure. Foil-type strain gages were attached to the geosynthetics in the laboratory and subsequently transported to the construction site. Once the gages were attached, several provisions were necessary to prevent damage to the instruments

Table 3.3. Subgrade field nuclear density values (Howard 2006).

Section	October 2004		June 2005	
	γ_d (pcf)	w%	γ_d (pcf)	w%
1	104.3	10.6	118.8	11.8
2	104.4	10.5	116.1	11.4
3	101.2	11.7	114.6	15.4
4	101.3	12.3	111.5	18.3
5	95.8	11.5	109.9	19.3
6	97.9	12.2	110.9	19.3
7	97.5	12.4	107.3	12.8
8	102.0	12.6	110.9	12.5
9	99.7	12.3	115.1	12.1
10	100.2	12.2	112.4	15.1
11	97.7	13.4	109.0	16.0
12	97.4	13.7	108.1	14.2
13	100.9	15.7	108.1	12.3
Average =	100.0	12.4	111.7	14.7

Note: October 2004 max dry density = 106 pcf. (95% max = 100.7 pcf)

Optimum Moisture Content (%OMC) = 16.8%

No max dry density determined for new fill applied in June 2005.
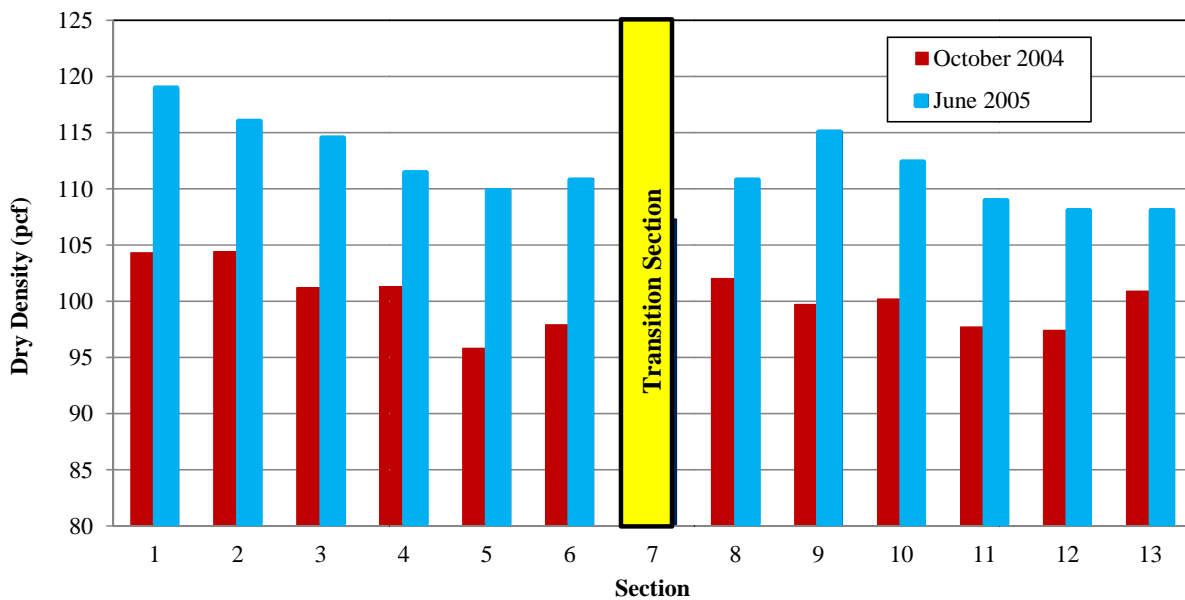
Figure 3.11. Subgrade field nuclear density values from Marked Tree site construction.

43

during transportation and installation (Brooks 2009). The instrumented geogrids were rolled from each end in a scroll-like fashion to make field alignment easier. By rolling each end to the center, the grid could be unrolled by first aligning the gage with its proper location on the subgrade. Geotextiles were also folded so that the active gage could easily be aligned to the proper location on the subgrade (Howard 2006).

Placement of each of the 56-ft (17.1-m) long geosynthetics was performed with care to ensure quality control and assurance. All geosynthetics were tensioned and placed on a smooth surface, free of wrinkles, using methods that simulated typical installation. It was necessary to locate the active geosynthetic strain gage within 1.2 inches (30mm) and prevent movement of the gage while the remainder of the geosynthetic was placed without reinforcing the area local to the gage. The procedure was developed entirely due to the instrumentation. Such a complicated procedure would not be practical or commonplace in construction. A typical installation would consist of rolling the material onto the subgrade relatively free of wrinkles and possibly tacking it into place (Howard 2006).

The following procedure was developed by Howard (2006) for the installation and protection of the instrumented Propex 2006 and Propex 2044 geotextiles. This procedure utilized nine people and two trucks. In addition to the planned protection measures, sand placed during earth pressure cell installation was present and provided a cushion for the gages. The following terms are commonly reoccurring during the procedure explanation, so to prevent from unnecessary repetition they are defined as follows:

Pins: Standard U-shaped landscaping pins approximately 6 inches (150 mm) long.

Pipe: 4-inch (10.2-cm) sewer and drain (S/D) pipe that was slightly longer than the widest geosynthetic.

Tensioner: Two wooden boards were fastened together with the top half of an S/D pipe attached to it. The composite board extruded form one truck tailgate to the other and had cross sectional dimensions of 3.0 x 5.6 inches (76 x 140 mm). The geosynthetic rolled over the top of the composite board during the tensioning process so the top half of the S/D pipe provided a smooth surface and prevented the geosynthetics from catching on bare wood (see Figure 3.12).

Installation method as defined in Howard (2006):

1) Locate the active gage over the center of the subgrade earth pressure cell and either unroll or unfold the entire geosynthetic.

2) Use standard surveying equipment to align the active geosynthetic strain gage and earth pressure cell center to within at most 1.2 in (30 mm).

3) Pull laterally (perpendicular to the traffic direction) on the geosynthetic at the gage location to remove all wrinkles and hold the material taunt while driving six pins uniformly across the width of the geosynthetic, ensuring all pins are at least 12 inches (300 mm) from the gages.

4) Place full buckets of sand behind the gages to help them remain stationary.

5) Measure and place a mark every 8 feet (2.44 m) on the geosynthetic on both sides of the gage. These marks will be used for pin placement in the geosynthetics.

6) Tension one side of the test material with reference to the gage. Slide the tensioner under the side of the geosynthetic being installed.

7) Position the two trucks as seen in Figure 3.12.

8) Persons 1 and 2 on Figure 3.12 straighten the geosynthetic, and then stand on the corners as shown, with persons 3 and 4 off the geosynthetic.

9) Persons 3 and 4 then walk toward the tensioner until enough force is present to start to lift the pipe with person 8 standing on it.

10) Once tension is applied, person 8 directs the trucks to pull forward very slowly and persons 7 and 9 roll the pipe forward at the same rate that the trucks move forward. During the lay down process, person 8 is ensuring adequate tension is maintained by adjusting the position of persons 3 and 4, controlling the rate of the trucks and pipe personnel to keep the geosynthetic straight and going under the pipe at an angle of approximately 45^0, and removing wrinkles from the geosynthetic as it traverses over the tensioner.

Figure 3.12. Geosynthetic tensioning technique (Howard 2006).

11) The process was continued until the first 8-ft (2.44-m) interval was reached. At this juncture, the lay down process was halted and persons 5 and 6 placed six pins equally across the geosynthetic.

12) The process was then repeated two more times, which left approximately 4 feet (1.2 m) of loose material at each end. The procedure was performed on both sides of the gage, beginning at the gage and traveling away from this area in the longitudinal direction.

13) The 4 feet (1.2 m) of loose material on either end overlapped the adjacent test section by 3 feet (0.91 m). The overlaps were pulled taunt by hand and six pins were placed equally across the geosynthetic. The laps were oriented so that when aggregate was bladed laterally onto the geosynthetics, the material would not tend to roll up.

14) Once the geosynthetics were installed, measures were taken to protect the foil strain gages during construction and service. For example, the cables were arranged to provide stain relief and the geogrid and geotextile strain gages were covered prior to testing. Figure 3.13 shows the small portion of the inverted core of a standard strip drain used to protect the geogrid strain gages, and Figure 3.14 shows the neoprene pads that were utilized to protect the geotextile strain gages. The cables were covered with fine sand (Figure 3.15) and crushed stone was then hand placed over the sand to a depth of approximately 6 in as seen in Figure 3.16.

Figure 3.13. Geogrid strain gage protection, strip drain (Howard 2006).

Figure 3.14. Geotextile strain gage protection, neoprene pad (Howard 2006).
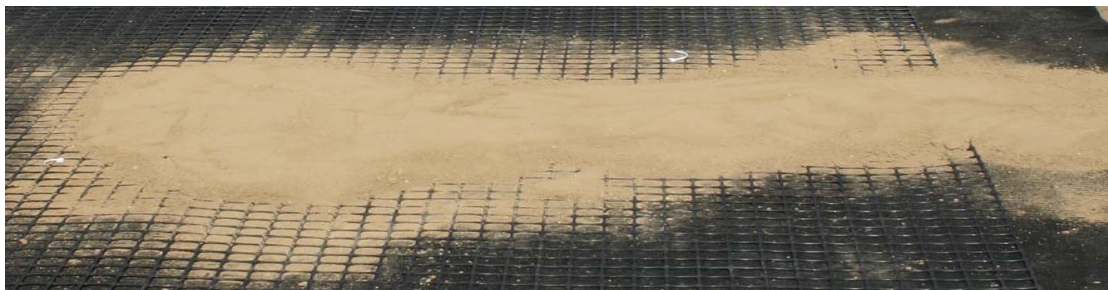
Figure 3.15. Sand covering geosynthetic strain gage and cable (Howard 2006).

Figure 3.16. Crushed stone covering fine sand, geosynthetic strain gage, and cable (Howard 2006).

A modified version of the aforementioned procedure was utilized for the instrumented Tensar BX 1200 geogrids and Propex 4553 geotextiles. Steps 7) – 10) were omitted, and the lay down process was performed entirely by hand. The Propex 4553 could manually be pulled taunt due to the increased deformation ability of the material, and the BX 1200 could be placed in the same orientation regardless of the lay down procedure (Howard 2006).

3.3.3 Base Course

Crushed stone aggregate was used for the construction of the base course. The properties of the crushed stone used for the construction can be found in Table 3.4. These values were obtained from Howard (2006). It should be noted that there is uncertainty about when and where throughout the testing site the average nuclear density gage values for dry unit weight were collected.

The base course was constructed by placing aggregate on the non-instrumented lane to provide a working platform next to the instrumented subgrade and geosynthetics. Aggregate was placed to a depth sufficient to obtain the first 6-inch (150-mm) lift of compacted material on both lanes (Figure 3.17). Once sufficient material was present along the entire test section, aggregate was laterally bladed onto the test sections as shown in Figure 3.18. Until aggregate covered the instrumented test sections, all sensitive areas were continuously marked with fluorescent paint

48

Table 3.4. Crushed stone properties (Howard 2006).

Property	Value
Geology	Dolomite
Classification	Arkansas Class 7
Dry Unit Weight (Modified Proctor)	142.4 - 144.0 pcf (2281 - 2307 kg/m^3)
Dry Unit Weight (Nuclear Density)*	148.5 - 150.3 pcf (2379 - 2408 kg/m^3)
Apparent Specific Gravity	2.80 - 2.81
Internal Friction Angle	43°
Cohesion	6 psi (41.4 kPa)
Plasticity	Non-plastic
Percent Passing 1.5 in (38 mm) sieve	100%
Fines	9.30%
Optimum Moisture	6.5 - 8.2%

*Believed to be too high.

Figure 3.17. Base course placement on non-instrumented lane (Howard 2006).

Figure 3.18. Lateral placement of crushed limestone on geosynthetics (Howard 2006).

and/or traffic cones. This process was carefully observed and no movement of the geosynthetics occurred. After compaction of the first lift of crushed stone, the contractor proceeded as normal to bring the entire test section to the appropriate grade and density (Howard 2006).

Vibration was used during the entire compaction process. A survivability study conducted prior to full scale construction verified vibration would not result in excessive loss of geosynthetic instrumentation. Representative density was far more critical to the overall objectives compared to the risk of losing the instruments. The target base course thickness was 10 inches (254 mm) in Sections 1 – 6 and 6 inches (150 mm) in Sections 8 – 13, variations were observed form the survey data, which was taken at the subgrade and base course surfaces. Sections 1B and 1A also had proposed base course thicknesses of 10 inches (254 mm), while sections 13A and 13B had proposed base course thicknesses of 6 inches (150 mm). The surveyed thicknesses of all 16 test sections can be found in Table 3.5. Note that Section 2 had the thinnest base (8.76 inches) in the 10-inch nominal base sections, while Section 1 had the thickest base

(11.58 inches). In the 6-inch nominal base sections, Section 10 had the thinnest base (5.64 inches), while Section 13B had the thickest base (6.72 inches).

Hand tools were used to excavate all holes and trenches necessary for base course sensor and cable placement. As in the subgrade, the entire base course was finished before any sensors were installed. Instrument locations were determined using standard surveying equipment to allow precise alignment with the previously installed subgrade sensors (Howard 2006).

3.3.4 Asphalt Layer

The design asphalt thickness was 2 inches (51 mm) in all test sections, and the entire pavement was surface course (0.5 in (12.7 mm) Superpave mix), placed in a single pass of the paving train. The asphalt strain gages and thermocouples were installed at locations determined using standard surveying equipment prior to paving. Paving modifications were necessary to avoid damage to these sensors while still producing a quality asphalt mat. The instrumented test sections were located in the middle of the frontage road so the contractor pave normally until the instrumented sections were approached (Howard 2006). Once the instrumented sections were reached, the paving train was stopped until sufficient asphalt was present to pave the entire length of the one lane research section. This process required approximately nine trucks. The paving train consisted of the following: 1) the truck hauling the asphalt, 2) shuttle buggy (Road Tec 74-001 SB-25 00B), 3) paver (Cedaraphids CR 461R), 4) breakdown roller (Ingersol Rand DD-138 steel wheel roller), and 5) finish roller (Ingersol Rand DD-130 steel wheel roller). To avoid the sensors located in the outer wheel path, the tires of the shuttle buggy drove within a few centimeters of the outside of the asphalt patch containing the sensors, and the loaded trucks pulled around the buggy from behind, and subsequently backed up to it to unload. The paver was also shifted and straddled the asphalt patches so that the tracks narrowly missed the strain gages.

51

Table 3.5. As-built base course surveyed thicknesses.

	Section	Surveyed Thickness[1]	
		(mm)	(in)
10" Nominal Base Thickness	1B	280.42	11.04
	1A	283.46	11.16
	1	294.13	11.58
	2	222.50	8.76
	3	231.14	9.10
	4	242.57	9.55
	5	250.70	9.87
	6	232.66	9.16
Transition	7	-	-
6" Nominal Base Thickness	8	167.89	6.61
	9	167.89	6.61
	10	143.26	5.64
	11	162.56	6.40
	12	160.27	6.31
	13	165.10	6.50
	13A	161.54	6.36
	13B	170.69	6.72

1. Base course thicknesses come from page 5-6,
Table 5.1, in Warren and Howard (2007b).

The roller pattern used for the test sections consisted of an initial single static pass with the breakdown roller followed by three vibratory passes with the breakdown roller and finally two static passes with the finish roller (Howard 2006).

As-built asphalt thickness values were observed using surveying techniques, as well as by extracting cores between test sections. The thickness values obtained from the extracted cores can be found in Table 3.6. The core thickness values reported were the average of readings taken at quarter points with a digital caliper. The survey data was determined unreliable due to its variability, lack of agreement with the extracted asphalt cores, and lack of agreement with the design asphalt thickness of 2 inches (51 mm). For some reason, Sections 1B, 1A, 13A, and 13B

all had asphalt thicknesses less than 1.5 inches. No other sections had asphalt thicknesses less than 2 inches.

3.4 Instrumented Testing Results (Summary)

The Marked Tree testing site was constructed to assess field performance of a flexible pavement structure reinforced with geosynthetics through instrumented test sections. The goal was to test the pavement over a wide range of temperature and moisture conditions with an emphasis on performance during the weakest (higher moisture content) conditions (Howard 2006). However, due to unusually dry conditions during the months leading up to and during testing, the expected benefits of the geosynthetics for wet conditions were not observed, making a true assessment of their benefits based on measured responses inconclusive. A post construction study also observed that only 77% of the installed environmental sensors provided functional signals and only 82% of the structural sensors were functional (Warren and Howard 2007b). These survival rates were considered acceptable when considering the harsh construction and environmental conditions the instruments were subjected to. There were water content probes installed that were deemed unreliable and the thermocouples were very problematic. Due to unexpected weather, harsh conditions, and time constraints the instrumented sections were only observed for approximately 6 months.

The original testing of this site was intended to be under normal traffic conditions for a year, but the construction of a nursing home on the land adjacent to this site with a driveway intersecting Section 8 caused the research team to accelerate the data collection to ensure the results of the study were not compromised by irregular traffic patterns from the nursing home. AHTD kept the frontage road closed to traffic until the construction of the nursing home was complete to provide a controlled testing environment for the accelerated testing process. AHTD

Table 3.6. As-built asphalt core thicknesses.

	Section	Core Thickness[1]	
		(mm)	(in)
10" Nominal Base Thickness	1B	280.42	11.04
	1A	283.46	11.16
	1	294.13	11.58
	2	222.50	8.76
	3	231.14	9.10
	4	242.57	9.55
	5	250.70	9.87
	6	232.66	9.16
Transition	7	-	-
6" Nominal Base Thickness	8	167.89	6.61
	9	167.89	6.61
	10	143.26	5.64
	11	162.56	6.40
	12	160.27	6.31
	13	165.10	6.50
	13A	161.54	6.36
	13B	170.69	6.72

1. Asphalt thicknesses come from page 118,
Table 5.2, in Howard (2006).

provided a dump truck for trafficking the site continuously for four one-week test intervals between September 2005 and March 2006 (Warren and Howard 2007b). Due to the dry conditions, the subgrade remained near optimum conditions, therefore the geosynthetic strain gages were unable to measure meaningful data; however, the asphalt strain gages and earth pressure cells provided reasonable results from the dynamic loading.

It was concluded that data acquisition methodology was successfully applied in a full scale test, and independent test section triggering was shown to be plausible and efficient. However, due to the dry conditions and variability in construction, the desired assessments of test section performances were made inconclusive from a practical standpoint. There was agreement in the measured stress and strain responses in comparison to calculated values for the overall test section. Unfortunately, the data could not be utilized for section to section

54

comparisons (Howard 2006). The most significant conclusion drawn in Howard (2006) would seem to be that the geosynthetic contributions were not evident. However, this conclusion was based on limited testing data at a site with uncharacteristically dry conditions. Howard (2006) recommended that it would benefit researchers to continue monitoring the instrumented test site for several years to eliminate the variability of unusually dry and/or wet seasons and capture representative conditions before absolute conclusions could be drawn. The conclusions discussed, as well as many others, can be found in Howard (2006), Warren and Howard (2007a), and Warren and Howard (2007b).

Chapter 4

4.0 Project Continuation

4.1 Overview

After limited observations and inconclusive results, the original Marked Tree research project, AHTD TRC 0406, came to a halt in the Spring of 2006. In the Fall of 2007, Dr. John McCartney and Dr. Brady Cox proposed to continue studying the Marked Tree site. This proposal was accepted with the project number AHTD TRC 0903 and a start date of July 2008. Their initial plan was to continue collecting data from the original instrumentation under both normal traffic and accelerated loading, and to supplement this data with other non-destructive testing methods for two years. Unfortunately, when the new research team arrived at the site in July of 2008, virtually all of the instrumentation, with the exception of the asphalt strain gauges, was no longer functioning. The dead instrumentation led the research group to rely on results collected from numerous non-intrusive surficial load tests and observations from a more recent internal investigation of each section obtained through forensic excavation. Later in this chapter, a summary of the tests conducted at the site will be presented. These test methods and results will be discussed in greater detail in the following chapter (Chapter 5). This chapter will also discuss the pavement condition as defined by distress surveys conducted by AHTD in June of 2010 and April of 2011, as well as the estimated traffic loading this road has been subjected to since construction ended in 2005.

4.2 Introduction

Although many researchers indicate that geosynthetic reinforcement leads to improved pavement performance (refer to Chapter 2), a field or laboratory test has not been identified to

consistently quantify the contribution of the geosynthetic to the pavement's overall performance. Accordingly, there is little experimental evidence to guide the optimal location of the geosynthetic, selection of the best geosynthetic for use in different situations (i.e., environmental conditions, subgrade materials, etc.), and indication of what soil and geosynthetic properties best indicate an improvement in pavement performance. The Marked Tree, AR site for TRC 0406 is a very unique site due to variable geosynthetics and base course thicknesses resting on very poor quality subgrade material. Originally, the site was also instrumented with multiple sensors installed to measure deformation, moisture content, temperature, precipitation, and earth pressure (Figure 3.1, Chapter 3).

However, the site was only monitored for a short time without significant traffic or weather changes and limited conclusions were drawn from this full-scale test site with such unique conditions. The goal of TRC 0903 was to continue the instrumentation monitoring of the different test sections and to determine global stiffness and modulus values for each section as a whole, and within each layer of the sections, respectively. This site provides a unique opportunity to assess the mechanisms of geosynthetic reinforcements in flexible pavements and to determine the relative importance of separation, lateral restraint, drainage, and base course thickness on pavement performance.

4.3 Initial Objectives of TRC 0903

The overall objective of TRC 0903 was to investigate the mechanisms of geosynthetic reinforcements installed in flexible pavements for low volume roads and to evaluate different field tests to infer the contribution of geosynthetic reinforcement to overall pavement performance. Additional goals of this study included direct comparison of the performance of various geosynthetic types used for reinforcement at the Marked Tree site (seven different

57

products were used) and evaluation of the pavement geometry (two different base course thicknesses were used). The initial, specific objectives of this study were as follows:

Objective 1: Review and re-interpret available information regarding soil and geosynthetic properties, pavement geometry, instrumentation layouts, and performance data (i.e. deflection basins from FWD testing) from TRC 0406, and develop a framework for comparison of the initial pavement performance with the current and future pavement performance.

Objective 2: Evaluated the current performance of the pavement test sections at the Marked Tree site; including visual pavement inspection (survey, cracking, rutting profiles, etc.), instrumentation assessment (survivability and calibration of existing sensors), and data acquisition system evaluation. A secondary objective would be to collect soil samples for additional hydraulic and mechanical assessment in the laboratory to complement field studies.

Objective 3: Re-start long-term monitoring program of the pavement test sections using instrumentation originally installed at Marked Tree site in order to evaluate the performance of the sections under normal vehicle traffic and environmental changes. Incorporate additional capacitance sensors in the roadway shoulder to better capture patterns in moisture content fluctuations in the subgrade.

Objective 4: Perform field measurements (dynamic and static) to determine the "global" performance of reinforced and unreinforced pavement test sections. Determine the global moduli using additional surface sensors (geophones) and the stress distributions and strain magnitudes using existing embedded sensors (strain gauges and pressure cells) under static and dynamic loads from a vibroseis truck. Consider the impacts of different surface loads (magnitude and frequency) and weather conditions.

Objective 5: Perform field measurements (dynamic) to determine the "individual" pavement layer moduli (compression and shear) in the reinforced and unreinforced pavement sections using shallow seismic borehole tests (crosshole and downhole) in non-critical areas of the pavement. Use the information gained from such testing along with visual inspection of boring data to consider the impacts of lateral restraint, separation, water content, and drainage conditions on layer moduli.

Objective 6: Evaluate results from the long-term monitoring program, global and individual layer moduli measurements in the pavement test sections, and comparisons of the performance of different test sections to draw conclusions with respect to the mechanisms of geosynthetic reinforcement (lateral restraint, pumping and fine particle migration due to cyclic increases in pore water pressure, aggregate intrusion into the subgrade, and moduli changes due to moisture flow).

Objective 7: Use comparisons between unreinforced and reinforced pavement test sections to perform a life-cycle cost analysis and develop specifications for using different types of geosynthetic reinforcements and pavement geometries.

Unfortunately, the objectives of this project had to be significantly adjusted once it was discovered that nearly all of the instrumentation previously installed was dead on arrival to the site. This prevented the group from continuously studying the long-term and seasonal effects on the test sections through the abundance of instrumentation. However, there has been extensive surface and subsurface testing and data collection and reduction conducted on the reinforced and unreinforced flexible pavement test sections. The following section will include a summary of the testing history from the current day back to the early FWD testing conducted in 2005.

4.4 Testing History

Surficial deformation and subsurface strength/stiffness tests have been conducted on the Marked Tree site as far back as September of 2005 to as recently as May of 2011. A summary of the dates and types of tests conducted is presented in Table 4.1. It should be noted that on some of the dates for a few of the tests, only 8 sections were tested (1B, 1A, 1, 5, 9, 13, 13A, and 13B) out of 16 possible sections, represented by a "5" in Table 4.1. These 8 sections were chosen because the research group first wanted to concentrate on the following major reinforcement configurations for both the 10-in (25-cm) and 6-in (15-cm) proposed base course thicknesses: geotextile, geogrid, unreinforced, and geotextile/geogrid composite. The data collected for the tests only conducted on 8 sections was not included in the final evaluation of the pavement test section performance (refer to Chapter 5) because eventually all 16 test sections were evaluated on a regular basis.

Cells in Table 4.1 that are labeled with a "1" represent tests that were conducted on all 16 test sections with data collected and reduced to analyze and compare relative pavement section performance. Cells that are numbered "3" or "4" represent tests that did not produce interpretable data and therefore were not included in the final analysis and ranking. As shown in the table,

59

Spectral Analysis of Surface Wave (SASW) testing was conducted at the Marked Tree site on three dates, however, that data will not be presented in this study. Some of the SASW results are presented by McCartney et al. (2011). The tests displayed in Table 4.1 only include deflection and strength/stiffness tests conducted at the Marked Tree site.

The FWD testing conducted in 2005 and 2006 was analyzed in Howard (2006) using a simple global modulus equation, but for this analysis, the calculated results were discarded and the raw deflection data was re-analyzed using methods that will be discussed in Chapter 5. All of the types of tests presented in Table 4.1, excluding SASW, will be discussed in Chapter 5.

4.5 Pavement Condition

The Marked Tree test site was constructed on a very low volume frontage road (Frontage Road 3) that runs parallel to Arkansas Highway 63. It was finished in September of 2005. In July of 2008, the pavement appeared to be in fairly good condition, with cracking and rutting limited to small areas directly above sensor locations at the center of each test section. This deformation appeared to be the result of relatively poor compaction around sensors and cables, which resulted in pavement compression over time. However, the pavement began to deteriorate during the life of the project and some areas in the westbound lane had rutted and cracked to "failure" [defined as rutting over 0.5 inches(1.3 cm)] by the Spring of 2010. A couple of the test sections in the eastbound lane also showed significant distress at this time (Section 10 in particular, which had the thinnest surveyed base course, as reported in Section 3.3.3). The cracking present in the test sections in the eastbound lane was determined to primarily be the result of the roadway construction (longitudinal cracks at the centerline), temperature effects (transverse cracking), and deformation immediately around sensor locations at the center of each test section (some limited alligator cracking). However, the rutting was deemed a result of traffic loading on a pavement

60

Table 4.1. Summary of deflection and strength/stiffness tests conducted at Marked Tree site.

Test Type	Date							
	2005 - 2006	July 2008	Dec 2008	Jan 2009	May 2009	Dec 2009	Oct 2010	May 2011
FWD	1 & 2			1	1	1		1
SASW		5	5		5			
PLT		3	5		5	1		
ADD		3	4		5	1		1
DCP						1	1	
In-Situ CBR							1	
LWD							1	
Res Mod/UU							1	
RDD								1

1. Testing conducted in all sections.

2. Testing Conducted four different times on the following dates: 9-13-05, 9-29-05, 12-20-05, 2-16-06.

3. Tests conducted over sensor locations; poor data, could not be interpreted.

4. Irregular ground force, data could not be interpreted.

5. Only tested Sections 1b, 1a, 1, 5, 9, 13, 13a,13b

structure constructed on poor subgrade soils. Traffic counts have been conducted at the test site that allow for a calculated estimate of the loads that have been applied to this road since construction. Distress surveys were also conducted in June of 2010 and April of 2011 that allow for developing a quantitative performance assessment for each test section.

4.5.1 Traffic Loading

The Arkansas Highway and Transportation Department (AHTD) has provided the research team with traffic volume data from a somewhat continuous traffic count starting on January 4, 2011 and continuing through August 31, 2011, excluding April 1, 2011 through May 26, 2011. The traffic volumes collected from these counts were analyzed and Equivalent Single Axle Loads (ESALs) per year were calculated/estimated for eastbound (EB) and westbound (WB) traffic at two different counter locations (East Counter and West Counter). The calculated ESALs per year for each counter and direction are provided in Figure 4.1. The two traffic counter locations were chosen so that the differences in ESAL's between Sections 1B-8 and Sections 9-13B could be obtained, recalling that the driveway for the nursing home intersects the

test sections within Section 8. Interestingly, this location almost perfectly split the 10-in (25.4-cm) base course sections from the 6-in (15.2 cm) sections, with part of Section 8 being the only 6-in (15.2-cm) section more heavily trafficked than the rest. Note that Sections 1B-8 received more than twice as many ESAL's per year (approximately 6,600) as Sections 9-13B (approximately 3,200).

The traffic data from AHTD was broken down into ten vehicle classifications, ranging from motorcycles to six or more axle single trailers. There was some uncertainty associated with how the absolute number for each classification was obtained, but the total traffic volume was considered reliable. The initial task was to calculate the total volume at each counter location, excluding motorcycle traffic. Then, with the classification totals calculated at the East Counter for the westbound direction (i.e., all incoming traffic); a percent of contribution to the total volume was calculated for each of the remaining nine classifications. Once that was calculated, a truck factor for each vehicle classification was calculated.

The truck factor was calculated using Load Equivalency Factors (LEF) from Table 20.3 in Garber and Hoel (2001). Since actual loads were not known for each axle configuration on each vehicle, a range of 12,000 to 20,000 lbs was used for single axles and a range of 16,000 to 32, 000 lbs was used for tandem axles. With these load ranges, there was a high and low LEF for each vehicle classification that was considered a truck. The truck factors for each vehicle classification were calculated by adding up the product of the number of each axle type per vehicle with the LEF for that certain load and axle type. The vehicle classifications and truck factors for each vehicle classification are displayed in Table 4.2.
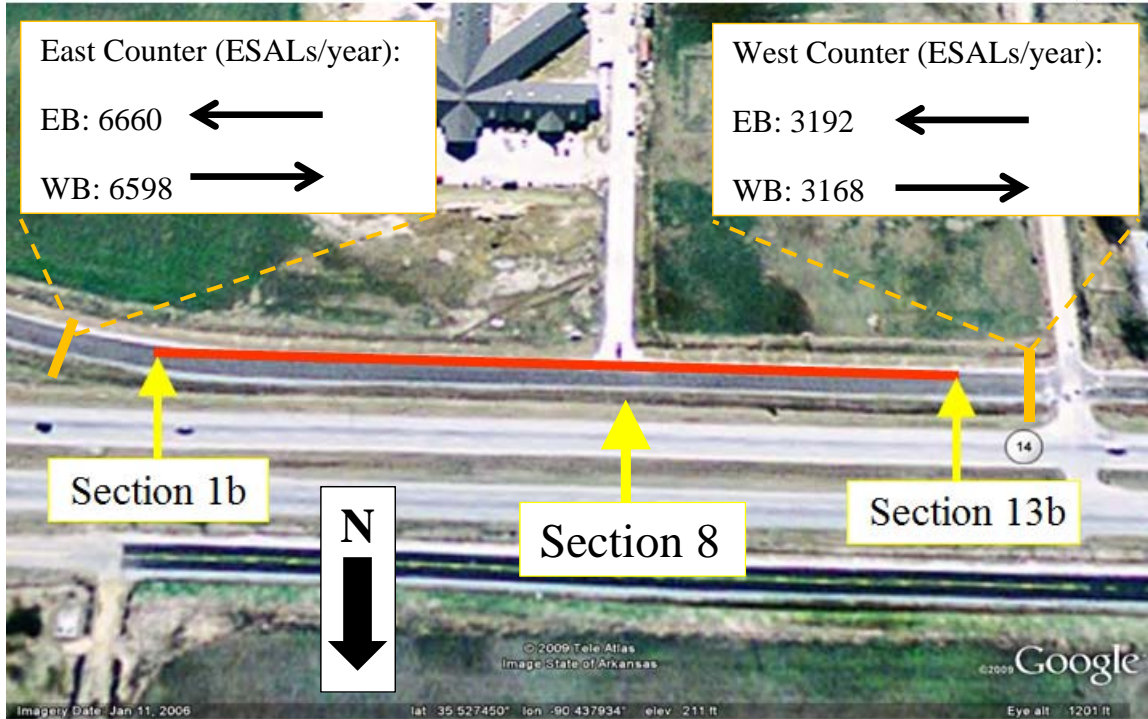
Figure 4.1. Estimated ESALs per year.

Once a truck factor was assigned to each vehicle for the high axle loads and the low axle loads, the respective truck factors were multiplied by the percent of contribution each classification had on the total volume calculation. The products were considered "weighted" truck factors that were then added together to create a "cumulative" truck factor for the high axle load condition and the low axle load condition. The cumulative truck factors were then multiplied by the total volumes at each counter (East and West) for each direction (EB and WB) to produce estimated ESAL values per year from the 159 day count. Since there was a high and low axle load condition, the high and low ESAL values were averaged for all four counting locations. These averages were finally factored to represent an estimated yearly ESAL value for each location, which are displayed in Figure 4.1. These ESAL values were deemed to be reasonably close to the design traffic loading values for this type roadway.

63

Table 4.2. Truck factors for each vehicle classification.

	Vehicle Classifications	Symbol	LEF	Tandem	LEF	Single	Truck Factor
1	Motorcycles	NEGLIGIBLE					0.000
2	Passenger Cars	P			0.00002	2	0.000
3	Two Axle, 4 Tire Single Units	SU			0.0877	2	0.175
4	Buses	S-BUS 36	0.121	1	0.189	1	0.310
5	Two Axle, 6 Tire Single Units	SU	0.047	1	0.189	1	0.236
5	Two Axle, 6 Tire Single Units	SU	0.857	1	1.51	1	2.367
6	Three Axle Single Units	SU	0.047	1	0.189	1	0.236
6	Three Axle Single Units	SU	0.857	1	1.51	1	2.367
7	Four or More Axle Single Units	SU	0.047	1	0.189	2	0.425
7	Four or More Axle Single Units	SU	0.857	1	1.51	2	3.877
8	Four or Less Axle Single Units	SU	0.047	1	0.189	2	0.425
8	Four or Less Axle Single Units	SU	0.857	1	1.51	2	3.877
9	Five Axle Single Trailers	WB-40	0.047	2	0.189	1	0.283
9	Five Axle Single Trailers	WB-40	0.857	2	1.51	1	3.224
10	Six or More Axle Single Trailers	WB-50	0.047	3	0.189	1	0.330
10	Six or More Axle Single Trailers	WB-50	0.857	3	1.51	1	4.081

Note: LEF values were found in Table 20.3 in Garber and Hoel (2001).

Truck Axle Load Range: Single Axle = 12,000 - 20,000 lbs

Tandem Axle = 16,000 - 32,000 lbs

4.5.2 Distress Survey

AHTD conducted distress surveys on every test section at the Marked Tree site in June of 2010 and April of 2011. These distress surveys allow the pavement condition/performance to be quantified. While rut depth in each wheel path, percent alligator cracking, and total longitudinal and transverse cracking were all recorded, the rut depths in each test section were deemed to be most related to pavement performance caused by traffic loading. As mentioned above, alligator cracking in the test sections in the eastbound lane was limited in every section except for Section 10 and was concentrated at the center of the section right above the sensor locations, and longitudinal and transverse cracking were deemed non-load based. Therefore, rutting in each section was determined to be the best indicator of relative pavement performance. Rutting was measured using a standard rut bar at three locations within every 50-ft (15.2-m) long test section in both the right and left wheel path in both the WB and EB lanes. Recall that only the EB lane

contained different types of geosynthetics, while the WB lane was reinforced with a single Carthage Mills FX-66 slit-film geotextile throughout (Section 3.3). Rut depths presented in Table 4.3 represent the average rut measurement within each 50-ft (15.2-m) long section of road. However, the test section rankings from 1-16 (1 being the best and 16 being the worst) are only based on the rutting in the eastbound lane because the westbound lane did not contain different geosynthetic types and limited tests were conducted in it. However, once failures were noticed in the westbound lane in the Spring of 2010, plans were made to test a couple of areas where failure was occurring. In October 2010, surficial tests and forensic excavation were conducted in the westbound lane across from sections 13 and 13B, referred to as 13W and 13BW herein. The rut depth values from the June 2010 and April 2011 distress surveys for the eastbound sections, as well as for 13W and 13BW, are displayed in Figures 4.2 and 4.3, respectively. Figures 4.2 and 4.3 also have a horizontal line across them denoting "failure" at 0.5 inches (1.3 cm) of rutting.

The average rut depths have been designated as the quantitative value of pavement performance that all other test results presented in subsequent chapters are compared to. However, the rutting data is not perfect and prior to discussing results a word of caution is exercised about trying to draw too much from this data. Rut depths were measured in approximately the same location for each survey date. However, the process of measuring rutting with a rut bar is not extremely precise and small differences in the location of the bar may certainly cause variations in the rut depths by +/- 1/8 of an inch or so (+/- 0.125 inches or +/- 3 mm). For example, in some sections (i.e., Section 3, 9, 10, 12, and 13A) the average rut depths from the June 2010 survey were slightly greater than the average rut depths from the April 2011 survey (refer to Table 4.3). These variations are generally minor and always within the tolerances noted above. So, it is not advisable, for example, to interpret the rutting data from April 2011

Table 4.3. Average rut depths calculated from distress surveys.

	Section	June 2010 WB	June 2010 EB	June 2010 EB Rank	April 2011 WB	April 2011 EB	April 2011 EB Rank
		WB	EB	EB Rank	WB	EB	EB Rank
10" Nominal Base Thickness	1B		0.17	1		0.31	9
	1A		0.23	7		0.25	6
	1		0.32	9		0.38	11
	2		0.22	6		0.29	7
	3		0.32	10		0.30	8
	4		0.20	3		0.23	3
	5		0.20	3		0.25	5
	6		0.19	2		0.19	1
Transition	7	-	-	-	-	-	-
6" Nominal Base Thickness	8		0.20	5		0.21	2
	9		0.25	8		0.24	4
	10		0.75	16		0.65	16
	11		0.44	14		0.47	14
	12		0.53	15		0.47	14
	13	0.91	0.43	13	1.01*	0.39	12
	13A		0.39	12		0.35	10
	13B	1.50	0.34	11	1.60*	0.41	13

* Denotes sections were patched, so conservatively added 0.1" to previous measurement.
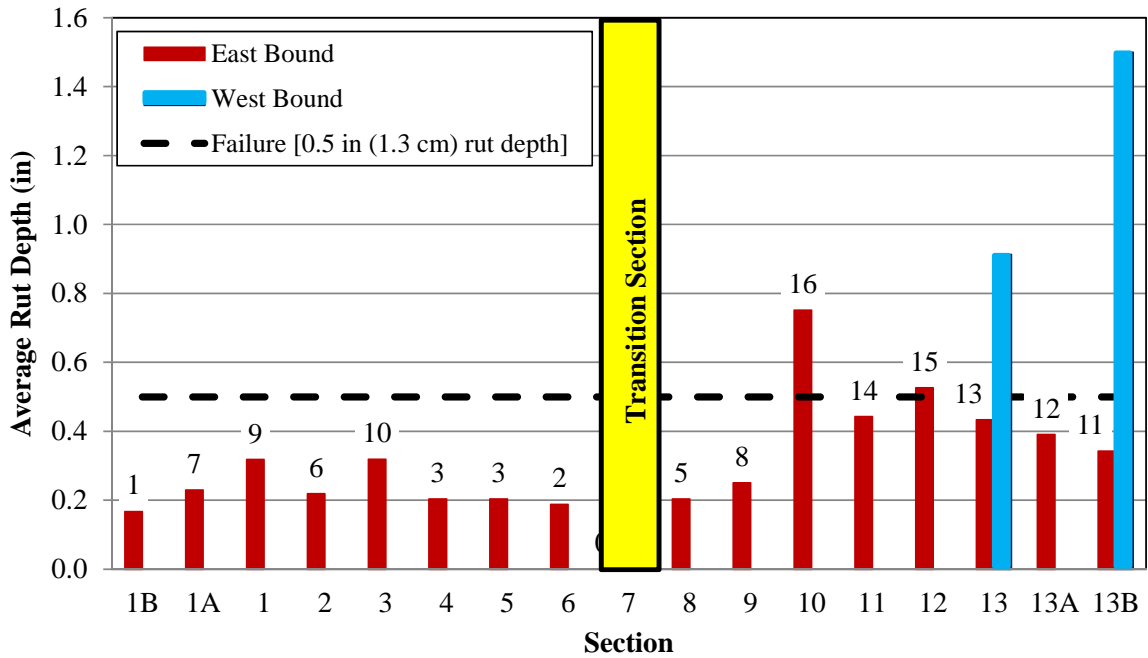
Figure 4.2. Average rut depths for measurements conducted in June of 2010.
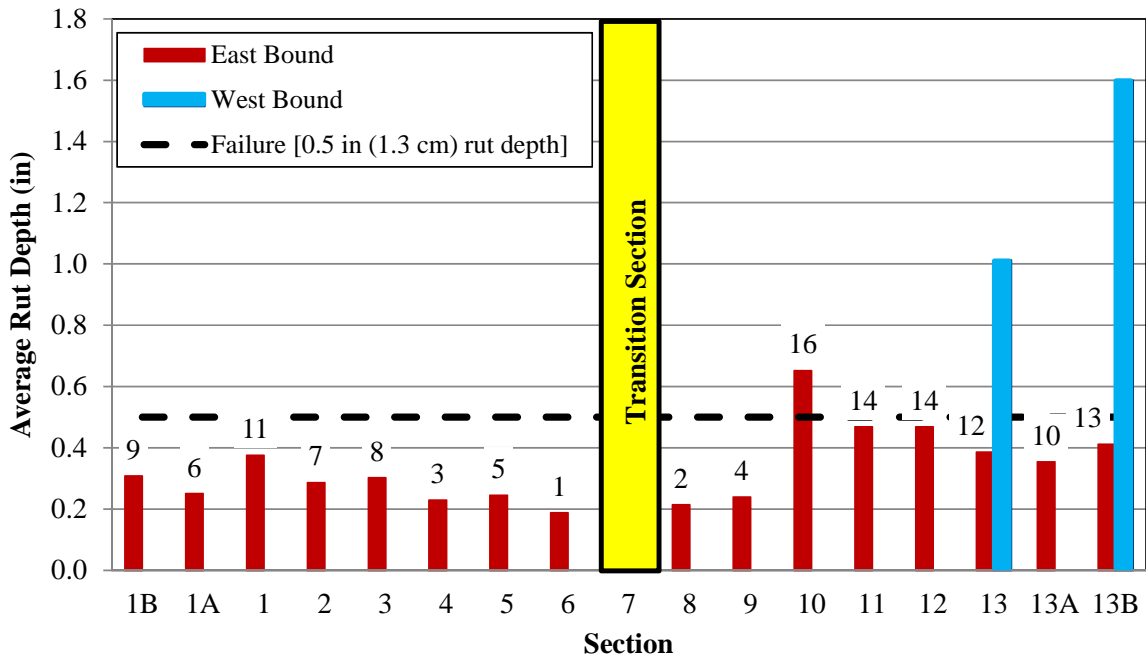
Figure 4.3. Average rut depths for measurements conducted in April of 2011.

(Table 4.3 and Figure 4.3) as proof that Section 6 (0.19 inches of rutting) is "better" than Section

8 (0.21 inches of rutting) or Section 5 (0.25 inches of rutting). The data isn't that precise.

General conclusions that can be drawn from this rut data include:

1) It seems there is a distinct difference in the rutting pattern in the eastbound lane that begins between Sections 9 and 10. While not completely perfect, most of the 10-inch (25-cm) nominal base course sections, and Sections 8 and 9 from the nominal 6-inch (15-cm) base course sections, appear to have less rutting than the remaining 6-inch (15-cm) nominal base course sections. *Remembering, that Sections 1B – 8 have received, on average, more than twice as many ESAL's as Sections 9 – 13B (refer to Figure 4.1).*

2) Based on the most-recent April 2011 data, Sections 10, 11, 12, 13W, and 13BW have clearly "failed" (i.e., approximately 0.5 inches or greater average rutting). All of these sections are in the 6-inch (15-cm) nominal base course sections and are reinforced with various types of geosynthetics at the subgrade-base course interface (refer to Figure 3.2)

3) The unreinforced section in the nominal 6-in (15-cm) base course zone (Section 13) has average rutting values that are less than 3-4 other eastbound reinforced test sections with the same nominal base course thickness and estimated ESAL's. Furthermore, it is directly adjacent to a portion of the westbound lane (Section 13W) that has failed that is reinforced with a slit-film geotextile.

4) The unreinforced section in the nominal 10-in (25-cm) base course zone (Section 1) has average rutting depths that are the worst (or close to the worst, depending on the date) among the eastbound test sections with the same nominal base course thickness and ESAL's.

5) The two sections that were reinforced with Tensar BX1200 geogrid (Sections 6 and 8) had the least amount of rutting in April 2011. However, the doubly-reinforced sections with Tensar geogrid and woven geotextile (Sections 5 and 12) had greater, yet still low, average rutting depths. This seems counter intuitive and, as mentioned above, the values are close enough to one another to be within the ability to measure accurately.

6) Section 8 has rutted less than any other nominal 6-in (15-cm) base section. This is interesting for at least three reasons: (a) Section 8 has received approximately twice as many ESAL's as the other 6-in sections; (b) The traffic flow in and out of the nursing home (refer to Figure 4.1) splits Section 8 in half, with much of the traffic crossing perpendicular across the middle of the section, and; (c) The nursing home driveway certainly helps to keep dynamic deflections and rutting lower than anticipated by buttressing Section 8. This buttressing effect is revealed in the deflection-based test results presented in Chapter 5.

7) The data does not appear to be of sufficient quality to draw conclusions about which specific types of geosynthetics outperform others within a given nominal base course thickness and similar ESAL's. Furthermore, no distinct pattern is discernible and it is highly likely that other factors (e.g., base or subgrade density, base or subgrade moisture content, base thickness, etc.) are influencing the varied pavement performance more than the specific type of geosynthetic.

The distress survey for Section 10 for each date is presented in Figures 4.4 and 4.5 as an example of where the rut depth and cracking data were derived from. These distress surveys also show the growth of the pavement cracking over time within Section 10 (the poorest performing test section). Note that the alligator cracking in the eastbound lane began at the center of the test section in the righthand (outside) wheel path where the instrumentation was installed during construction. It is possible that this distress allowed more water to infiltrate the pavement and further weaken the section over time.
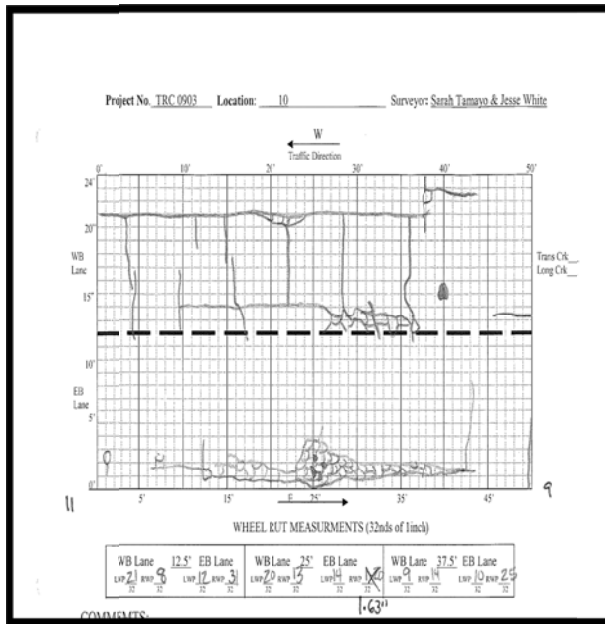
Figure 4.4. Section 10 June 2010 distress survey.
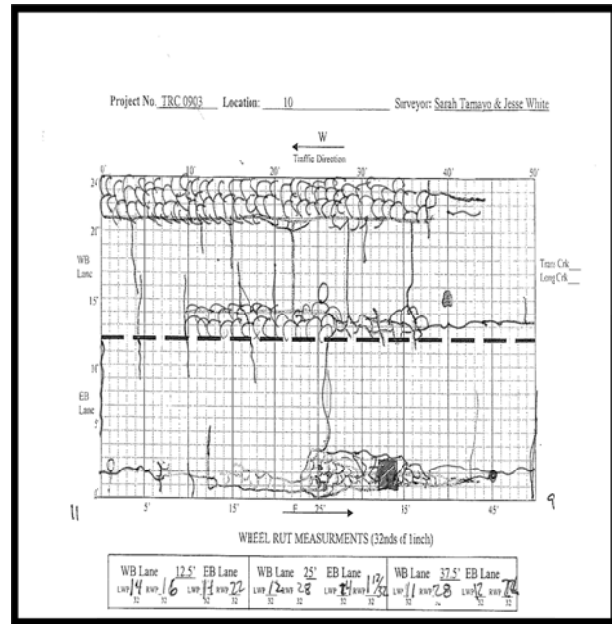
Figure 4.5. Section 10 April 2011 distress survey.

4.6 Conclusions

Since of September 2005, Sections 1B – 8 have been trafficked by approximately 39,600 ESALs (approximately 6,600 ESALs/year) while Sections 9-13B have been trafficked by approximately 19,200 ESALs (approximately 3,200 ESALs/year). As of April 2011, only five areas/sections of the pavement structure had "failed" [average rut depth over approximately 0.5 inches (1.3 cm)]. The five failed sections/areas were 6-in (15.2-cm,) nominal base sections (10, 11, 12, 13W, and 13BW). No failures had occurred in the 10-in (25.4-cm) nominal base sections. Generally, Sections 1B – 9 have rutted less than Sections 10 – 13B, while Sections 1B – 8 have received approximately twice as many ESALs as Sections 10 – 13B.

The data is not extensive enough to determine which types of geosynthetics outperform others within a given nominal base course thickness and similar ESALs. Furthermore, no distinct pattern is evident because there is high probability that other factors (i.e., layer densities,

moisture content, base thickness, etc.) are influencing the varied pavement performance more than the specific type of geosynthetic.

Chapter 5

5.0 Deflection-Based Tests to Infer Relative Performance

5.1 Overview

Pavement performance data (rutting) and loading (ESALs) were presented in Chapter 4 for the geosynthetic test sections at the Marked Tree site. It was noted that no clear pattern could be discerned within either nominal base course thickness regarding which type of reinforcement, or lack thereof, was "best". However, it was clear that certain 6-in (15-cm) nominal base course sections had "failed" (Sections 10, 11, 12, 13W, and 13BW) despite having less than half the estimated ESAL's of the 10-in (15.4-cm) nominal base course sections. Furthermore, it appeared that in general the rutting was less in Sections 1B – 9 than in Sections 10 – 13B, possibly as a result of weaker/different subsurface conditions.

This chapter presents results from the deflection-based testing methods introduced in Chapter 4, Table 4.1 (i.e., FWD, PLT, ADD, LWD, and RDD) as a means to determine if these tests could have predicted, or inferred, the observed pattern in rutting prior to "failure". In particular, these test results are investigated as a means to determine which test(s) and associated method(s) of data analysis might be most useful to infer relative pavement performance. In the following sections, the procedures used to conduct each test, the data analysis methodologies employed, and the test results are presented. While typical results are presented from tests conducted in each nominal base course thickness (i.e., 10-in (25-cm) thick and 6-in (15-cm) thick nominal base course), most of the testing results are presented in tables and then plotted as a function of section number (i.e., Section 1B – Section 13B) for relative comparison. Furthermore, the test results from each section are ranked 1 through 16, from "best" to "worst",

as a means to infer relative performance in a quantitative manner. Results from tests conducted on multiple dates are presented individually, and then the rankings are summed to create a composite ranking value that is compared to the average rut depth values presented in Table 4.4 (Figures 4.2 and 4.3). In the end, the rankings from all tests deemed to produce reliable results (i.e., those tests whose rankings from "best" to "worst" generally agreed with the pavement rutting performance) were used to create a total composite ranking (with each test receiving equal weight) so that the deflection-based test results could be summed up in a single ranking to quantify relative performance of the various geosynthetic-reinforced sections at the Marked Tree site and possibly reveal subtle differences that were not yet discernible in the rutting data.

5.2 Falling Weight Deflectometer (FWD)

The Falling Weight Deflectometer (FWD) test is a measure of vertical surface deflections caused by a falling weight impulse load on the pavement surface. Dynamic deflections from this impulse load are measured with an array of transducers (geophones) that are spaced radially away from the loading footprint. The data can be used in inferring the performance of the global pavement structure or individual pavement layers (ASTM D4964-09). It is typical to see the data used to calculate a global modulus of the pavement structure or moduli of each layer of the structure.

Arkansas Highway and Transportation Department (AHTD) assisted the research group by conducting FWD tests on many dates and supplying UA personnel with the raw deflection data for analysis. From September of 2005 through May of 2011 AHTD conducted FWD tests at the Marked Tree site on eight dates. Four of those test dates occurred early in the life of the pavement in later 2005 and early 2006 as part of the original Marked Tree project (AHTD TRC – 0406; refer to Chapter 3).

5.2.1 FWD Testing Procedure

The FWD tests were conducted in the same general location within each test section on all eight testing dates. A photograph of the FWD used at the Marked Tree site is provided in Figure 5.1. The drop locations are presented in Figure 5.2. The dates that FWD tests were performed can be found in Table 4.1. The FWD tests conducted between September 2005 and May 2009 were generally conducted using two drops at each location with an approximate force of 9,000 lbs (40 kN) each. However, on December 2009 and May 2011, the FWD tests were performed using only one drop at each location with an approximate force of 10,000 lbs (44.5 kN).

The sensor array consisted of nine transducers at the following distances from the drop location in inches (cm): 0 (0.0), 8 (20.3), 12 (30.5), 18 (45.7), 24 (61.0), 36 (91.4), 48 (121.9), 60 (152.4), and 72 (182.9). The loading surface, or load footprint, was approximately 100 in^2 (645.2 cm^2), resulting in pressures of approximately 90 psi (620 kPa) and 100 psi (689 kPa) for the 9,000 lb (40 kN) and 10,000 lb (44 kN) loads, respectively.

5.2.2 FWD Data Analysis

The data collected from each drop of the FWD assists in the creation of a deflection basin for each section by using the deflections recorded at each geophone. These deflection basins have been compiled for each test section on all the dates the FWD test has been conducted. For the dates that had multiple drops at each location, September 2005 through May 2009, the results were averaged to develop one deflection basin per section on each date. Figure 5.3 is an example of typical deflection basins for both a 10-in (25.4-cm) and a 6-in (15.2-cm) nominal base course thickness. Note the deflection basin in the section with a 10-in (25.4-cm) nominal base thickness is substantially shallower than that of the section with a 6-in (15.2-cm) nominal base thickness.
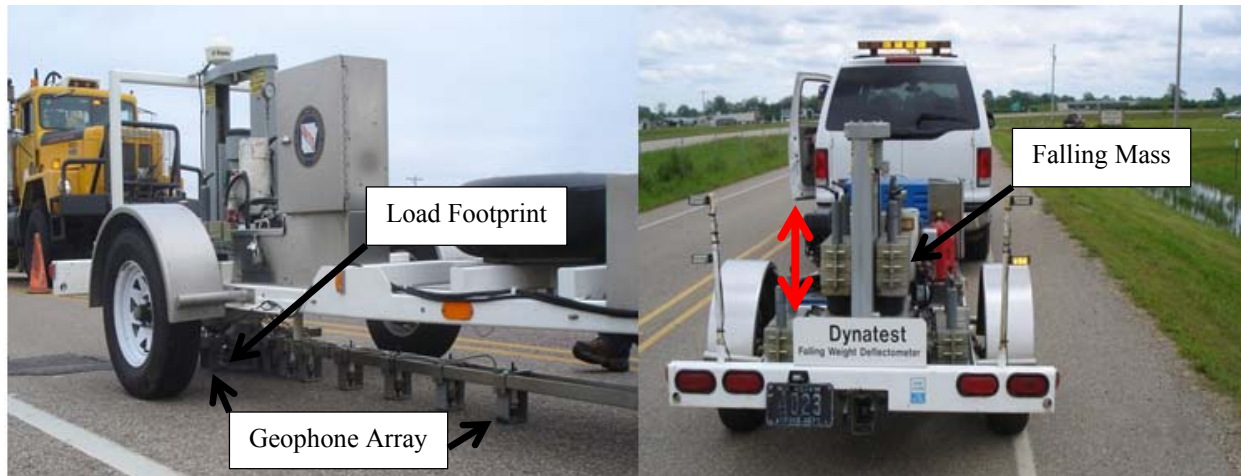
Figure 5.1. Side and rear view of AHTD's FWD at Marked Tree site.
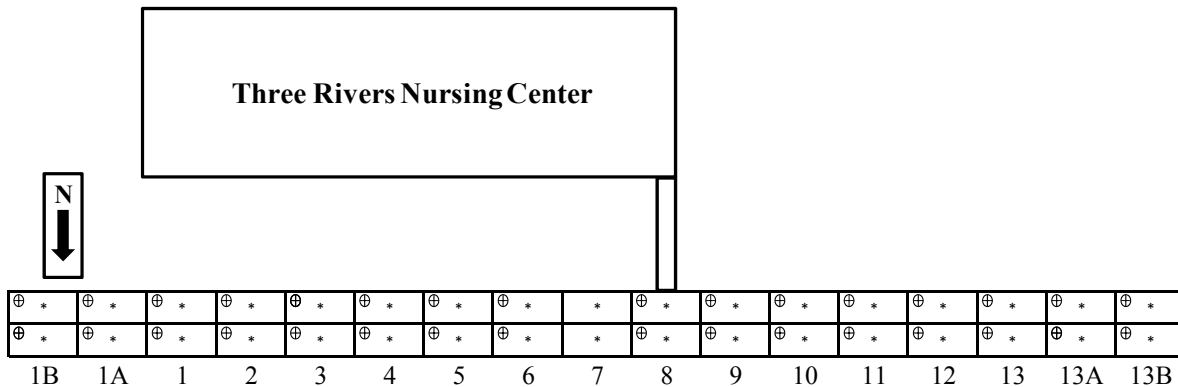
⊕ Denotes FWD drop locations 15-ft (4.6-m) east of the center of each section.

Figure 5.2. FWD testing locations at the Marked Tree site.

The deflection results from each FWD test were used in the calculations for two values used to infer the performance of each section on all dates. The two values are referred to as the total deflected area (Area) of the deflection basin in units of in^2 and the AREA$_{12}$ value of the deflection basin (dimensionless). To calculate the total deflected area, the trapezoidal rule was employed, using Equation 5.1 as follows:
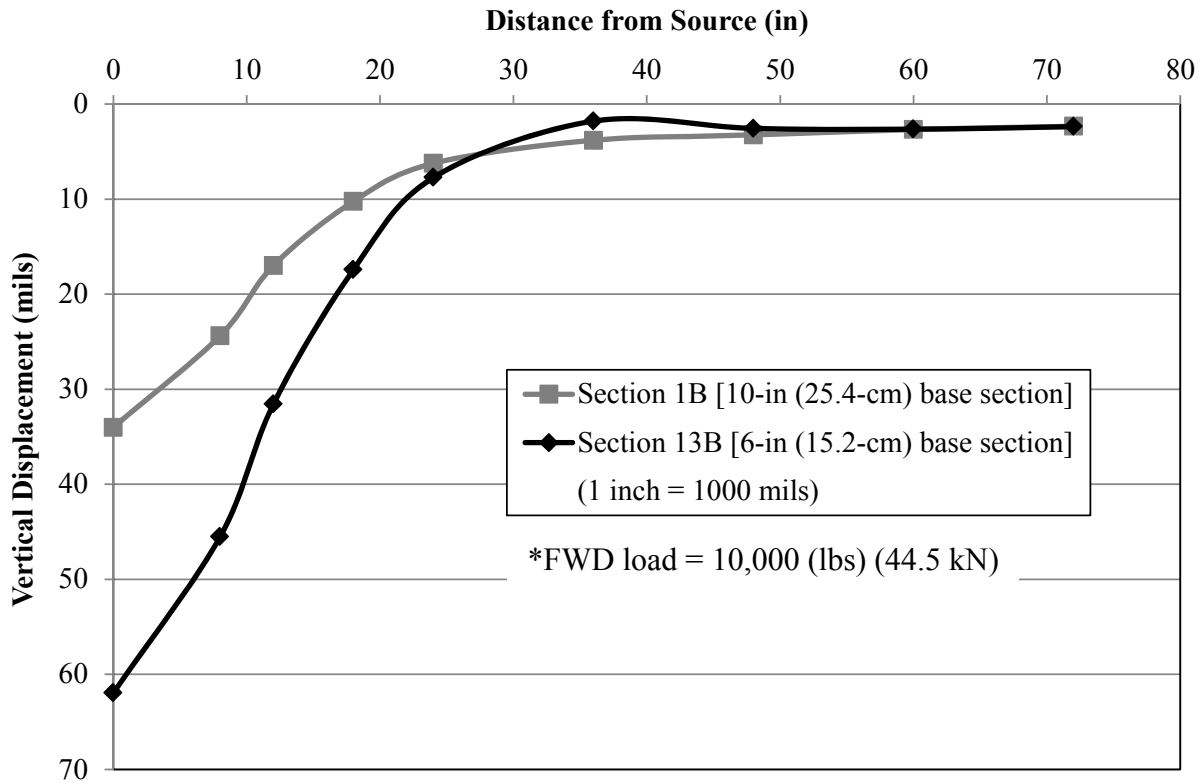
Figure 5.3. Typical FWD deflection basins for Sections 1B and 13B from the May 2011 Marked Tree site visit.

$$Area = [(\frac{d_0+d_8}{2}) * (x_8 - x_0)] + \cdots [(\frac{d_{60}+d_{72}}{2}) * (x_{72} - x_{60})] \qquad (5.1)$$

Where: Area = total deflected area, in^2

d_0, d_8,…d_{72} = peak vertical deflection measured at a distance specified by the subscript, in

x_0, x_8,…x_{72} = distance from the load source as specified by the subscript, in

The AREA$_{12}$ value calculated using the FWD results is a deflection basin curvature index for flexible pavements that represents the deflection basin from the geophone 0 in (0.0 cm) away from the source up to the geophone 12 in (30.5 cm) away from the source. AREA$_{12}$ is a dimensionless value and is not the actual deflected area up to the 12 in (30.5 cm) geophone, but rather a relative indicator of pavement stiffness. An AREA$_{12}$ value of 12 represents an infinitely

stiff upper layer with identical deflections at all three sensors, while an $AREA_{12}$ calculation of

6.91 represents uniform layer moduli of elasticity (FHWA 2006). The equation used for

calculating $AREA_{12}$ was obtained from FHWA (2006):

$$AREA_{12} = 2 * [2 + 3\left(\frac{d_8}{d_0}\right) + \left(\frac{d_{12}}{d_0}\right)]$$ (5.2)

Where: $AREA_{12}$ = curvature index of the first 12 inches (30.5 cm) of the deflection basin

d_0 = vertical deflection at 0 inches from the source, in

d_8 = vertical deflection at 8 inches from the source, in

d_{12} = vertical deflection at 12 inches from the source, in

Note that the FWD data was used exclusively to obtain these two single-valued estimates

of pavement deflection (i.e., total deflected area and AREA12) as a means to quantify relative

pavement performance. The FWD deflection basins were also processed in various other ways to

estimate global and individual layer moduli. However, it was determined that the raw deflection

values provided the most direct path for comparing one section to another for any given testing

date. It will also be noted that on any given testing date the pavement temperature did not vary

significantly over the couple of hours required to complete testing, as verified through

temperature readings.

5.2.3 FWD Results

The total deflected area (Area) and $AREA_{12}$ were calculated for each test section on each

date the FWD testing was performed. When ranking the total deflected area values, the lowest

Area value receives the best ranking and the highest Area receives the worst ranking. When

ranking the $AREA_{12}$ values, the highest value receives the best ranking, while the lowest value

receives the worst ranking.

The total deflected Area and $AREA_{12}$ results with associated rankings for each testing date are tabulated in Tables 5.1 through 5.8. It is seen that in the majority of the sections, the relative rankings for either analysis method are not exactly the same from one test date to the next. For example, Section 1A ranked 1 out of 16 in terms of total deflected Area on September 13, 2005 (Table 5.1). However, this section ranked 6 out of 16 in terms of total deflected Area on September 29, 2005 (Table 5.2). On the other hand, Section 1B consistently ranked 5 out of 16 in terms of total deflected area on both of these dates. Furthermore, the absolute deflected areas can vary widely from test date to test date based on seasonal variations in temperature and moisture content of the pavement. As a means to synthesize the FWD deflection results from all test dates into a quantitative relative comparison between sections, the rankings from each test date were summed, providing a composite ranking value on which to base a new, overall ranking of the sections. The summed composite ranking values from the eight FWD test dates and the overall section rankings are presented in Table 5.9 and plotted in Figures 5.4 and 5.5 for total deflected Area and $AREA_{12}$, respectively.

The composite total deflected area FWD rankings (Figure 5.4) do not correlate well with the general trends in the average rut depths (i.e., rutting generally lower and similar in Sections 1B – 9) presented in Figures 4.2 and 4.3. However, Section 10 has the worst ranking (16) for both total deflected Area and rutting, and Section 11 and 12 both have poor rankings for both. While one might expect the total deflected Areas in the 10-in (25.4-cm) nominal base sections to consistently rank lower (i.e., less deflection) than the 6-in (15.2-cm) nominal base sections, this trend was not perfectly observed, with three of the 6-in sections (including the null/unreinforced section – Section 13) ranking better than some of the 10-in sections. A much clearer distinction between the 10-in and 6-in (25.4-cm and 15.2-cm) sections was observed from the exact same

77

Table 5.1. FWD deflection basin area results from September 13, 2005 at the Marked Tree site.

	Section	Area (in^2)	Rank	AREA$_{12}$	Rank
	1B	0.56	5	9.04	10
	1A	0.45	1	8.77	14
10"	1	0.64	9	9.26	3
Nominal	2	0.68	11	9.10	6
Base	3	0.71	14	9.31	2
Thickness	4	0.74	15	9.08	7
	5	0.64	8	9.31	1
	6	0.53	3	9.07	9
Transition	7	-	-	-	-
	8	0.54	4	8.74	15
	9	0.62	7	9.11	5
6"	10	0.83	16	8.16	16
Nominal	11	0.69	12	9.07	8
Base	12	0.65	10	9.25	4
Thickness	13	0.48	2	8.96	13
	13A	0.57	6	8.96	12
	13B	0.70	13	9.03	11

Table 5.2. FWD deflection basin area results from September 29, 2005 at the Marked Tree site.

	Section	Area (in^2)	Rank	AREA$_{12}$	Rank
	1B	0.58	5	9.23	9
	1A	0.58	6	9.15	11
10"	1	0.73	11	9.42	2
Nominal	2	0.65	8	9.49	1
Base	3	0.72	10	9.42	2
Thickness	4	0.75	13	9.34	5
	5	0.54	2	9.28	7
	6	0.54	2	9.28	7
Transition	7	-	-	-	-
	8	0.59	7	8.89	14
	9	0.70	9	8.93	13
6"	10	1.03	16	7.84	16
Nominal	11	0.81	14	9.38	4
Base	12	0.88	15	9.33	6
Thickness	13	0.49	1	8.80	15
	13A	0.56	4	9.01	12
	13B	0.73	12	9.20	10

Table 5.3. FWD deflection basin area results from December 20, 2005 at the Marked Tree site.

	Section	Area (in^2)	Rank	$AREA_{12}$	Rank
	1B	0.60	10	9.29	13
	1A	0.46	2	9.39	10
10"	1	0.54	6	9.62	4
Nominal	2	0.55	7	9.51	7
Base	3	0.56	8	9.64	3
Thickness	4	0.60	10	9.66	2
	5	0.63	13	9.87	1
	6	0.52	5	9.60	5
Transition	7	-	-	-	-
	8	0.50	4	9.01	15
	9	0.56	8	9.32	12
6"	10	0.63	13	8.78	16
Nominal	11	0.65	15	9.54	6
Base	12	0.73	16	9.32	11
Thickness	13	0.45	1	9.48	8
	13A	0.46	3	9.48	9
	13B	0.62	12	9.10	14

Table 5.4. FWD deflection basin area results from February 16, 2006 at the Marked Tree site.

	Section	Area (in^2)	Rank	$AREA_{12}$	Rank
	1B	0.62	10	9.40	10
	1A	0.47	1	9.44	9
10"	1	0.54	5	9.54	7
Nominal	2	0.60	9	9.55	5
Base	3	0.58	8	9.64	2
Thickness	4	0.66	12	9.61	3
	5	0.68	13	9.90	1
	6	0.54	6	9.52	8
Transition	7	-	-	-	-
	8	0.53	4	9.18	15
	9	0.56	7	9.36	13
6"	10	0.80	16	8.51	16
Nominal	11	0.62	11	9.39	11
Base	12	0.73	15	9.34	14
Thickness	13	0.52	2	9.55	6
	13A	0.53	3	9.36	12
	13B	0.72	14	9.59	4

Table 5.5. FWD deflection basin area results from January 21, 2009 at the Marked Tree site.

	Section	Area (in^2)	Rank	AREA$_{12}$	Rank
	1B	0.50	6	8.93	10
	1A	0.46	1	9.12	5
10"	1	0.46	2	9.06	6
Nominal	2	0.49	3	9.13	4
Base	3	0.51	8	9.21	2
Thickness	4	0.57	11	8.98	9
	5	0.56	10	9.27	1
	6	0.51	7	9.19	3
Transition	7	-	-	-	-
	8	0.56	9	8.51	15
	9	0.58	13	8.92	11
6"	10	0.69	16	8.39	16
Nominal	11	0.58	12	8.55	14
Base	12	0.64	15	8.67	13
Thickness	13	0.50	5	8.91	12
	13A	0.50	4	9.02	8
	13B	0.60	14	9.03	7

Table 5.6. FWD deflection basin area results from May 11, 2009 at the Marked Tree site.

	Section	Area (in^2)	Rank	AREA$_{12}$	Rank
	1B	0.49	3	9.12	9
	1B	0.45	1	9.29	6
10"	1	0.49	2	9.22	7
Nominal	2	0.54	6	9.41	3
Base	3	0.53	4	9.49	2
Thickness	4	0.66	15	9.40	4
	5	0.61	10	9.49	1
	6	0.57	8	9.36	5
Transition	7	-	-	-	-
	8	0.54	5	8.61	16
	9	0.61	11	9.06	10
6"	10	0.65	14	8.80	15
Nominal	11	0.63	12	9.04	11
Base	12	0.63	13	8.98	13
Thickness	13	0.56	7	8.91	14
	13A	0.59	9	8.99	12
	13B	0.69	16	9.15	8

Table 5.7. FWD deflection basin area results from December 15, 2009 at the Marked Tree site.

	Section	Area (in^2)	Rank	AREA$_{12}$	Rank
10" Nominal Base Thickness	1B	0.63	5	9.53	6
	1A	0.54	1	9.43	9
	1	0.58	2	9.46	8
	2	0.62	4	9.67	4
	3	0.65	6	9.68	3
	4	0.75	11	9.74	2
	5	0.68	8	10.02	1
	6	0.61	3	9.64	5
Transition	7	-	-	-	-
6" Nominal Base Thickness	8	0.70	9	9.37	11
	9	0.78	13	9.21	14
	10	0.87	16	9.13	15
	11	0.80	14	9.12	16
	12	0.76	12	9.28	13
	13	0.71	10	9.40	10
	13A	0.67	7	9.51	7
	13B	0.81	15	9.33	12

Table 5.8. FWD deflection basin area results from May 24, 2011 at the Marked Tree site.

	Section	Area (in^2)	Rank	AREA$_{12}$	Rank
10" Nominal Base Thickness	1B	0.60	1	9.30	13
	1A	0.64	2	9.47	8
	1	0.70	6	9.61	5
	2	0.80	10	9.67	3
	3	0.78	8	9.51	7
	4	0.66	3	9.79	1
	5	0.78	8	9.74	2
	6	0.66	3	9.61	4
Transition	7	-	-	-	-
6" Nominal Base Thickness	8	0.69	5	9.27	15
	9	0.85	12	9.37	11
	10	1.05	16	9.55	6
	11	0.81	11	9.29	14
	12	0.90	14	8.95	16
	13	0.76	7	9.32	12
	13A	0.85	13	9.41	10
	13B	0.95	15	9.43	9

Table 5.9. Composite deflection basin area rankings from all eight FWD testing dates at the Marked Tree site.

	Section	Area Composite Rank	Rank	AREA$_{12}$ Composite Rank	Rank
10" Nominal Base Thickness	1B	45	5	80	9
	1A	15	1	72	7
	1	43	4	42	5
	2	58	8	33	3
	3	66	9	23	2
	4	90	12	33	3
	5	72	10	15	1
	6	37	3	46	6
Transition	7	-	-	-	-
6" Nominal Base Thickness	8	47	6	116	15
	9	80	11	89	12
	10	123	16	116	15
	11	101	13	84	11
	12	110	14	90	13
	13	35	2	90	13
	13A	49	7	82	10
	13B	111	15	75	8

The composite rankings were calculated by summing the total deflected area
and the AREA12 values from each test date and ranking the sums accordingly.
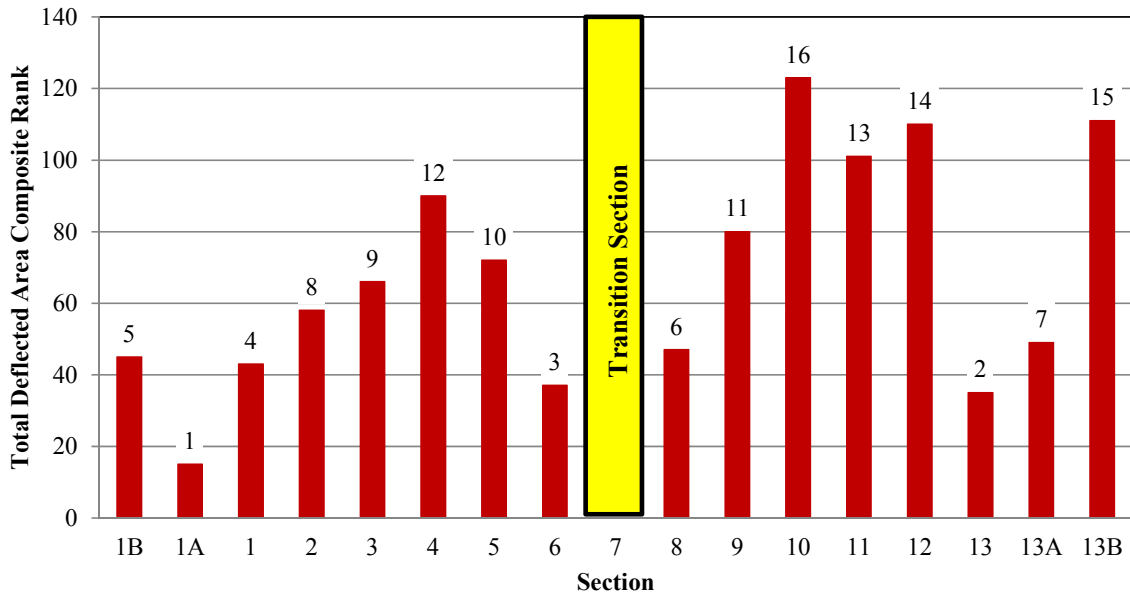
Figure 5.4. Total deflected area composite rankings from eight FWD tests conducted at the Marked Tree site.
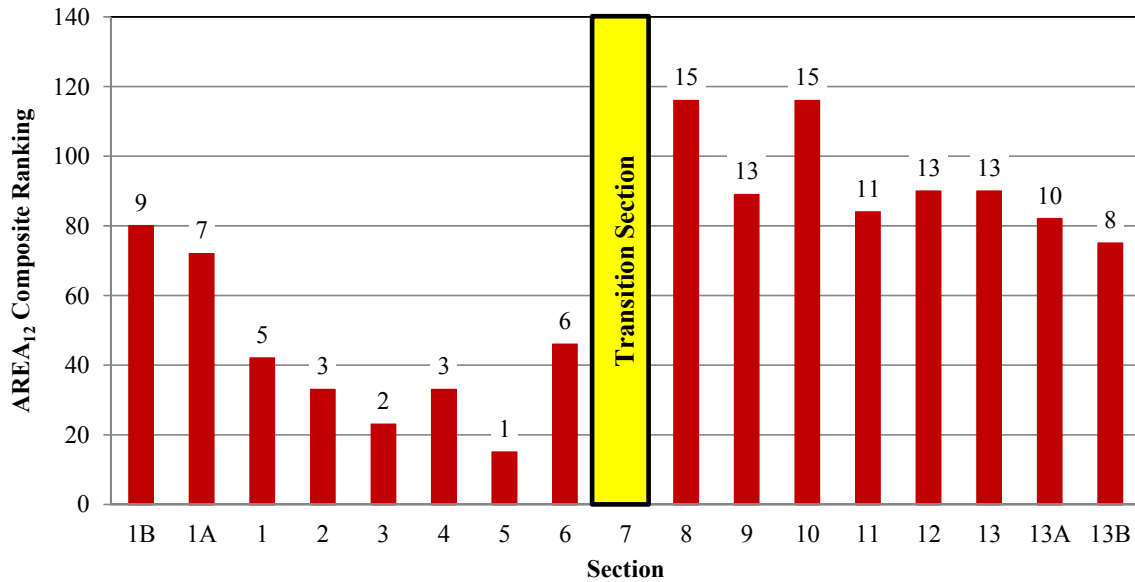
Figure 5.5. $AREA_{12}$ composite rankings from eight FWD tests conducted at the Marked Tree site.

deflection basins based on the composite $AREA_{12}$ rankings (Figure 5.5). With the exception of only one 6-in (15.2-cm) section (Section 13B), the 10-in (25.4-cm) nominal base sections are all ranked more favorably than the 6-in (15.2-cm) nominal base sections. The composite $AREA_{12}$ values also indicate that Section 10 is the worst performing section (tied for rank 15), as indicated by the average rut depth rankings (Figure 4.6). However, Section 8 also ranks 15 in the average $AREA_{12}$ evaluation, yet ranks 2 in the average rut depth measurements. Clearly the correlations between FWD deflection basins and rutting are not perfect.

5.3 Plate Load Test (PLT)

Plate load tests (PLTs) are static loading tests conducted in the field for evaluation and design of pavement structures (ASTM D1195-09). The pavement structure is subjected to relatively slow repetitive loading cycles while measuring the surface deflections that occur during the loading and unloading processes. The load is typically applied to a 12-in (30.5 cm) square steel plate (Coduto 2001) that transfers the point load into a distributed pressure applied

to the pavement structure. A global stiffness value in psi/in (kPa/mm) for the pavement structure is obtained by observing the amount of pavement deformation with respect to the stress being applied. The depth of influence of the plate load is assumed to be approximately twice the plate width/diameter (Coduto 2001).

The research group from the University of Arkansas conducted plate load tests at the Marked Tree site on four dates (refer to Table 4.1); however, only the data obtained from the December 2009 site visit is included herein because this was the only date when plate load tests were conducted in all sections.

5.3.1 PLT Testing Procedure

The plate load tests at the Marked Tree site were conducted on the asphalt surface 15 feet (4.6 m) east of the sensor locations in each section. The pressures were applied to the pavement through a 12-in (30.5-cm) diameter steel plate loaded by applying resistance through a bottle jack from the back-end of the University of Arkansas's vibroseis truck (Figure 5.6). The loads applied to the plate ranged from approximately 0 - 9,500 lbs (0 – 42.3 kN) and were measured by recording the response of a load cell mounted directly on top of the loading plate. The loads resulted in applied pressures that ranged from approximately 0 - 84 psi (0 – 579 kPa). The surface deflections of the pavement structure were monitored with two linear variable differential transformers (LVDTs) on diametrically opposite sides of the loading plate. The testing configuration is shown in Figure 5.7.

The loading cycle was applied to the flexible pavement at least four times. During the loading and unloading process, the LVDTs continuously measured the response of the pavement structure. The initial loading cycle was considered as a seating load, and the results from that

84

Figure 5.6. University of Arkansas vibroseis truck.

cycle were not used in any of the stiffness calculations. The results from the three subsequent

load cycles were used to develop the global stiffness values of each section.

5.3.2 PLT Data Analysis

The asphalt provides a visco-elastic response to the results of a PLT, so several cycles of

loading and unloading were applied in an attempt to characterize this response. The continuous

deflection and rebound measurements recorded from the two LVDTs during the cyclic loading

and unloading during the PLTs shown in Figures 5.8 and 5.9 were averaged to estimate a mean

deflection value at the center of the loading plate. This average approximately accounted for

limited differential settlement of the loading plate. The mean deflection values were plotted
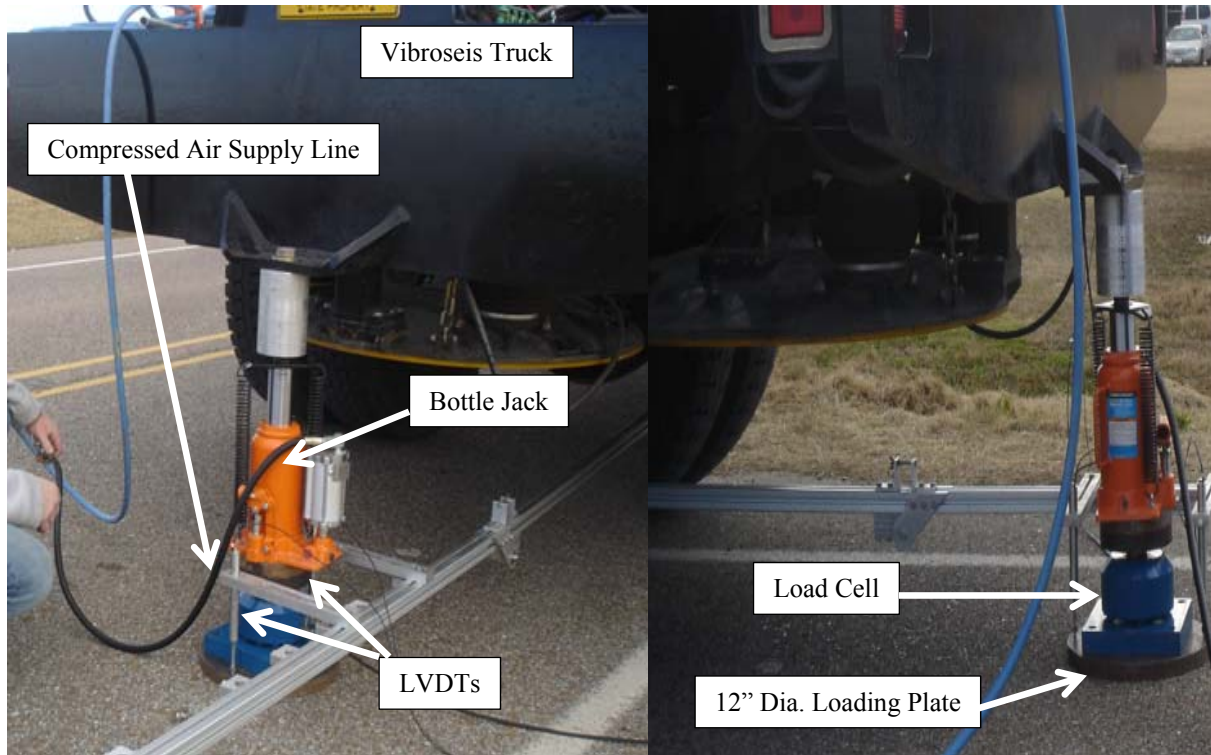
Figure 5.7. Rear and side view, respectively, of the PLT testing configuration at the Marked Tree site.

against the stresses that were applied. Typical response curves for both a 10-in (25.4-cm) and 6-in (15.2-cm) nominal base course section are provided in Figures 5.8 and 5.9, respectively. It is noticed from the typical curves that the 10-in (25.4-cm) base sections generally had significantly steeper slopes than the 6-in (15.2-cm) base sections.

The global stiffness values were calculated by averaging the three slopes of the loading portion of the response curves from approximately 30 psi to 70 psi (206 – 482 kPa). The slopes over this pressure range were generally very linear, and these magnitudes of contact pressure are typical for many vehicle tires.
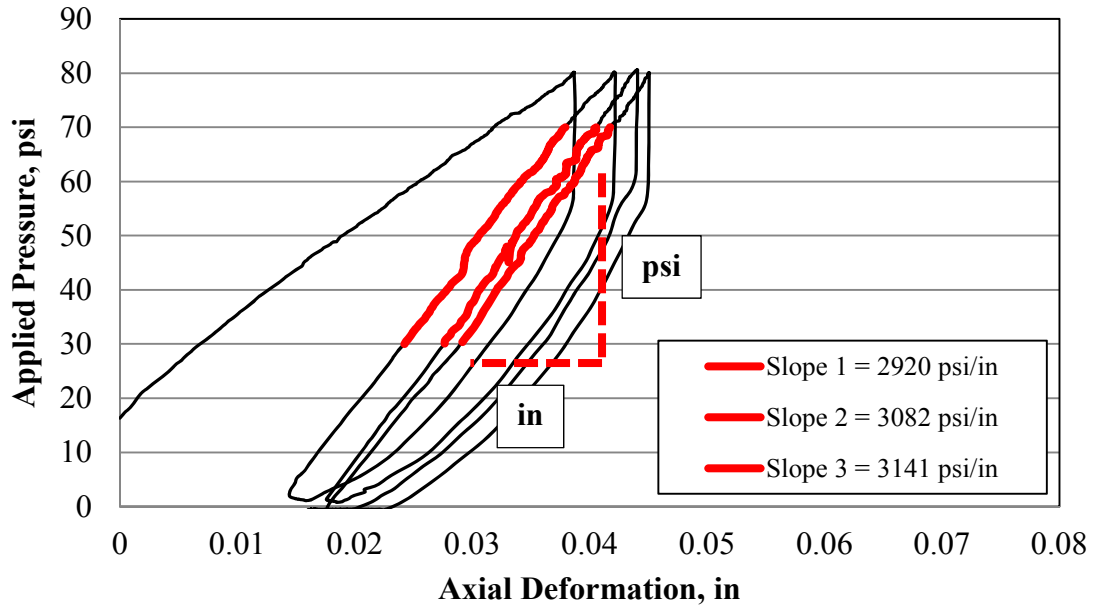
Figure 5.8. Typical PLT response curve for a 10-in (25.4 cm) base section (Section 6).
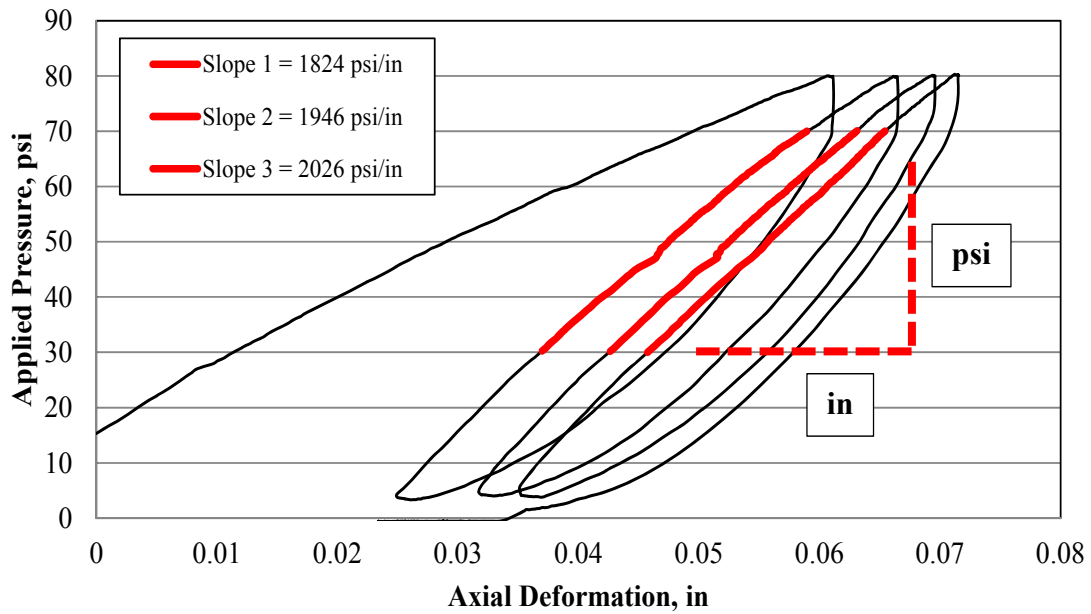
Figure 5.9. Typical PLT response curve for a 6-in (15.2 cm) base section (Section 13B).

87

5.3.3 PLT Results

The PLT global stiffness results from December 2009 were ranked by applying the best rank (1) to the highest stiffness value and the lowest rank (16) to the lowest stiffness value. The stiffness values and rank for each section are provided in Table 5.10 and plotted in Figure 5.10. These stiffness values represent the average amount of pressure (psi) necessary to achieve one inch of surface deflection. The results presented in Figure 5.10 indicate that Section 1, the unreinforced 10-in (25.4-cm) base section, is globally the stiffest pavement section. This result is likely directly correlated to the fact that Section 1 has the greatest combined thickness of asphalt and base course (refer to Chapter 6, Figure 6.13). As with the FWD results and the rut depth measurements, Section 10 has the lowest PLT stiffness ranking. With only one exception, the PLT results from the 10-in (25.4-cm) base sections are greater than the 6-in (15.2-cm) base sections. This is expected since the zone of influence from the loading plate is expected to include more subgrade soil in the thinner base course sections. Furthermore, the PLT results clearly show the general trend observed in the rutting data (i.e., Sections 1B – 9 generally have less deflection than Sections 10 – 13B), and also indicate that the "failed" sections (Sections 10, 11 and 12) have the lowest global stiffness values (note that Sections 13W and 13BW were not tested with the PLT in December 2009). The PLT stiffness values seem to be a better, though not perfect, indicator of pavement performance than the FWD.

Table 5.10. Average stiffness values calculated from PLT tests conducted at Marked Tree site in December 2009.

	Section	Average Stiffness (psi/in)	Standard Deviation (psi/in)	Rank
	1B	4040	376	3
	1A	4138	403	2
10"	1	5467	293	1
Nominal	2	3119	276	6
Base	3	3226	102	4
Thickness	4	2450	113	9
	5	2751	140	8
	6	3048	114	7
Transition	7	-	-	-
	8	3128	211	5
	9	2400	250	10
6"	10	1548	71	16
Nominal	11	1641	66	15
Base	12	1914	58	14
Thickness	13	2056	97	11
	13A	1920	98	13
	13B	1932	102	12
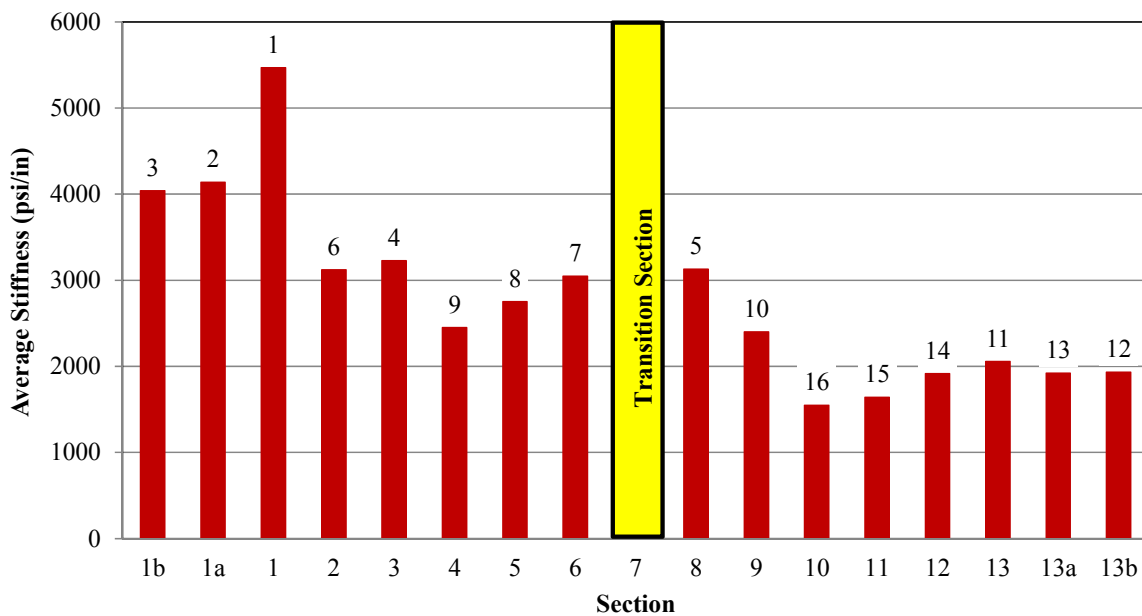
Figure 5.10. Average stiffness values calculated from PLT tests conducted at Marked Tree site in December, 2009.

5.4 Accelerated Dynamic Deflectometer (ADD)

Accelerated dynamic deflectometer (ADD) testing is a cyclic plate load test where a static hold-down force with a superimposed dynamic force is applied to the surface of a pavement structure to observe relative surface deformations as a function of number of loading cycles. The loads are applied to the pavement surface through an approximately 200 in^2 (1290 cm^2) rectangular wooden loading footprint to simulate a dual-tire footprint. The pavement deformations caused by the dynamic loading are monitored by an array of LVDTs that span farther than the expected zone of meaningful surface deformation. The LVDTs are located the same distances away from the loading footprint as the geophones in FWD testing. The results from this test are similar to the deflection basins observed from FWD testing; only the ADD test can be used to monitor both dynamic and residual/accumulating deformation as a function of applied load and number of loading cycles.

ADD tests were conducted at the Marked Tree site on five dates (refer to Table 4.1), but the only dates that are discussed herein are December 2009 and May 2011. These were the only two dates when ADD testing was conducted in all 16 sections. The ADD tests were performed in a similar manner on both dates, but the University of Arkansas's vibroseis truck was employed for applying the loads in December 2009, while a larger vibroseis truck owned by the University of Texas was used for load applications in May 2011. The larger truck allowed for greater static and dynamic forces to be applied during testing in order to "fail" the pavement.

5.4.1 ADD Testing Procedure

In December 2009, ADD tests were performed on all 16 test sections at the Marked Tree site. These tests were conducted approximately 16 feet (4.9 m) east of the center of each section.

These tests were performed with the University of Arkansas's vibroseis truck. The testing configuration is shown in Figure 5.11.

The spacing of the LVDT array is the same as the standard spacing of the FWD geophone array. The distances from the source are as follows in inches (cm): 0 (0.0), 8 (20.3), 12 (30.5), 18 (45.7), 24 (61.0), 36 (91.4), 48 (121.9), 60 (152.4), and 72 (182.9). The LVDTs were supported by a 16-ft (4.9-m) long aluminum frame, which extended beyond the zone of influence of the cyclic loading. For the December 2009 ADD testing, the static hold-down force applied to the loading footprint was 9,000 lbs (40 kN). The dynamic load was ± 5,000 lbs (22 kN), resulting in minimum and peak loads of 4,000 lbs (18 kN) and 14,000 lbs (62 kN), respectively. The dynamic load was applied at a frequency of 50 Hz and loading was conducted for approximately 30,000 cycles.

In May 2011, a larger vibroseis truck from the University of Texas at Austing was modified to apply the loads for the ADD testing. The testing configuration only changed slightly because the dynamic loading mechanism on the truck from the University of Texas at Austin was located near the middle of the truck rather than the end, which is illustrated in Figure 5.12. The May 2011 testing was conducted with a static hold-down force of 12,000 lbs (53 kN) and a dynamic load of ±10,000 lbs (44 kN), resulting in minimum and peak loads of 2,000 lbs (9 kN) and 22,000 lbs (97 kN), respectively. The dynamic load was applied at the same 50 Hz frequency for up to 10,000 cycles. Many of the 6-in (15.2-cm) sections could not withstand the entire 10,000 cycles before significant [plus 1 inch (2.5 cm)] deformation occurred.
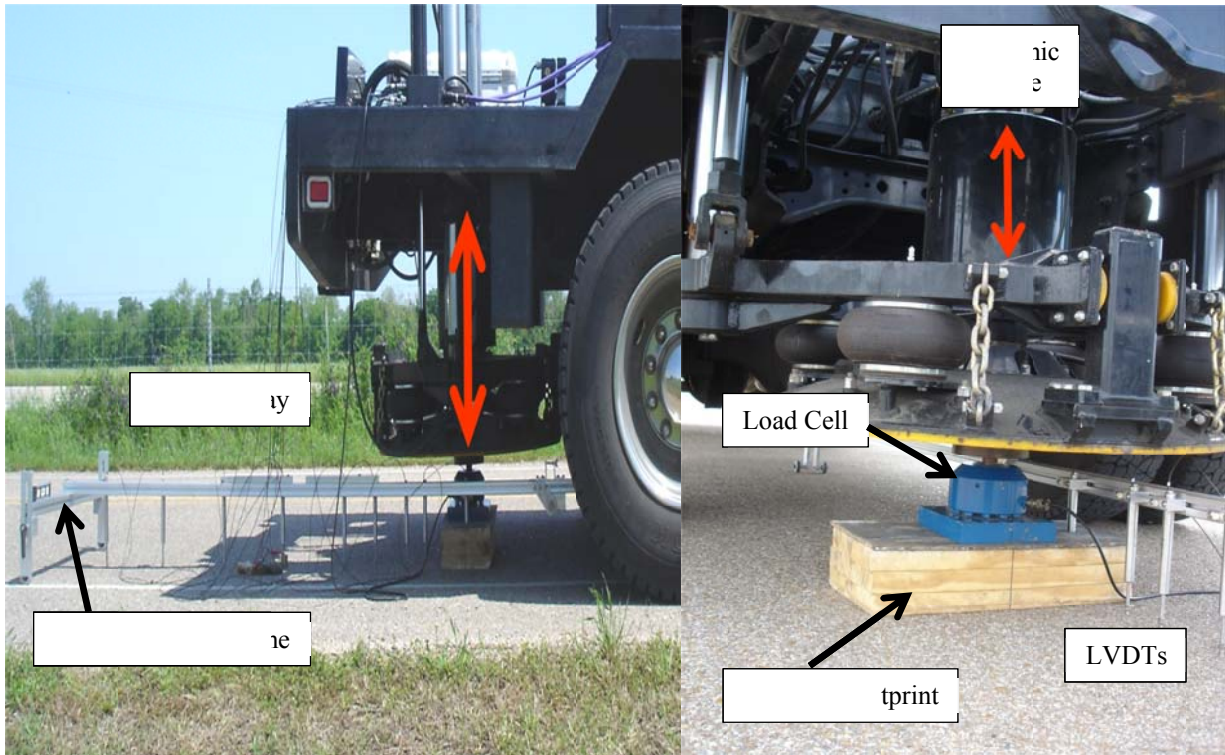
Figure 5.11. ADD testing configuration using the University of Arkansas vibroseis truck.
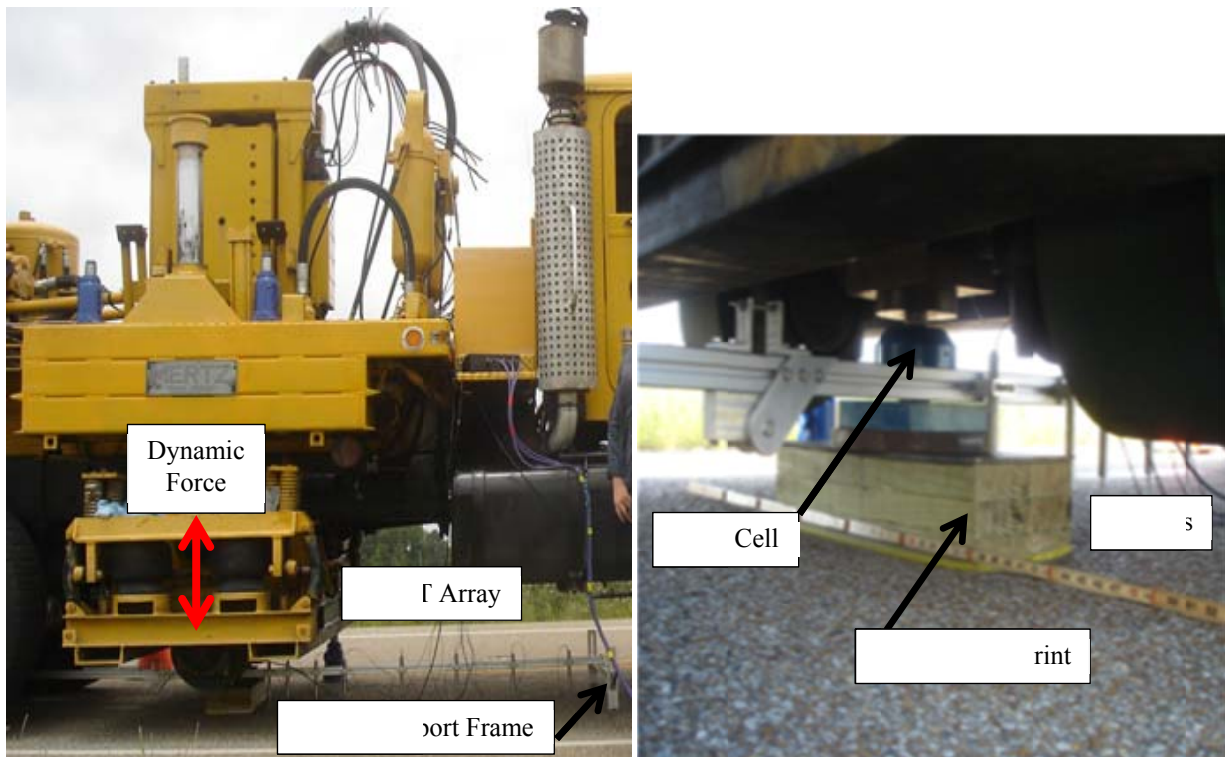
Figure 5.12. ADD testing configuration using the University of Texas vibroseis truck.

5.4.2 ADD Data Analysis

The data collected from a single cycle of ADD testing is in a similar form to the data from an FWD test (deflection basins). However, LVDTs are used in ADD testing, which enable the tracking of both dynamic and residual/accumulating deformation. Static and dynamic deformation basins are measured with the LVDT array as a function of the number of loading cycles. Typical deformation basins for a 10-in (25.4-cm) and a 6-in (15.2-cm) base section after various numbers of loading cycles are shown in Figures 5.13 and 5.14, respectively. The deformation basins were used to calculate the following three values to allow relative comparison between sections: total deformed area, deflected area up to 12 inches (30.5 cm), and the difference in deflection between the sensor located 12 inches (20.3 cm) from the applied load the sensor at the center of the applied load (Δ_{12}).

The total deformed area was calculated using the trapezoidal rule, as previously described for the FWD data analysis for total deflected area (Equation 5.1). However, this form of the trapezoidal rule only applies when the deformations between the two LVDTs have the same sign convention. Many of the 6-in base course sections experienced heave rather than deflection at a few of the LVDT locations under higher numbers of loading cycles (refer to Figure 5.14), which is why the term total deformed area is used rather than total deflected area. When the deformation from one LVDT to the next changed from deflection to heave, or vice versa, the following equation (Equation 5.3) was employed:

$$Area = \left[\frac{\frac{d_1^2*(x_2-x_1)}{(ABS(d_1)+ABS(d_2))}}{2}\right] + \left[\frac{\frac{d_1^2*(x_2-x_1)}{(ABS(d_1)+ABS(d_2))}}{2}\right] \qquad (5.3)$$
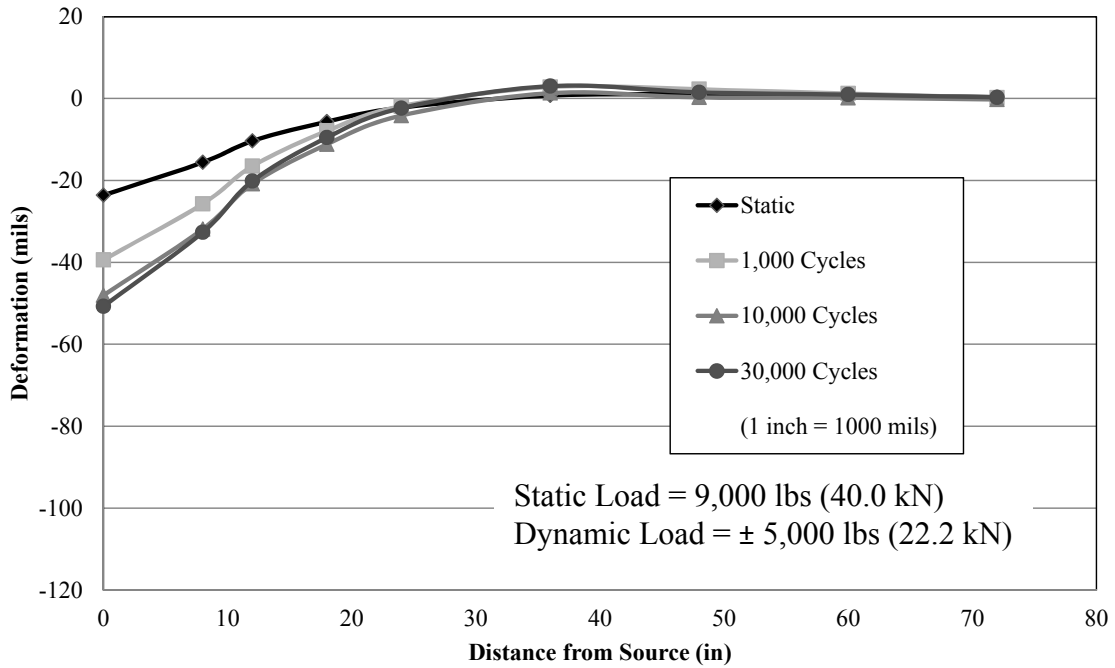
Figure 5.13. Typical ADD deformation basin for a 10-in (25.4 cm) base section (Section 5) from testing in December 2009.
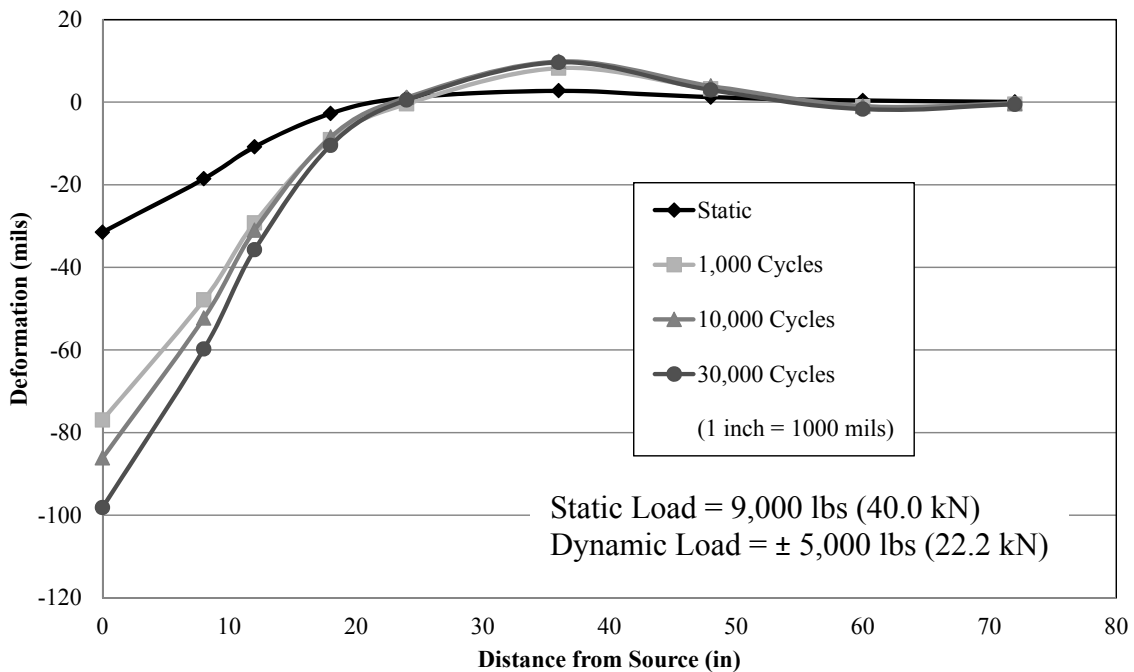
Figure 5.14. Typical ADD deformation basin for a 6-in (15.2 cm) base section (Section 13B) from testing in December 2009.

Where: Area = total deformed area, in^2

d$_1$ and d$_2$ = vertical deformation (deflection or heave) at specified LVDTs, in

x_1 and x_2 = distances from load source at specified LVDTs

ABS = absolute value of vertical deformation at specified LVDT

The subscripts 1 and 2 in Equation 5.3 represent the first and second LVDT locations with respect to the location of the applied load. The equation provided is the general form used for calculating the area of deformation between any two LVDT locations that have deflection at one and heave at the other. The absolute values of the deformations must be used for the calculation because deflection values are positive and heave values are negative. The total deformed area is a sum of all deformations calculated using the trapezoidal rule, as well as the deformations calculated using the equation for the deflection to heave transition zone.

Calculation of the deflected area up to 12 inches (30.5 cm) was performed because in all sections, except Section 10 in May 2011, and all loading cases, d_0, d_8 and d_{12} were all deflection values (no heave). This value allows for a comparison of deflected area at each section for a deflection basin with a 12-in (30.5-cm) radius around the source because heave only occurred at distances greater than 12 inches (30.5-cm) from the source. To account for the heave that occurred at Section 10 during the May 2011 visit, the deflection basin was shifted down by the amount of heave that occurred at the 18-in (45.7-cm) LVDT for this calculation only. The trapezoidal rule was implemented for these calculations.

The Δ_{12} values are differential deflection values between the LVDT at 0 inches (0 cm) away from the source and the LVDT at 12 inches (30.5 cm) away from the source for each recorded number of loading cycles at every section in terms of inches (cm). The equation for Δ_{12} (Equation 5.4) is as follows:

$$\Delta_{12} = d_0 - d_{12} \tag{5.4}$$

Where: Δ_{12} is in inches

d_0 = vertical deflection at 0 inches away from the source, in

d_{12} = vertical deflection at 12 inches away from the source, in

The one exception to the equation for Δ_{12} was for Section 10 on the May 2011 visit. Section 10 experienced heave between the 8-in (20.3-cm) LVDT and the 12-in (30.5-cm) LVDT. Since the d_{12} value for Section 10 was negative (heave), it was added to d_0 to account for the total deformation occurring between the two points rather than the differential settlement between the two points.

5.4.3 ADD Results

All of the results calculated using the methods described above for ADD data analysis are presented in this section. The results are presented in two different groups, either December 2009 or May 2011. The results are separated because, as mentioned above, the testing conducted in December 2009 was conducted at lesser load values than the loads applied to the pavement during the ADD testing performed during May 2011.

5.4.3.1 December 2009 ADD Results

The ADD tests conducted at the Marked Tree site during the December 2009 site visit were conducted with a static load of 9,000 lbs (40 kN) and a dynamic load of 5,000 lbs (22 kN) at a loading frequency of 50 Hz. The results presented for the December 2009 site visit are for the following loading stages: static, 1,000 cycles, 10,000 cycles, and 30,000 cycles. The resulting total deformed areas, deflected area up to 12 inches (30.5 cm), and Δ_{12} values, as well as

associated ranks, for each loading condition are provided in Tables 5.11 through 5.14, respectively.

5.4.3.2 May 2011 ADD Results

The ADD tests conducted at the Marked Tree site during the May 2011 site visit were conducted with a static load of 12,000 lbs (53 kN) and a dynamic load of 10,000 lbs (44 kN) at a loading frequency of 50 Hz. Due to the large increase in the magnitude of loading, the number of loading cycles that each test section endured prior to "failure" [i.e., a footprint deflection > 0.5 in (1.3 cm)] was typically less than what was applied to each test section during the December 2009 site visit. The results presented for the May 2011 site visit are from the following loading stages: static, 1,000 cycles, and 2,500 cycles. The resulting total deformed areas, deflected area up to 12 inches (30.5 cm), and Δ_{12}, as well as associated ranks, for each loading condition are provided in Tables 5.15 through 5.17.

ADD testing was also performed in the west bound lane adjacent to Sections 13 and 13B (referred to herein as 13W and 13BW) during the May 2011 Marked Tree site visit, but these two areas were not tested during the December 2009 site visit and are not presented in the May 2011 ADD testing results.

5.4.3.3 ADD Composite Ranking

As a means to synthesize the ADD results from both test dates and numerous loading cycles into a quantitative relative comparison between sections, the rankings from each method of analysis (i.e., total deformed area, deflected area up to 12 inches (30.5 cm), and Δ_{12}) were summed, providing a composite ranking value on which to base a new, overall ranking of the sections. The summed composite ranking values from the ADD data and the overall section rankings are presented in Table 5.18. The composite ranking values and overall section rankings

Table 5.11. Static loading results from ADD testing on December 2009 at the Marked Tree site.

	Section	Total Deformed Area (in^2)	Rank	Area up to 12" (in^2)	Rank	Δ_{12} (in)	Rank
	1B	0.2272	1	0.1472	2	0.0108	4
	1A	0.2626	3	0.1655	4	0.0082	1
10"	1	0.2389	2	0.1430	1	0.0086	2
Nominal	2	0.3362	9	0.2059	8	0.0094	3
Base	3	0.2686	4	0.1595	3	0.0137	11
Thickness	4	0.3217	8	0.2040	7	0.0135	9
	5	0.3193	7	0.2088	9	0.0132	7
	6	0.4637	15	0.2271	11	0.0121	5
Transition	7	-	-	-	-	-	-
	8	0.2779	5	0.2006	6	0.0132	6
	9	0.3694	11	0.2705	13	0.0179	12
6"	10	0.4728	16	0.3733	16	0.0301	16
Nominal	11	0.4272	13	0.3404	15	0.0257	15
Base	12	0.4361	14	0.3215	14	0.0193	13
Thickness	13	0.2962	6	0.2205	10	0.0133	8
	13A	0.3744	12	0.1763	5	0.0137	10
	13B	0.3654	10	0.2589	12	0.0207	14

Table 5.12. ADD test results after 1,000 loading cycles on December 2009 at the Marked Tree site.

	Section	Total Deformed Area (in^2)	Rank	Area up to 12" (in^2)	Rank	Δ_{12} (in)	Rank
	1B	0.4554	1	0.2965	2	0.0186	5
	1A	0.4952	2	0.2833	1	0.0134	1
10"	1	0.5447	7	0.3249	3	0.0156	2
Nominal	2	0.6991	10	0.3880	7	0.0161	3
Base	3	0.5172	4	0.3552	5	0.0251	9
Thickness	4	0.5001	3	0.3694	6	0.0230	7
	5	0.5221	5	0.3451	4	0.0229	6
	6	0.8066	14	0.4117	9	0.0218	5
Transition	7	-	-	-	-	-	-
	8	0.5423	6	0.3927	8	0.0264	10
	9	0.6511	9	0.4865	11	0.0326	12
6"	10	0.8382	15	0.6453	15	0.0566	16
Nominal	11	0.7910	13	0.6189	14	0.0501	15
Base	12	0.7384	11	0.5613	13	0.0365	13
Thickness	13	0.5839	8	0.4196	10	0.0231	8
	13A	0.7573	12	0.5020	12	0.0304	11
	13B	0.9340	16	0.6535	16	0.0478	14

Table 5.13. ADD test results after 10,000 loading cycles on December 2009 at the Marked Tree site.

	Section	Total Deformed Area (in^2)	Rank	Area up to 12" (in^2)	Rank	Δ_{12} (in)	Rank
	1B	0.5301	1	0.3545	1	0.0223	4
	1A	0.7035	5	0.3568	2	0.0156	1
10"	1	0.7206	6	0.3891	3	0.0183	2
Nominal	2	0.8230	12	0.4525	7	0.0192	3
Base	3	0.5916	2	0.4130	4	0.0299	9
Thickness	4	0.7451	7	0.4789	9	0.0278	8
	5	0.6014	3	0.4252	5	0.0272	6
	6	0.8692	13	0.4469	6	0.0245	5
Transition	7	-	-	-	-	-	-
	8	0.6957	4	0.4621	8	0.0314	10
	9	0.7941	8	0.5621	12	0.0392	12
6"	10	1.0105	15	0.7679	16	0.0681	16
Nominal	11	0.9601	14	0.7419	15	0.0611	15
Base	12	0.8172	11	0.6203	13	0.0428	13
Thickness	13	0.8085	10	0.5023	10	0.0274	7
	13A	0.8001	9	0.5469	11	0.0350	11
	13B	1.0380	16	0.7203	14	0.0551	14

Table 5.14. ADD test results after 30,000 loading cycles on December 2009 at the Marked Tree site.

	Section	Total Deformed Area (in^2)	Rank	Area up to 12" (in^2)	Rank	Δ_{12} (in)	Rank
	1B	0.5911	1	0.3901	1	0.0259	4
	1A	0.7565	4	0.3939	2	0.0179	1
10"	1	0.7350	3	0.4061	3	0.0202	2
Nominal	2	0.9495	12	0.5105	7	0.0221	3
Base	3	0.7565	5	0.4972	6	0.0340	9
Thickness	4	0.8014	6	0.5328	9	0.0317	7
	5	0.6299	2	0.4392	4	0.0306	6
	6	0.8597	9	0.4671	5	0.0268	5
Transition	7	-	-	-	-	-	-
	8	0.8039	7	0.5275	8	0.0360	10
	9	0.9077	11	0.6257	12	0.0441	12
6"	10	1.1126	15	0.8648	16	0.0777	16
Nominal	11	1.0978	14	0.8414	15	0.0701	15
Base	12	0.9514	13	0.7154	13	0.0483	13
Thickness	13	0.8225	8	0.5353	10	0.0329	8
	13A	0.8762	10	0.6226	11	0.0388	11
	13B	1.1509	16	0.8226	14	0.0624	14

for total deformed area, deflected area up to 12 inches (30.5 cm), and Δ_{12} are presented in Figures 5.15, 5.16, and 5.17, respectively.

With only one exception (Section 8), both the total deformed area (Figure 5.15) and the deflected area up to 12 inches (30.5 cm) (Figure 5.16) clearly indicate that the 10-in (25.4-cm) nominal base sections outperform the 6-in (15.2-cm) nominal base sections in terms of surface deflections under dynamic loading. Surprisingly, for both methods of data analysis, Section 8 ranks highest among the 6-in (15.2-cm) sections, while Section 6 ranks lowest among the 10-in (25.4-cm) sections despite the fact that these two sections have the same geosynthetic reinforcement (refer to Figure 3.2). Section 8 also ranked higher than some of the 10-in (25.4-cm) nominal base course sections in terms of PLT stiffness (refer to Figure 5.10) and rutting (refer to Figures 4.2 and 4.3). It is hypothesized that the buttressing/confining effect of the driveway that intersects Section 8 has a positive impact on the deformation characteristics of this section. All three methods of analysis (total deformed area, deflected area up to 12" (30.5 cm), and Δ_{12}) indicated the general pattern noted in the rutting data (Figures 4.2 and 4.3); that Sections 1B-9 generally outperform the other sections. Furthermore, all three ADD data analysis methods also indicated that Section 10 performed the worst under dynamic loading and that Sections 11 and 12 also performed very poorly, agreeing with the average rut depth values that indicated these sections had "failed". However, similar to the PLT results and contrary to the rutting data, all three methods of ADD data analysis also consistently ranked Section 1 (the unreinforced section with 10-in nominal base thickness) as the 2nd best section. Again, this is likely due to the fact that Section 1 has the thickest summed total of asphalt and base course (refer to Figure 6.13).

Table 5.15. Static loading results from ADD testing on May 2011 at the Marked Tree site.

	Section	Total Deformed Area (in^2)	Rank	Area up to 12" (in^2)	Rank	Δ_{12} (in)	Rank
10" Nominal Base Thickness	1B	0.5925	1	0.3701	2	0.0293	2
	1A	0.6040	2	0.3424	1	0.0255	1
	1	0.6148	4	0.3935	3	0.0311	3
	2	0.6064	3	0.4391	4	0.0381	4
	3	0.6271	5	0.4783	5	0.0412	5
	4	0.7525	8	0.5506	8	0.0457	7
	5	0.6879	7	0.4936	6	0.0429	6
	6	1.0810	11	0.6741	10	0.0526	9
Transition	7	-	-	-	-	-	-
6" Nominal Base Thickness	8	0.6734	6	0.5040	7	0.0483	8
	9	0.9042	9	0.6547	9	0.0558	10
	10	3.4214	16	1.8351	16	0.0995	15
	11	1.1457	12	0.8622	12	0.0916	12
	12	1.4028	13	0.9517	13	0.0942	13
	13	1.4745	14	1.1027	14	0.0943	14
	13A	1.0537	10	0.7828	11	0.0898	11
	13B	1.5212	15	1.1225	15	0.1316	16

Table 5.16. ADD test results after 1,000 loading cycles on May 2011 at the Marked Tree site.

	Section	Total Deformed Area (in^2)	Rank	Area up to 12" (in^2)	Rank	Δ_{12} (in)	Rank
10" Nominal Base Thickness	1B	3.0758	6	2.3567	6	0.2023	4
	1A	3.3324	8	2.0472	2	0.1572	1
	1	2.4253	1	1.9424	1	0.1919	2
	2	2.5590	2	2.0587	3	0.2063	5
	3	2.5754	3	2.0721	4	0.2009	3
	4	3.1033	7	2.3941	8	0.2411	7
	5	2.6942	4	2.1491	5	0.2311	6
	6	3.0407	5	2.4698	9	0.2463	8
Transition	7	-	-	-	-	-	-
6" Nominal Base Thickness	8	3.4570	9	2.3911	7	0.2772	9
	9	3.8598	10	2.5992	10	0.3074	10
	10	8.3671	16	7.7965	16	0.4652	16
	11	5.6691	13	3.7668	14	0.4211	14
	12	5.6073	12	3.7050	13	0.4057	12
	13	6.9192	15	4.9547	15	0.4578	15
	13A	5.6719	14	3.5406	12	0.4088	13
	13B	4.9119	11	3.3286	11	0.3813	11

Table 5.17. ADD test results after 2,500 loading cycles on May 2011 at the Marked Tree site.

	Section	Total Deformed Area (in^2)	Rank	Area up to 12" (in^2)	Rank	Δ_{12} (in)	Rank
10" Nominal Base Thickness	1B	4.0409	9	3.1084	10	0.2671	5
	1A	3.3350	5	2.2020	2	0.1731	1
	1	2.6160	1	2.1478	1	0.2212	2
	2	2.8793	2	2.3329	3	0.2546	3
	3	3.1860	4	2.4652	4	0.2589	4
	4	3.8043	7	2.9049	8	0.3079	7
	5	3.1301	3	2.6197	5	0.3095	8
	6	3.4055	6	2.8328	7	0.3015	6
Transition	7	-	-	-	-	-	-
6" Nominal Base Thickness	8	3.9600	8	2.6409	6	0.3272	9
	9	4.6982	10	3.0100	9	0.4024	10
	10	10.5498	16	9.8114	16	0.6484	16
	11	7.1365	14	4.6271	14	0.5625	15
	12	6.9674	13	4.4241	13	0.5319	13
	13	8.0724	15	5.6781	15	0.5561	14
	13A	6.7785	12	4.0711	12	0.5048	12
	13B	6.0062	11	3.8487	11	0.4791	11

Table 5.18. Composite rankings from ADD data analysis.

	Section	Total Deformed Area		Area up to 12"		Δ_{12}	
		Composite	Rank	Composite	Rank	Composite	Rank
10" Nominal Base Thickness	1B	20	1	24	3	28	4
	1A	29	4	14	1	7	1
	1	24	2	15	2	15	2
	2	50	8	39	6	24	3
	3	27	3	31	4	50	7
	4	46	7	55	8	52	8
	5	31	5	38	5	45	6
	6	73	10	57	9	43	5
Transition	7	-	-	-	-	-	-
6" Nominal Base Thickness	8	45	6	50	7	62	9
	9	68	9	76	11	78	11
	10	109	16	111	16	111	16
	11	93	14	99	15	101	15
	12	87	13	92	13	90	13
	13	76	11	84	12	74	10
	13A	79	12	74	10	79	12
	13B	95	15	93	14	94	14
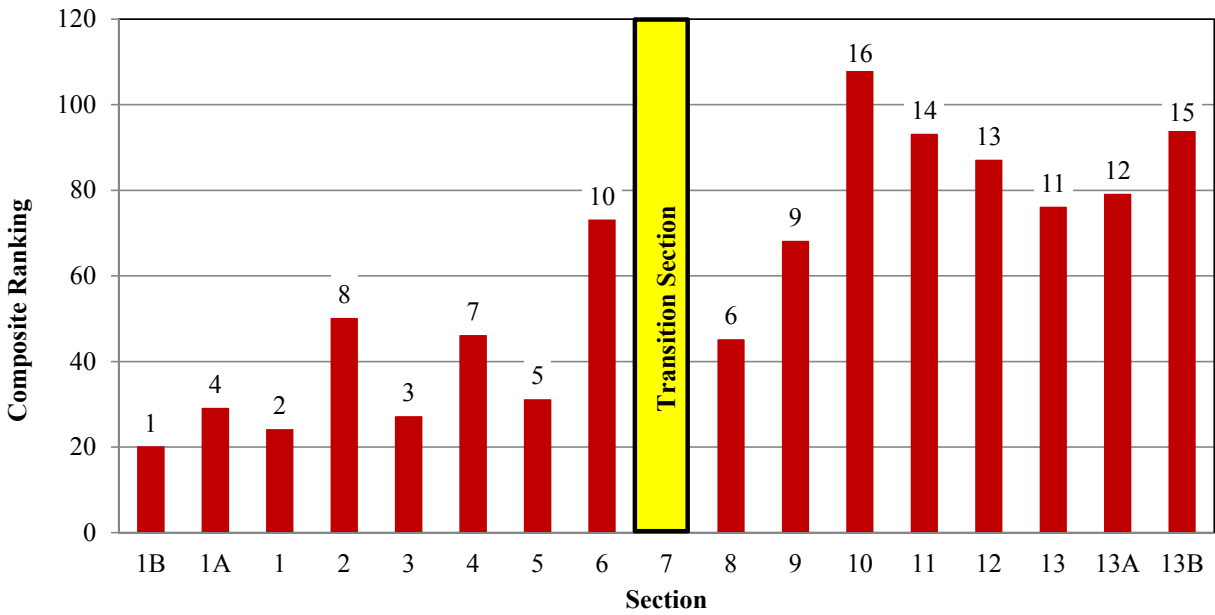
Figure 5.15. Total deformed area composite ranking from ADD testing at Marked Tree site.
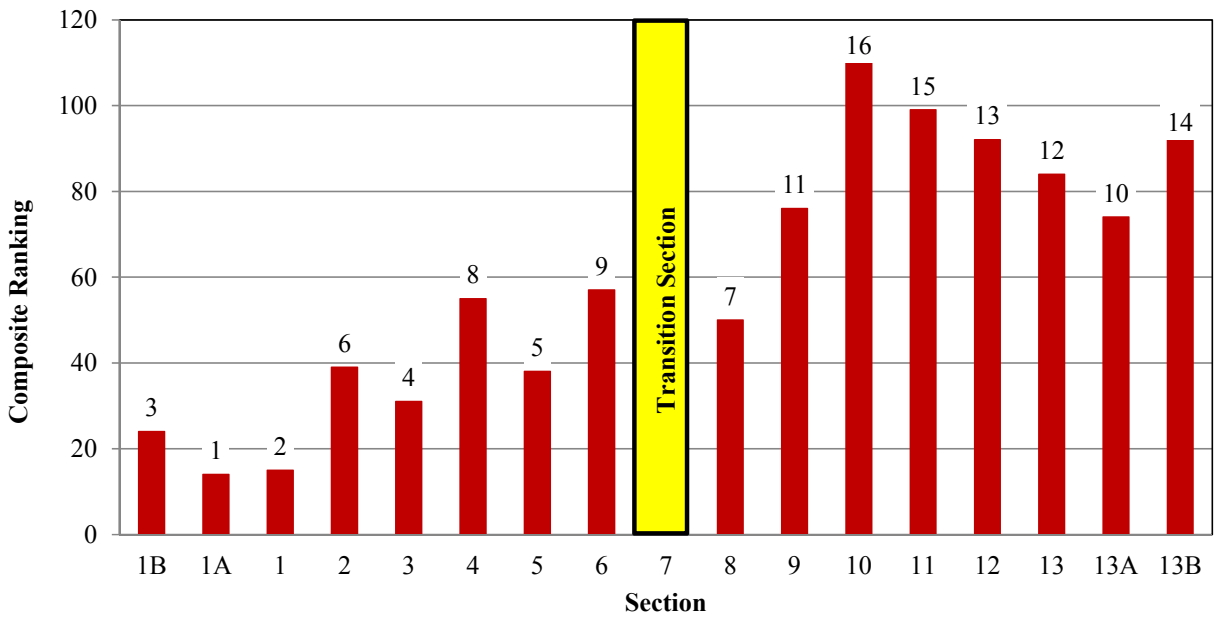
Figure 5.16. Deflected area up to 12" composite ranking from ADD testing at Marked Tree site.
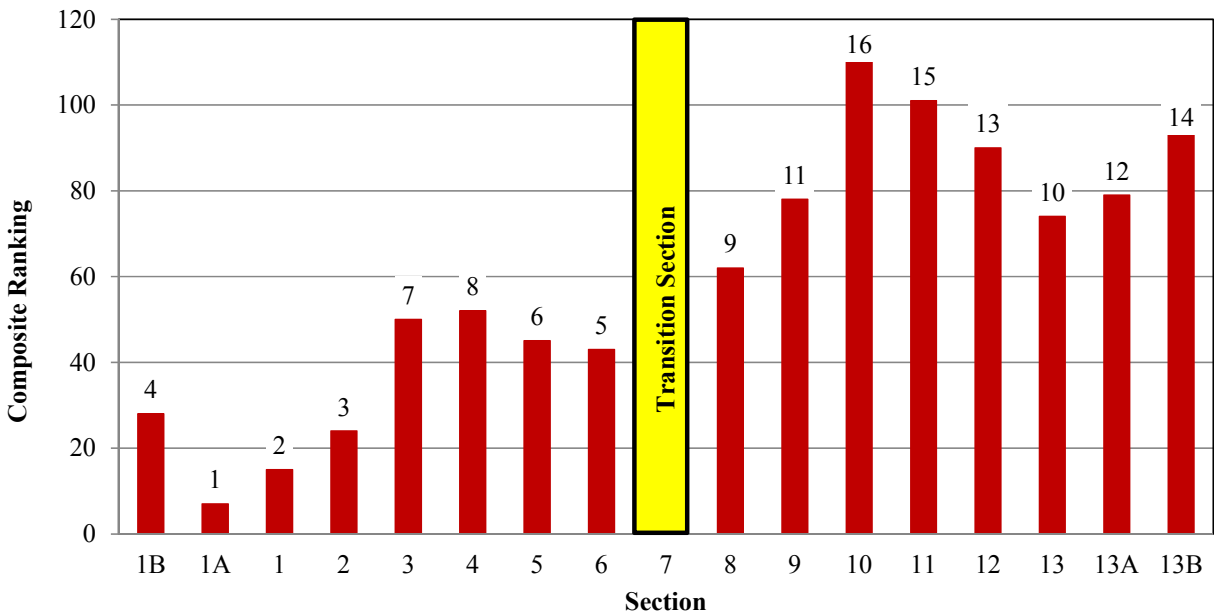
Figure 5.17. Δ_{12} composite ranking from ADD testing at Marked Tree site.

No clear distinctions between various types of geosynthetics were observed in the ADD results from either base course thickness, yet the ADD data and the PLT data both seem to agree better with pavement performance than the FWD data.

5.5 Light Weight Deflectometer (LWD)

The Light Weight Deflectometer (LWD) is a portable version of an FWD, often referred to as a Portable Falling-Weight Deflectometer (PFWD). During LWD testing, a falling weight is raised to a desired height and allowed to fall freely onto a buffer system (refer to Figures 5.18 and 5.19). The buffer system transmits the load pulse through a loading plate that evenly distributes the load onto the testing surface. A load cell is positioned within the LWD apparatus to measure the impulse loads for every drop. Peak deflections are measured for every drop by a geophone mounted inside the LWD apparatus, measuring deflections through the center of the loading plate. An array of geophones can also be connected to the LWD to measure the

deflection basin caused by the impulse load. The peak deflections and impulse load are generally displayed and recorded through a personal digital assistant (PDA) wirelessly linked to the load cell and geophones. Deflections and loads may be either correlated directly to pavement performance or used to determine in-situ material characteristics of the pavement layers (ASTM E2583 – 2007).

LWD tests were conducted at the Marked Tree site during the October 2010 site visit. The tests were first conducted on the asphalt, and then on top of the base course layers of each test section after removing at 2-ft by 2-ft (0.61-m x 0.61-m) piece of asphalt (refer to Chapter 6). The areas in the westbound lane adjacent to Sections 13 and 13B, referred to as 13W and 13BW, were tested along with the 16 test sections, but tests were only performed on top of the asphalt in these sections. All LWD tests only utilized the single geophone at the center of the loading area. An LWD global modulus (E_{LWD}) was calculated from these tests and ranked for all sections.

The testing procedure, data analysis method, and testing results from the October 2010 visit to the Marked Tree site are presented in the following sections.

5.5.1 LWD Testing Procedure

LWD tests were conducted at the Marked Tree site during the October 2010 site visit. These tests were performed on the asphalt and base course surfaces of all 16 test sections, as well as on the asphalt of the areas referred to as 13W and 13BW. The LWD device utilized was a Dynatest 3031 Lightweight Deflectometer. A schematic of the apparatus is presented in Figure 5.18. The group used a falling mass arrangement that equaled 33 lbs (15 kg) that impacted a buffer system consisting of four Dynatest buffer pads. LWD tests were also conducted on each surface using a 12-in (30.5-cm) diameter loading plate and a 6-in (15.2-cm) diameter loading plate. To alternate from the 12-in (30.5-cm) loading plate to the 6-in (15.2-cm) loading plate, the

snap locks must be released and the 12-in (30.5-cm) plate attachment must be rotated freely to ensure it is disconnected from the 6-in (15.2-cm) loading plate. Unfortunately, the attachment plate was not properly disengaged before conducting the tests with the 6-in (15.2-cm) loading plate. Therefore, data collected using the 6-in (15.2-cm) loading plate was discarded due to procedural error.

The LWD tests on top of the asphalt layer were conducted approximately 15 feet (4.6 m) east of the center of each test section. The base course testing was conducted within the 2-ft x 2-ft (0.61-m x 0.61-m) testing area once the asphalt layer was removed (excavation described in Chapter 6). A gripped rubber mat was placed between the loading plate and the testing surface to improve load distribution for both testing surfaces. Five falling weight sequences were performed on the testing surfaces at each section with each size of loading plate. The load and deflection values collected during each falling weight sequence were stored and displayed on a PDA connected to the LWD through Bluetooth. Pictures of LWD tests being performed on the base and asphalt are displayed in Figure 5.19.

5.6.2 LWD Data Analysis

The main unit of the LWD records the load cell and geophone data continuously throughout the dynamic pulse from the falling weight, which is the time elapsed from the falling weight impacting the buffer stack until the falling weight becomes stationary. Typical load-deflection pulses for a 6-in (15.2-cm) and a 10-in (25.4-cm) nominal base thickness section on both asphalt and base are presented in Figures 5.20 and 5.21, respectively. From the load-deflection pulse data, the peak load and resulting peak deflection values were recorded. Note how the peak force values remained the same while the peak deflection values were generally greater in the 6-in sections than the 10-in sections on both asphalt and base surfaces.

106
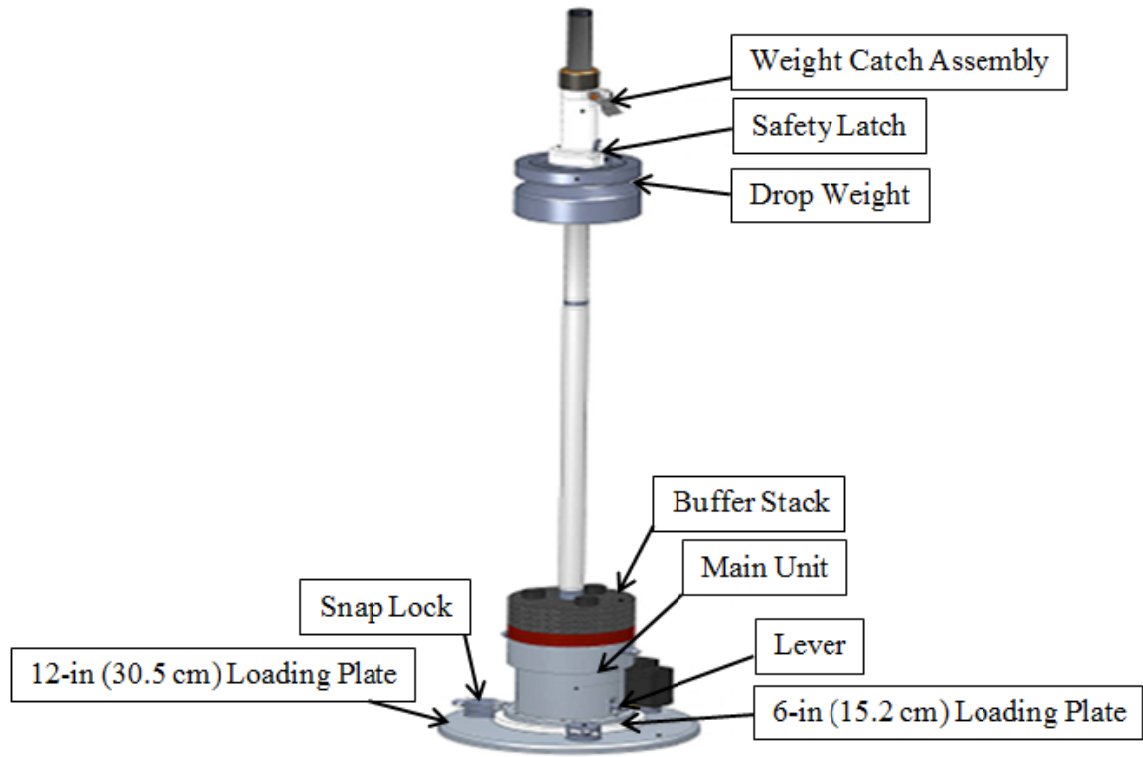
Figure 5.18. Dynatest 3031 LWD schematic.

Figure 5.19. LWD tests conducted on asphalt and base course layers at Marked Tree site.

The peak load and resulting peak deflection values are the key components in the calculation of the LWD global modulus (E_{LWD}). The E_{LWD} was calculated for all sections on both the asphalt and base surfaces. The equation for calculating the E_{LWD} (Equation 5.5) derived by Dynatest from Equation 8-26 in Das (1997) is as follows:

$$E_{LWD} = \frac{2*(1-v^2)*\sigma*R}{\delta} \hspace{3cm} (5.5)$$

Where: E_{LWD} = LWD global modulus (MPa)

v = Poisson's Ratio (0.33 for asphalt and 0.25 for base)

σ = maximum applied stress (kPa)

R = loading plate radius (mm)

δ = maximum surface deflection (µm)

5.6.3 LWD Results

The calculated E_{LWD} values and ranks from the 12-in (30.5-cm) loading plate on top of both the asphalt and base layers are presented in Tables 5.19 and 5.20, respectively, and Figures 5.22 and 5.23, respectively.

The LWD rankings on the asphalt and base do not clearly reveal differences between different types of geosynthetics in either the 10-in (25.4-cm) or 6-in (15.2-cm) base sections. However, in general, the 10-in (25.4-cm) base sections tend to have higher global E_{LWD} values than the 6-in (15.2-cm) base sections, with a few exceptions. Interestingly, Section 10, which was the lowest ranked section in terms of rutting and all other test results presented previously (i.e., FWD, PLT and ADD), did not rank lowest (12 out of 16) based on LWD tests performed on the asphalt surface (Figure 5.22), but did rank lowest based on LWD tests performed on the base layers.

108
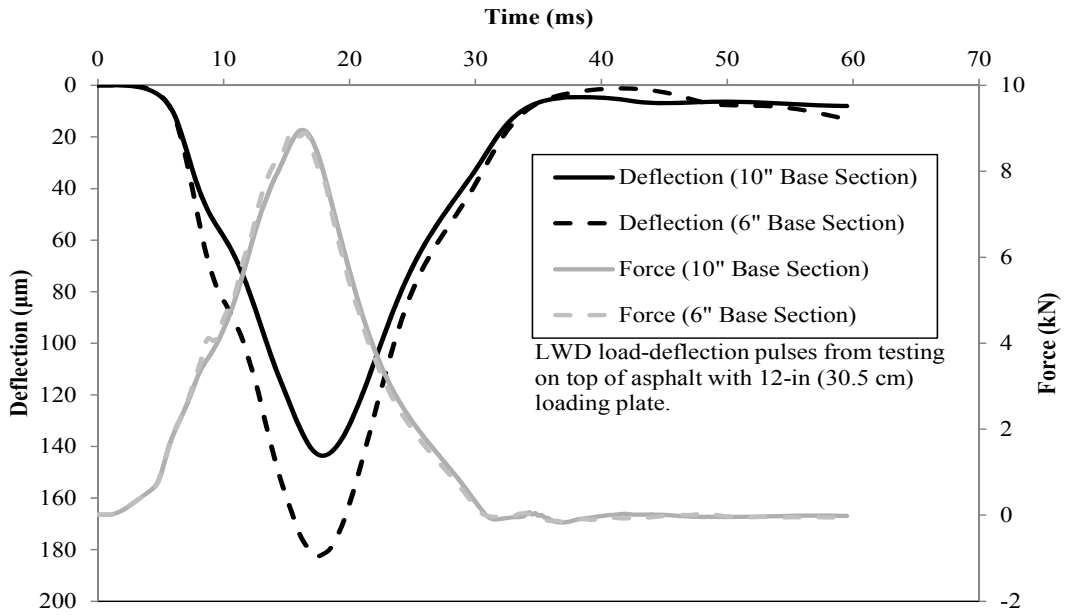
Figure 5.20. Typical load-deflection pulses from LWD testing on the asphalt surface with 12-in (30.5-cm) loading plate at the Marked Tree site on 10-in (25.4-cm) and 6-in (15.2-cm) thick base course layers.
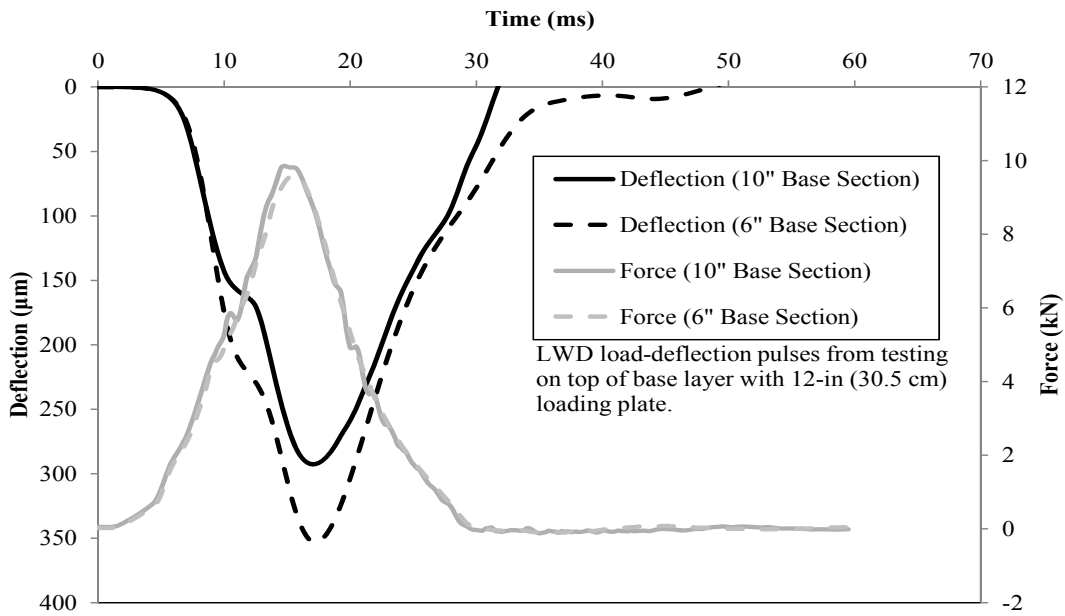
Figure 5.21. Typical load-deflection pulses from LWD testing on the base layer with 12-in (30.5-cm) loading plate at the Marked Tree site on 10-in (25.4-cm) and 6-in (15.2-cm) thick base course layers.

Table 5.19. E_{LWD} results from LWD testing on the asphalt with 12-in (30.5-cm) diameter load plate.

	Section	Eastbound			Westbound		
		E_{LWD} (MPa)	E_{LWD} (ksi)	Rank	E_{LWD} (MPa)	E_{LWD} (ksi)	Rank*
10" Nominal Base Thickness	1B	237	34.44	7			
	1A	253	36.75	5			
	1	253	36.76	4			
	2	229	33.15	9			
	3	255	37.04	3			
	4	214	31.02	10			
	5	296	42.99	1			
	6	263	38.20	2			
Transition	7	-	-	-	-	-	
6" Nominal Base Thickness	8	193	27.97	11			
	9	170	24.73	13			
	10	176	25.53	12			
	11	168	24.34	14			
	12	136	19.67	16			
	13	244	35.44	6	142	20.53	15
	13A	234	33.95	8			
	13B	136	19.79	15	120	17.34	18

*Represents potential rank if westbound lane was used in ranking
(Eastbound ranks would change accordingly).
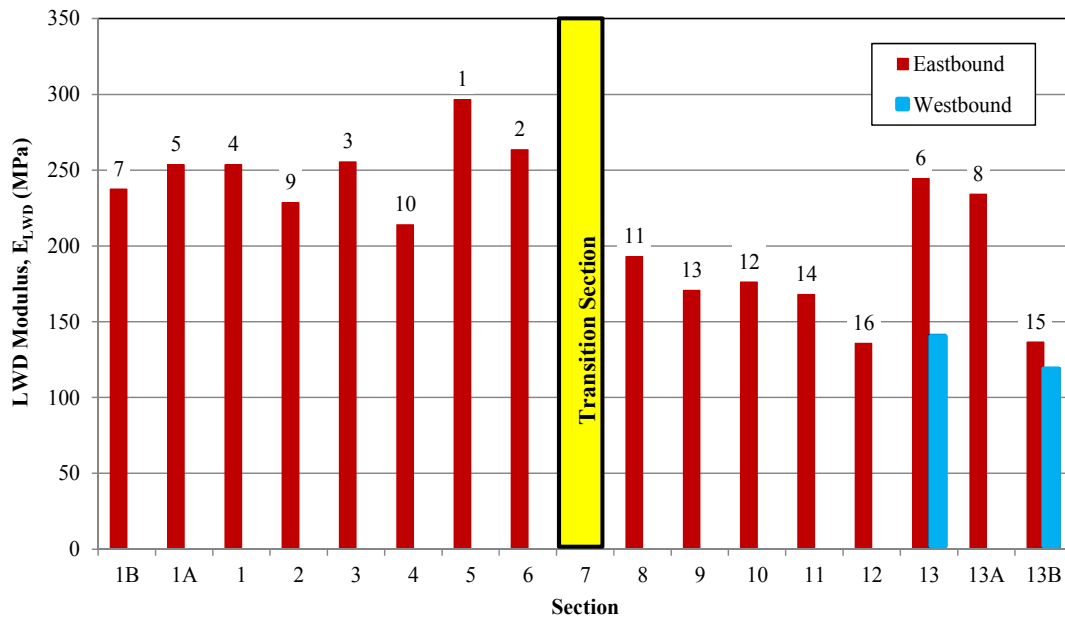
Figure 5.22. E_{LWD} results from LWD testing on the asphalt with 12-in (30.5-cm) diameter load plate

110

Table 5.20. E$_{LWD}$ results from LWD testing on the base with a 12-in (30.5-cm) diameter loading plate.

| | Section | Eastbound | | |
		E$_{LWD}$ (MPa)	E$_{LWD}$ (ksi)	Rank
10" Nominal Base Thickness	1B	114	16.59	12
	1A	169	24.55	3
	1	180	26.04	2
	2	131	19.02	8
	3	130	18.88	9
	4	153	22.19	4
	5	192	27.87	1
	6	149	21.55	5
Transition	7	-	-	-
6" Nominal Base Thickness	8	127	18.39	10
	9	94	13.64	15
	10	62	8.99	16
	11	115	16.70	11
	12	98	14.28	13
	13	139	20.12	7
	13A	147	21.33	6
	13B	95	13.83	14
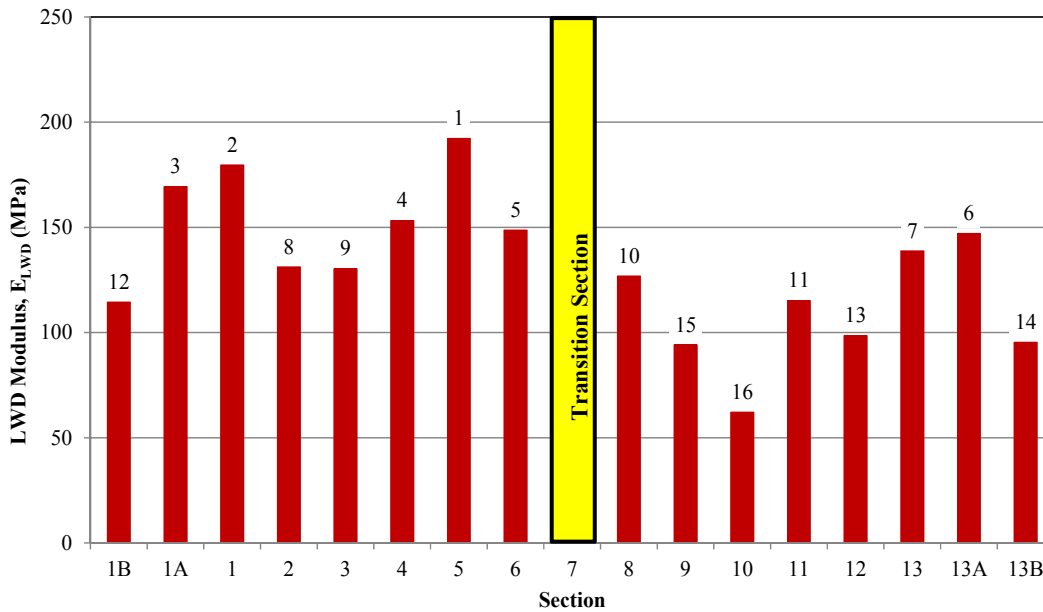
Figure 5.23. E$_{LWD}$ results from LWD testing on the base with a 12-in (30.5-cm) diameter loading plate.

111

The LWD rankings from testing atop the base layer seem to be more similar to the average rut depth rankings than the LWD rankings from testing atop the asphalt layer. However, Sections 13 and 13A show much better relative performance from both forms of LWD testing than the average rut depth values credit them with. Furthermore, while Section 8 is ranked 2 in the average rut depth analysis, it is ranked 11 and 10 for the LWD analyses when tested atop the asphalt and base layers, respectively. The LWD results do not seem to correlate with rutting as well as the PLT and ADD tests.

5.6 Rolling Dynamic Deflectometer (RDD)

The rolling dynamic deflectometer (RDD) is a large truck on which a servo-hydraulic vibrator is mounted. The vibrator is used to apply large vertical dynamic loads to rolling wheels that come into contact with the pavement. The vibrator can apply a total vertical dynamic load up to 33,000 lbs (147 kN). A receiver wheel located midway between the loading wheels is primarily used to monitor the dynamic deflections. Additional rolling receivers are located at greater distances from the applied load, enabling the measurement of dynamic deflection basins. The truck is driven at a slow speed and continuous profiles of pavement deflection are measured under heavy loading conditions (Bay et al. 1995). The RDD test is typically performed at velocities of approximately 1 to 2 ft/sec (0.3 to 0.6 m/s) (Bay and Stokoe 1998). A schematic of the RDD, with the important components pointed out, from Bay and Stokoe (1998) is displayed in Figure 5.24.
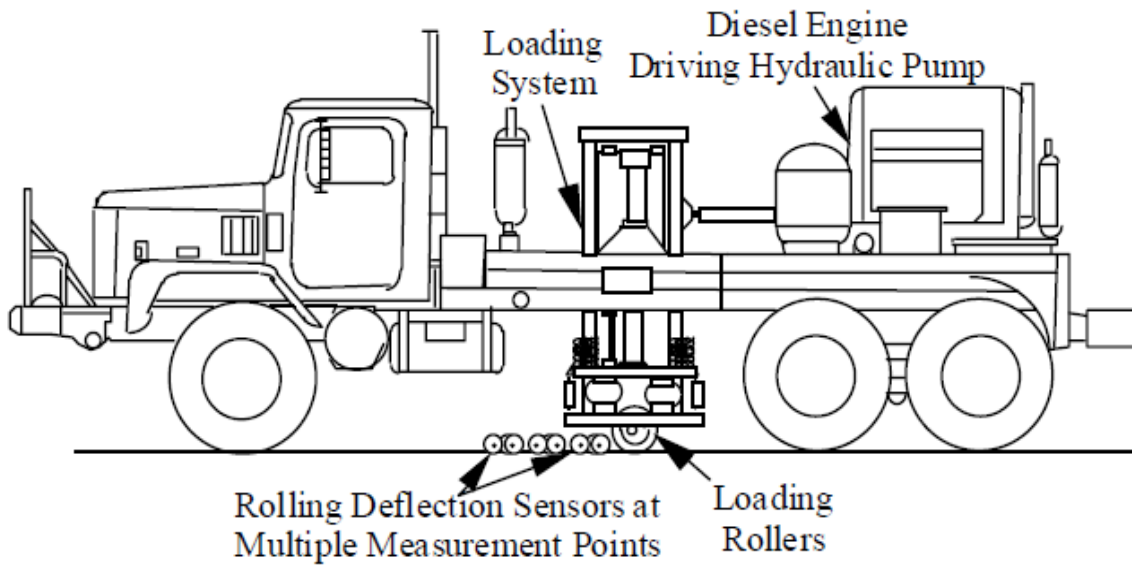
Figure 5.24. Schematic of RDD with important testing features labeled (Bay and Stokoe 1998).

The University of Texas's RDD was mobilized to the Marked Tree site for testing during the May 2011 site visit. The testing was conducted very quickly compared to the majority of the tests conducted at the site. The RDD was driven down the eastbound lane in the eastern direction, referred to as the first path. The RDD was then driven down the westbound lane in the eastern direction, completing the second path. Continuous deflection profiles were created from the data collected during the RDD test.

5.6.1 RDD Test Procedure

The RDD test paths were in the center of the east and west bound lanes, traveling from approximately 300 feet (91.4 m) west of Section 13B to approximately 300 feet (91.4 m) east of Section 1B [approximately 1450 ft (442 m) total]. The static load applied during the testing was 8 kips (35.6 kN), and the dynamic load was 6 kips (26.7 kN) peak-to-peak. The loading frequency was 30 Hz. The RDD was equipped with three sensors positioned in the center of the

lane. Sensor 1 was located between the loading rollers. Sensor 2 was positioned 2.5 feet (0.76 m) in front of Sensor 1, and Sensor 2 was positioned 2 feet (0.61 m) in front of Sensor 2.

The RDD test was conducted by applying the combined loads (dynamic superimposed on the static), and then slowly driving over the center of each lane, traveling from west to east. The applied forces and displacements at each rolling sensor were constantly monitored during testing. The position of the RDD was constantly calculated using a distance encoding device based on the known starting position (Bay and Stokoe 1998). A picture of the RDD at the Marked Tree site is displayed in Figure 5.25.

5.6.2 RDD Data Analysis

During the RDD testing, a continuous deflection profile was calculated for each path. Raw deflection values were averaged over 1-ft (0.3-m) increments to smooth out noise. Only the Sensor 1 deflection data is presented herein. The continuous deflection profiles in the eastbound and westbound lanes are presented in Figure 5.26. Note that all of the highest deflections occurred in the westbound lane, particularly across from Section 10 and Sections 12, 13 and 13A, in the areas where significant rutting leading to failure had occurred. It is also important to point out that while the deflections in the westbound lane across from Section 13B (referred to as Section 13BW) were low this section had recently been patched due to excessive rutting, which resulted in lower dynamic deflections. The deflection values from the profiles within each 50-ft (15.2-m) long section were averaged to obtain a single deflection value for each section.

Figure 5.25. University of Texas's RDD at the Marked Tree site.
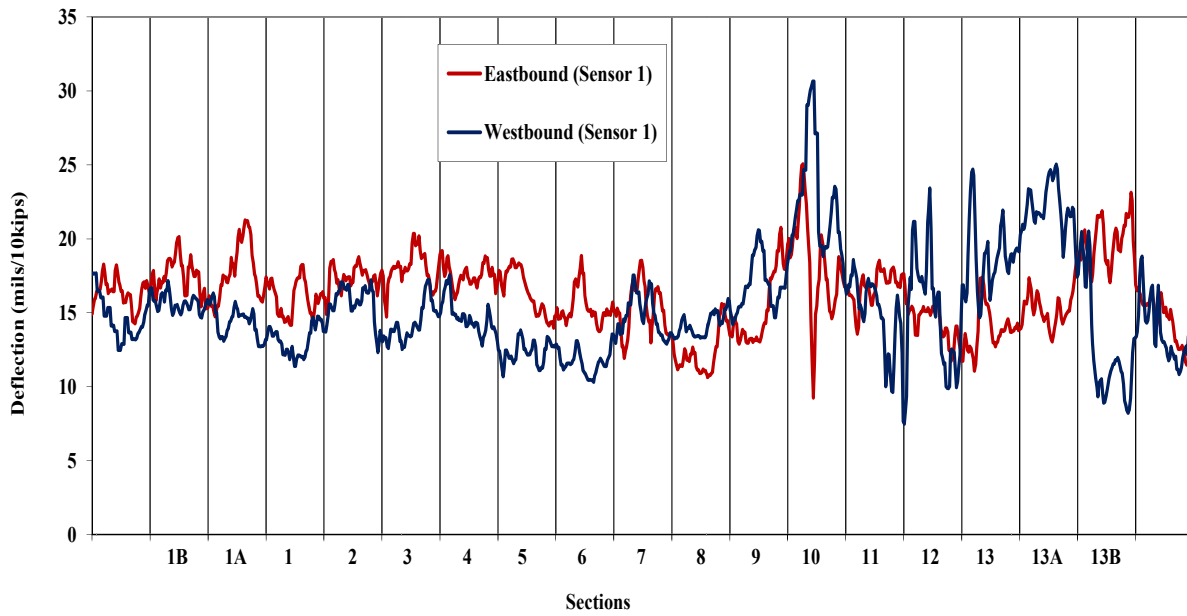
Figure 5.26. RDD Sensor 1 continuous deflection profile of the eastbound and westbound lanes at the Marked Tree site.

5.6.3 RDD Results

Only the RDD results from Sensor 1 were analyzed and ranked. Sensor 1 is located between the rolling loading wheels. The average deflection values are presented in terms of mils/10 kips. The results and ranks are presented in Table 5.21. Figure 5.27 is a graphical representation of the average deflection results. The deflection values in Table 5.21 indicate that the 10-in (25.4-cm) base sections only cover a range of 2.5 mils/10 kips, ranging from 15.4 to 17.9 mils/10 kips, while the 6-in (15.2-cm) base sections are more variable and cover a range of 7.5 mils/10 kips, ranging from 12.3 to 19.8 mils/10 kips. The RDD results do not really follow the same trend as the rutting results (i.e., generally better performance in Sections 1B – 9 than Sections 10 – 13B), and do not segregate the 10-in (25.4-cm) sections from the 6-in (15.2-cm) sections as clearly as the PLT and ADD results presented previously. Many of the 6-in (15.2-cm) sections yielded lower deflection values on average. This is perplexing because the continuous deflection profiles clearly detected anomalies (patches in the asphalt) that were present in the pavement. It is possible that either the static or dynamic load fluctuated slightly while driving down the pavement. However, Section 8 (the buttressed section) is one of the better performing sections in terms of RDD deflection, which agrees well with the average rut depth measurements that rank Section 8 second. Section 10 performed poorly during the RDD testing (ranked 15), which also has the worst average rut depth within the eastbound sections. Section 13B was the poorest performing section during the RDD testing, which is somewhat consistent with the ADD results presented herein. Yet, Section 13B does not have nearly the greatest average rut depth in comparison to all other 6-in (15.2-cm) sections.

Table 5.21. Average Sensor 1 deflections from RDD testing at the Marked Tree site.

	Section	East Bound		West Bound	
		Avg. Deflection (mils/10 kips)	Rank	Avg. Deflection (mils/10 kips)	Rank*
10" Nominal Base Thickness	1B	17.5	11		
	1A	17.7	13		
	1	16.0	7		
	2	17.3	10		
	3	17.9	14		
	4	17.5	12		
	5	16.4	8		
	6	15.4	6		
Transition	7	-	-	-	-
6" Nominal Base Thickness	8	12.3	1		
	9	15.3	4		
	10	18.2	15		
	11	16.8	9		
	12	14.3	3		
	13	13.9	2	18.5	17
	13A	15.4	5		
	13B	19.8	16	12.7	2

* Represents potential rank if west bound lane was included in ranking
(East Bound rankings would change accordingly).
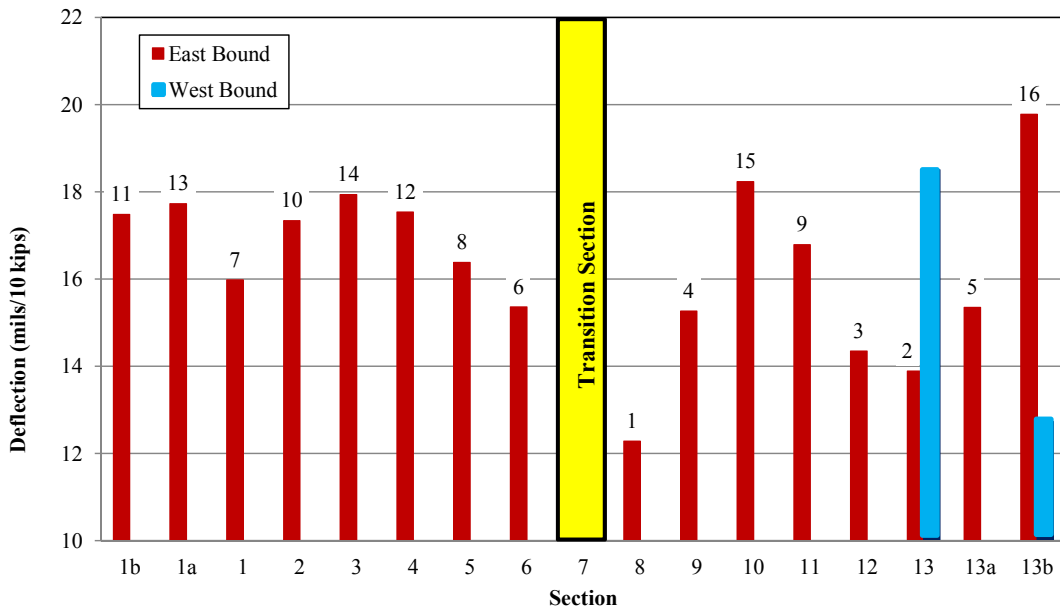
Figure 5.27. Sensor 1 average deflections from RDD testing at the Marked Tree site.

117

5.7 Composite Ranking from all Deflection-Based Test Results from the Marked Tree Site

A total composite ranking from the deflection-based testing performed at the Marked Tree site was calculated and used to rank the test sections. The composite value is the summation of the ranks from all the data analysis methods presented in the previous sections from the following tests: FWD, PLT, ADD, LWD, and RDD. Test-specific composite rankings were calculated for the deflection-based tests that had multiple data analysis methods associated with them (i.e., FWD, ADD, and LWD) prior to compiling the final composite ranking presented in this section. The test-specific composite rankings were created to avoid weighing the results from one test where multiple types of data analysis yielded a lot of rankings (e.g., ADD) more heavily than another test with only a single type of analysis and ranking (e.g., RDD). The test-specific composite values were then ranked from lowest composite value to highest composite value, receiving new overall rankings from 1 to 16, respectively. The composite rank values and new overall rankings are presented in Table 5.22 and are graphically represented in Figure 5.28. Note that the rankings in Table 5.22 and Figure 5.28 can be misleading. Though Section 1B and Section 6 are ranked 6 and 7, respectively, the difference in the composite values is exactly one, while Sections 9 and 12 are ranked 12 and 13, respectively; the difference in the composite values is 11.

The overall composite rankings agree with the average rut depth in the sense that Section 10 is the worst in terms of actual performance (average rut depth) and relative performance (composite ranking from deflection-based tests). However, Section 8 is ranked 7 in the deflection-based tests composite rankings, which is the best ranking of any 6-in (15.2-cm) nominal base section, but Section 8 has the second least amount of average rut depth among all

118

Table 5.22. Composite ranking from all deflection-based tests conducted at the Marked Tree site.

	Section	Composite	Rank
10" Nominal Base Thickness	1B	35	6
	1A	23	2
	1	14	1
	2	36	7
	3	32	5
	4	42	10
	5	26	3
	6	26	3
Transition	7	-	-
6" Nominal Base Thickness	8	36	7
	9	49	12
	10	76	16
	11	64	14
	12	60	13
	13	39	9
	13A	46	11
	13B	71	15

Note: composite values are composed of the summation of rankings from FWD, PLT, ADD, LWD, and RDD testing.
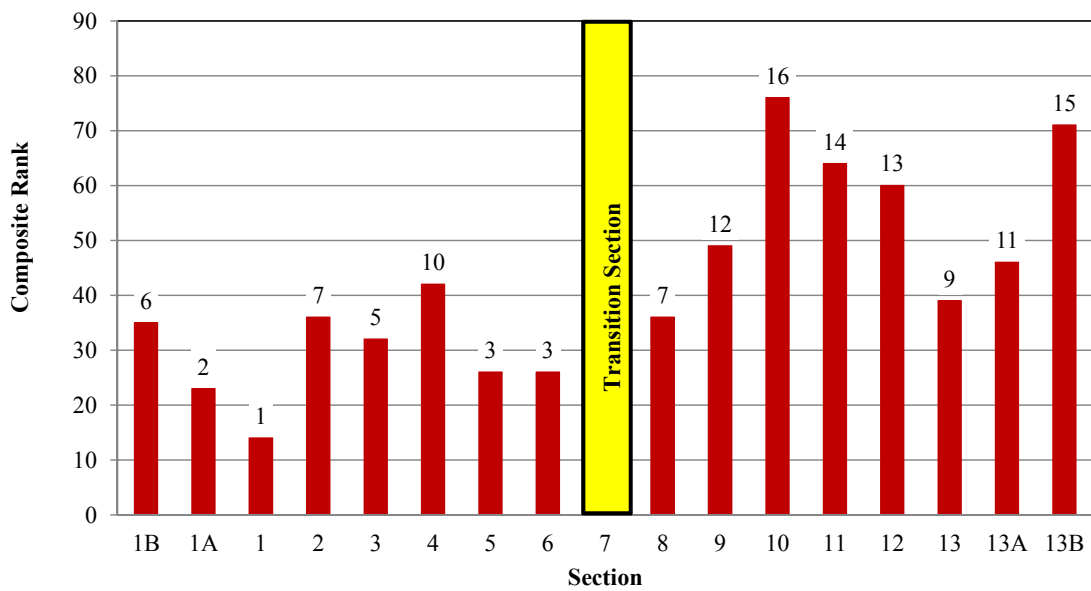
Figure 5.28. Composite ranking from all deflection-based testing at the Marked Tree site.

sections (refer to Figure 4.3). Additionally, Section 1 is ranked first in overall deflection-based tests, yet ranked worst among the 10-in (25.4-cm) nominal base course sections in terms of rutting. Obviously, the overall deflection-based composite rankings do not match exactly with the average rut depth rankings, but the composite deflection-based rankings somewhat agree with the general rutting trend of better performance in Sections 1B – 9 and poorer performance in Sections 10 – 13B. Furthermore, the overall deflection-based results also rank Sections 10, 11 and 12 (the three sections in the eastbound lane that had "failed" in terms of rutting) as three out of the top four poorest sections, excluding the two westbound areas (13W and 13BW) which were not tested during most of the deflection-based testing. It seems clear, based on rutting and the overall deflection-based results that the nominal base thicknesses [(10-inches (25.4-cm) versus 6-inches (15.2-cm)] significantly influences relative pavement performance and overwhelms subtle differences in geosynthetic type (or even no reinforcement) within any give base course thickness.

5.8 Composite Ranking from PLT and ADD Test Results from Marked Tree Site

It is clear from comparing the rankings for the individual deflection-based tests that the PLT and ADD tests yielded results that more closely correlated to rut depth than the other three deflection-based tests (FWD, LWD, and RDD). To determine if the combined results from these two deflection-based tests (PLT and ADD) could more closely approximate pavement performance than the composite of all five deflection-based tests (refer to Figure 5.28) the research group decided to develop a composite ranking only based on the final rankings for the PLT and ADD tests. These composite values are tabulated in Table 5.23 and graphically presented in Figure 5.29.

Table 5.23. Composite ranking from PLT and ADD tests conducted at the Marked Tree site.

	Section	Composite	Rank
10" Nominal Base Thickness	1B	6	3
	1A	3	1
	1	3	1
	2	11	5
	3	8	4
	4	16	8
	5	14	7
	6	16	8
Transition	7	-	-
6" Nominal Base Thickness	8	13	6
	9	20	10
	10	32	16
	11	30	15
	12	27	14
	13	23	11
	13A	24	12
	13B	26	13

Note: composite values are composed of the summation of rankings from PLT and ADD testing.
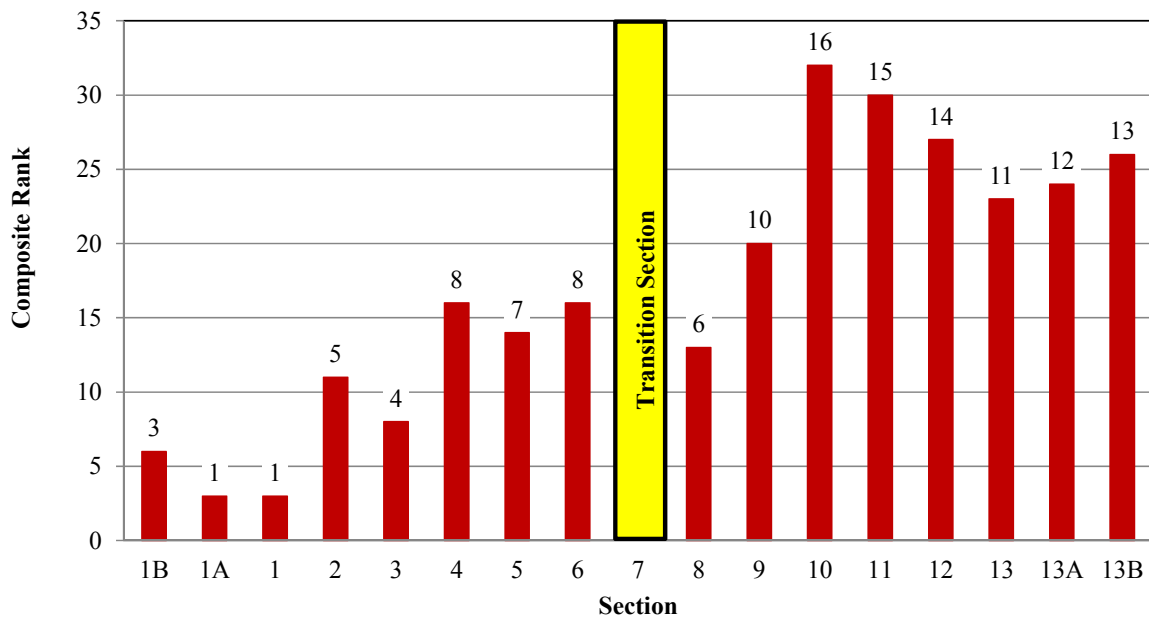
Figure 5.29. Composite ranking from PLT and ADD testing at the Marked Tree site.

In comparison with the average rut depth rankings presented in Figure 4.3, it is clear that the composite rank of the PLT and ADD rankings has the same general rutting trend of better performance in Sections 1B – 9 and poorer performance in Sections 10 – 13B. Furthermore, the overall deflection-based results also rank Sections 10, 11 and 12 (the three sections in the eastbound lane that had "failed" in terms of rutting) as the three worst sections in terms of deflection-based results from PLT and ADD. Additionally, Section 8 was the best 6-in (15.2-cm) nominal base section in terms of both deflection-based results from PLT/ADD and rutting measurements. However, the deflection-based results from PLT and ADD still indicate that Section 1 (unreinforced) is one of the best sections overall despite being the worst 10-in (25.4-cm) nominal section in terms of rutting. The combined PLT and ADD results are a slight improvement over the composite results from all deflection-based tests, but still do not match the rutting measurements exactly.

Again, no clear pattern exists in the combined PLT and ADD data that would suggest a difference in performance base on geosynthetic type, or even a favorable difference between reinforced and unreinforced sections within a given nominal base course thickness.

5.8 Conclusions from Deflection-Based Test Results

Results from PLT and ADD deflection-based tests (Figure 5.29) clearly identified Sections 10, 11 and 12 as the worst sections in the eastbound lane (note that deflection-based tests were generally not conducted in Sections 13W and 13BW in the westbound lane). These sections were also the same sections that had "failed" based on rutting measurements (Figures4.2 and 4.3). Therefore, one may conclude that these tests were successful at inferring relative pavement performance in terms of identifying sections that had, or were about to, rut to the point

of "failure". Furthermore, the PLT and ADD deflection-based tests also clearly indicated the general rutting trend of better performance in Sections 1B – 9 and poorer performance in Sections 10 – 13B. However, beyond successfully identifying failed sections and showing general agreement in rutting trends, the deflection-based tests did not perfectly correlate with the more subtle differences in pavement performance as quantified by average rut depth values. For example, Section 1 (unreinforced) has the highest combined PLT and ADD deflection-based composite ranking, yet Section 1 has the greatest average rut depth among the 10-in (25.4-cm) base sections. Still, the average April 2011 rut depth difference between the best ranked section (Section 6) and the 11th ranked section (Section 1) is only approximately 0.19 in (0.48 cm) and due to the method for collecting the average rut depth values they can only be considered accurate within approximately +/- 0.125 in (0.318 cm).

Trends indicating benefits from the addition of geosynthetics are hard to observe in either the rutting measurements or results from the deflection-based tests. Among the deflection-based tests analyzed herein, the PLT and ADD test agreed best with the average rut depth values and these tests should be further studied to determine if they can detect more subtle differences in relative pavement performance. Some sort of data normalization based on absolute base course thickness or pavement stiffness may be required to detect these subtle differences. No doubt others will seek to analyze and interpret this data in a different manner in the future.

Chapter 6

6.0 Forensic Excavation and Subsurface Layer Properties

6.1 Overview

In the Spring of 2010, AHTD personnel noticed that some of the sections of Frontage Road 3, especially in the westbound lane, were failing or nearing failure. In a few locations, rut depths exceeded several inches (refer to Figure 6.1). The research group was faced with answering the question of what factor, or combination of factors, was responsible for failure in certain sections and not others. So, it was decided that a forensic excavation needed to be conducted in each of the test sections in the eastbound lane, as well as a couple of areas in the westbound lanes opposite Sections 13 and 13B (referred to as Sections 13W and 13BW) where significant rutting was observed.

The forensic excavation was conducted during the October 2010 site visit. Additional in-situ test were conducted and samples were gathered in all sections for laboratory testing. These samples included bagged samples, bulk samples, and Shelby tube samples. The process of the forensic excavation, as well as the layer and soil properties determined through the forensic excavation, are discussed in this chapter. A composite rank of the soil and layer properties deemed to be influencing failure is calculated and compared to the average rut depth values presented in Chapter 4 (refer to Table 4.4 and Figure 4.6) to determine why failure occurred in certain sections and not others.

6.2 Introduction

Prior to the October 2010 Marked Tree site visit, the research group decided to conduct tests on top of the asphalt layer, the base layer, and the subgrade layer in a 2-ft x 2-ft (0.61-m x

Figure 6.1. Rut depth exceeding 3 inches (7.6 cm) in Section 13BW during May 2010.

0.61-m) square testing area in the outside (right) wheel path 8-ft east of the center of each section. To conduct tests on top of the base layer and the subgrade layer, the asphalt and base layers, respectively, had to be removed sequentially from each section. Prior to removal of the asphalt, LWD tests were conducted on the 2-ft x 2-ft (0.61-m x 0.61-m) square testing area in each section. After removing the asphalt and measuring its thickness, LWD, nuclear density, dynamic cone penetrometer (DCP), and in-situ California Bearing Ratio (CBR) tests were conducted on the base layer in each section. Nuclear density gage readings were collected in 2-inch (5.1-cm) increments by advancing the nuclear gage probe through the base material. During removal of the base layers, bag and bucket bulk samples were obtained every 2 inches (5.1 cm) for testing of in-situ moisture content and base layer gradation as a function of depth. After removing the base layers and measuring their thickness, nuclear density gage readings were

125

collected in 2-inch (5.1 cm) increments through the top 12 inches (30.5 cm) of the subgrade. Then, in-situ CBR tests were conducted on the subgrade layer and undisturbed (Shelby tube) samples were pushed in the northeast and southwest corners of the testing area. Additionally, bag samples for in-situ moisture content and plasticity index were collected every 2 inches (5.1 cm) of subgrade down to 6 inches (15.2 cm).

The in-situ DCP and CBR tests conducted on the base and subgrade layers were used to determine the relative stiffness of the two layers in each section. Additionally, resilient modulus (Mr) and unconsolidated undrained (UU) triaxial tests were conducted on the Shelby tube samples collected in the subgrade to evaluate the stiffness/strength properties of the subgrade soils. The excavation, sampling, and testing procedures previously discussed will be described in greater detail, along with the results, in the following sections.

6.3 Forensic Excavation

On the October 2010 Marked Tree site visit, the research group conducted a forensic excavation in each test section, including 13W and 13BW. The forensic excavation was conducted so the research group could perform in-situ tests on, and collect samples of, the base layer and subgrade layer to attempt to determine why certain sections were performing more poorly than others. The forensic excavation was conducted in the following sequence for each test section:

1. The locations for the 2-ft x 2-ft (0.61-m x 0.61-m) excavation and testing locations were marked 15 feet (4.6 m) east of the sensor locations in each section on the outside wheel path (Figure 6.2).

2. LWD tests were conducted on the asphalt layer using a 12-in (30.5-cm) diameter plate and a 6-in (15.2-cm) diameter plate. (refer to Section 5.5 and Figure 5.19).

3. The perimeter of the 2-ft x 2-ft (0.61-m x 0.61-m) layer of asphalt was carefully cut using a concrete saw (Figure 6.3a) and the asphalt layer was removed with a pry-bar
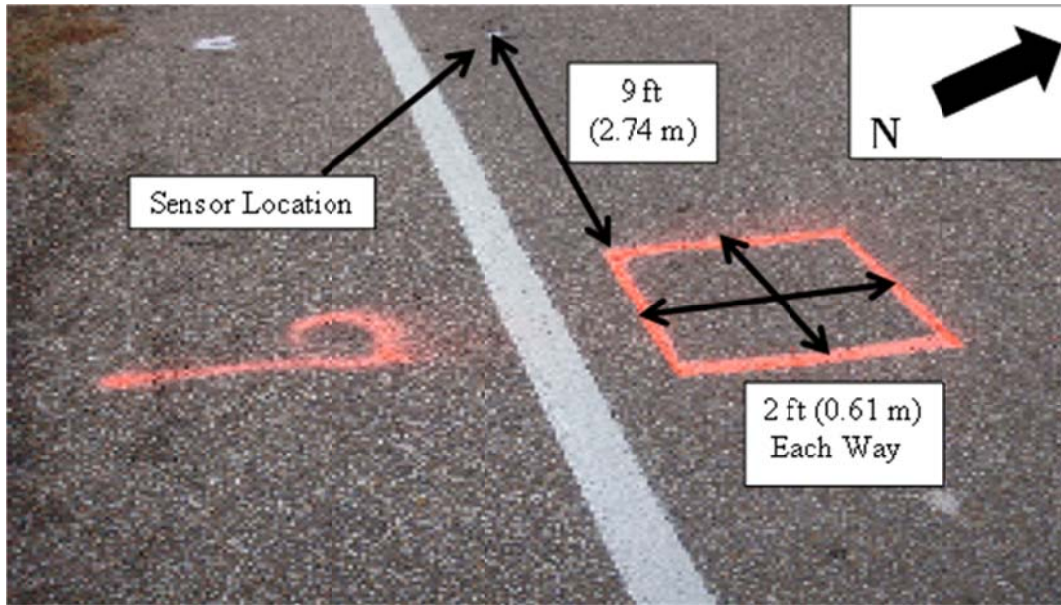
Figure 6.2. Excavation and testing area at Section 9 during October 2010 Marked Tree site visit.

(Figure 6.3b). No water was used during the asphalt cutting to ensure accuracy of in-situ moisture content data for the base and subgrade.

4. Asphalt layer thickness measurements were conducted at each corner and in the center of the excavation area using a small scale and a metal rut bar.

5. Nuclear density gauge readings were collected by continuously advancing the probe every 2 inches (5.1 cm) through the base in the northwest corner of the excavation area (Figure 6.4a).

6. DCP tests were conducted through the base and well into the subgrade [at least 47 inches (120 cm)] in the southeast corner of the excavation area (Figure 6.5).

7. LWD tests were conducted on the base layer using a 12-in (30.5-cm) diameter plate and a 6-in (15.2-cm) diameter plate (refer to Figure 5.19).

8. In-situ CBR tests were conducted on the base layer (Figure 6.6a).

9. In-situ moisture content and bulk samples were collected every 2 inches (5.1 cm) of base course (Figure 6.7).

10. The base course was completely excavated to the subgrade-base interface for Sections 1 and 13 (Figure 6.8), and the base was completely excavated to the subgrade-geosynthetic interface for all other sections (Figure 6.9). The geosynthetics were cut out of the test area and stored in bags for testing discussed in Boga (2011).

<div align="center">(a)   (b)</div>

Figure 6.3. Cutting (a) and removal (b) of asphalt layer for base course testing and sampling.

<div align="center">(a)   (b)</div>

Figure 6.4. Nuclear density gauge readings conducted on the base (a) and subgrade (b) layers.

Figure 6.5. DCP test conducted in southeast corner of excavation area of Section 13W.

(a)   (b)

Figure 6.6. CBR tests conducted on base (a) and subgrade (b) layers.

Figure 6.7. Base layer excavation and sampling at Section 2.

Figure 6.8. Base-subgrade interface of Section 1 (no geosynthetics).

Figure 6.9. Subgrade-geosynthetic interface of Section 1A (Mirafi geogrid).

11. Base course and asphalt combined thickness (total thickness) measurements were conducted at each corner and in the center of the section using a steel tape and a metal rut bar. Base course thicknesses were inferred from subtracting the asphalt layer thicknesses from the total thickness measurements.

12. Once the subgrade layer was reached, nuclear density gauge readings were collected by continuously advancing the probe every 2 inches (5.1 cm) through the subgrade to a depth of 12 inches (15.2 cm) (Figure 6.4b).

13. In-situ CBR tests were conducted on the subgrade layer (Figure 6.6b).

14. Shelby tubes [30-in (76.2-cm) long; 3-in (7.6-cm) diameter] were pushed to a depth of 24 inches (60.9 cm) in the northeast and southwest corners of each excavation area to collect undisturbed samples for lab testing (Figure 6.10).

15. Bag samples for in-situ moisture content and plasticity index testing were collected every 2 inches (5.1 cm) for the first 6 inches (15.2 cm) of subgrade.

The soil properties determined from the in-situ testing and laboratory testing conducted as part of the forensic excavation are discussed in the following sections.

Figure 6.10. Shelby tube pushed in southwest corner of excavation area.

6.4 Layer Properties

Prior to visiting the Marked Tree site on October 2010, the research group was uncertain of the current subgrade and base properties within each test section. During construction of the test sections, survey data presented in Howard (2006) was collected to document the approximate thicknesses of the asphalt and base layers. However, there was limited data provided on the constructed density and moisture content of the base or subgrade (refer to Chapter 3).This section presents the layer thickness, in-situ moisture content, dry density, and plasticity index information gathered in each section during the October 2010 forensic excavation.

6.4.1 Layer Thicknesses

The layer thicknesses were calculated as the different layers were extracted from the 2-ft x 2-ft (0.61-m x 0.61-m) square testing area. For example, once the asphalt layer was removed,

there were five thickness measurements collected: one in the center and one at each of the four corners. To ensure continuity in the thickness measurements between layers, a flat metal bar was placed across the test area, and thicknesses were measured relative to the nearest edge of the bar. The bar used for measuring thicknesses was the same bar used for measuring rut depths and is referred to herein as a "rut bar".

The five asphalt thickness values were averaged together to obtain one comparable value for each section. These thickness values were also obtained for the areas adjacent to Sections 13 and 13B in the west bound lane, referred to as 13W and 13BW. The same procedure was used to obtain the average base course thickness in each section. The averaged values and rankings assigned to each section are presented in Table 6.1 and Figures 6.11, 6.12, and 6.13. Figure 6.11 is a plot of the asphalt thicknesses, Figure 6.12 is a plot of the base thicknesses, and Figure 6.13 is a plot of the total asphalt plus base thickness. The rankings for each section are located over the bar for each section, excluding the west bound lane sections, which were not included in the overall rankings since these sections had not previously been a focus of testing at the site. However, the reader is reminded that these sections (13W and 13BW) were added to the forensic excavation because failure (major rutting) had occurred in them.

The asphalt thicknesses at the site vary from 2.0 – 2.65 inches (5.1 – 6.7 cm). There is no clear pattern for changes in asphalt thickness in the 10-in (25.4-cm) nominal base course sections, but the asphalt thickness tends to increase from Section 8 to Section 13B in the 6-in (15.2-cm) nominal base course sections.

The base course thicknesses in the 10-in (25.4-cm) nominal sections vary from 8.9 – 11.3 inches (22.6 – 28.7 cm), with Section 4 and Section 1 (unreinforced) having the least and greatest base thicknesses, respectively. Furthermore, the total base plus asphalt thicknesses in the

Table 6.1. Layer thicknesses collected during October 2010 site visit.

	Section	Eastbound Thicknesses (in)			Rank	Westbound Thicknesses (in)			Rank*
		Asphalt	Base	Total		Asphalt	Base	Total	
10" Nominal Base Thickness	1b	2.30	9.33	11.63	7				
	1a	2.24	9.64	11.88	5				
	1	2.08	11.33	13.40	1				
	2	2.23	9.95	12.17	3				
	3	2.39	9.64	12.03	4				
	4	2.08	8.90	10.98	8				
	5	2.46	10.14	12.60	2				
	6	2.13	9.70	11.83	6				
	7	-	-	-	-	-	-	-	-
6" Nominal Base Thickness	8	2.00	7.18	9.18	9				
	9	2.15	6.50	8.65	12				
	10	2.23	5.60	7.83	16				
	11	2.15	6.48	8.63	13				
	12	2.31	5.76	8.08	15				
	13	2.38	6.55	8.93	10	2.21	5.67	7.88	16
	13a	2.55	6.13	8.68	11				
	13b	2.65	5.45	8.10	14	1.92	5.33	7.25	18

Note: Rank was decided by Total Thickness; Total Thickness is the sum of asphalt and base thicknesses.
* Represents potential rank if west bound lane was included in ranking (East Bound rankings would change accordingly).
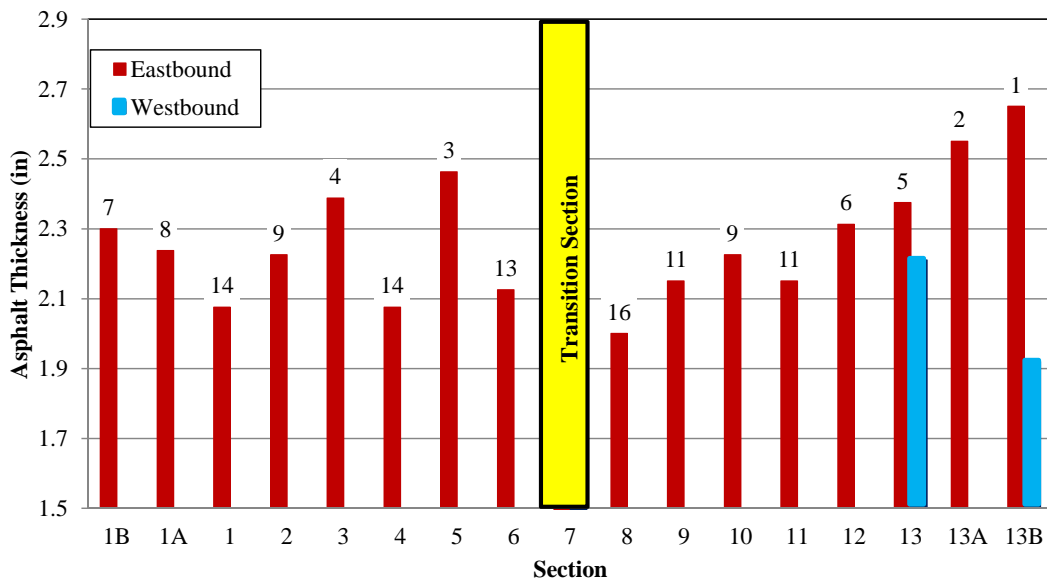
Figure 6.11. Asphalt thicknesses collected during October 2010 site visit.

134
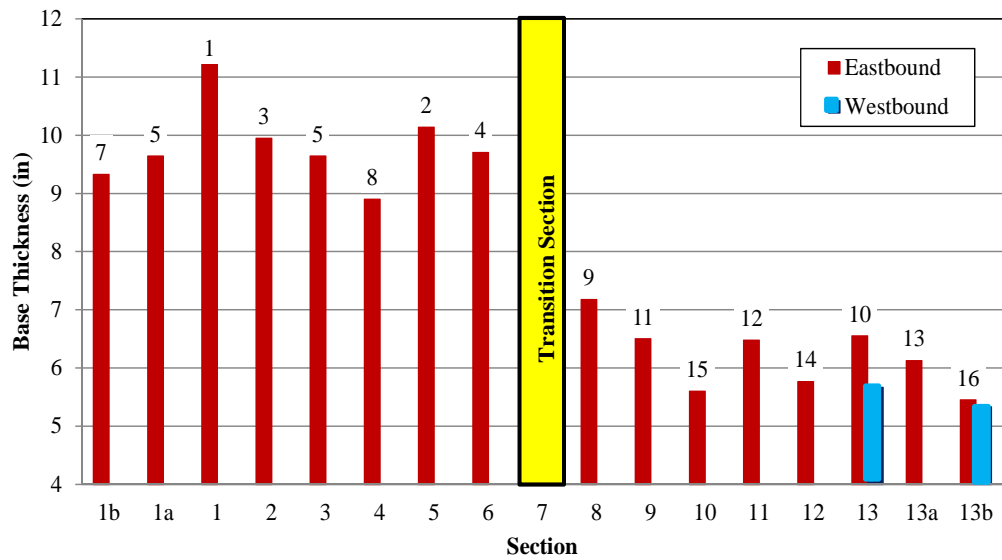
Figure 6.12. Base thicknesses collected during October 2010 site visit.
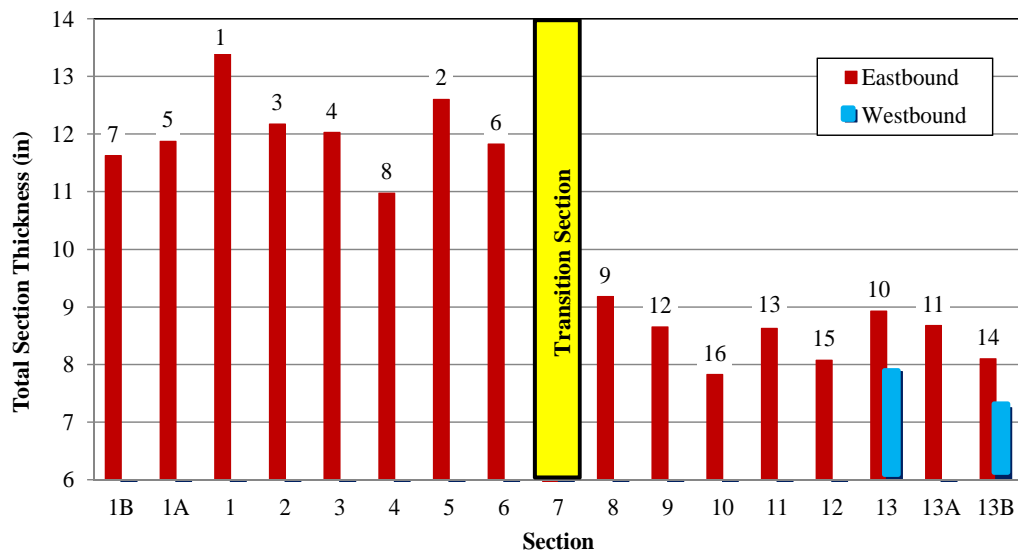
Figure 6.13. Total asphalt and base section thicknesses collected during October 2010 site visit.

10-in (25.4-cm) nominal sections vary from 10.98 – 13.4 inches, again with Section 4 and Section 1 (unreinforced) having the least and greatest asphalt plus base thicknesses, respectively.

Coincidentally (or perhaps not), Sections 4 and 1 are also generally ranked as "worst" and "best" among the 10-in (25.4-cm) nominal base course sections via the combined PLT and ADD deflection-based rankings (refer to Figure 5.29). These deflection-based tests are heavily influenced by the thickness of the pavement material over the subgrade. The base course thicknesses in the 6-in (15.2-cm) nominal sections vary from 5.5 – 7.2 inches (14.0 – 18.3 cm), with Section 13B and Section 8 having the least and greatest base thicknesses, respectively. Furthermore, the total base plus asphalt thicknesses in the 6-in (15.2-cm) nominal sections vary from 7.8 – 9.2 inches (19.9 – 23.3 cm), with Sections 10 and 8 having the least and greatest asphalt plus base thicknesses, respectively. Coincidentally (or perhaps not), Sections 10 and 8 are also generally ranked as "worst" and "best" among the 6-in nominal base course sections via the combined PLT and ADD deflection-based rankings. Furthermore, all of the sections that have "failed" (Sections 10, 11, 12, 13W and 13BW) according to the rutting data [> 0.5 in (1.3 cm) of rutting] also have the lowest combined asphalt and base course thicknesses (approximately 8 inches or less; refer to Figure 6.13). This cannot be coincidental. It should also be noted here that a very clear interface existed between the base and subgrade during excavation of the unreinforced sections (i.e., Sections 1 and 13), and that no significant loss of base course into the subgrade or migration of fines into the base course was observed. Migration of fines into the subgrade was studied in depth by Boga (2011).

6.4.2 Moisture Content

Moisture content of the base and subgrade layers plays a significant role in the performance of any pavement. Furthermore, it is important to investigate the role that different geosynthetic reinforcements play in how moisture moves throughout the pavement structure. During the October 2010 visit, the ground on the shoulder and ditch line south of the roadway

was very dry, creating desiccation cracks several feet deep (Figure 6.14). Despite the fact that the surrounding ground was extremely dry, pooling/slowly flowing water was found on top of the subgrade in certain sections. An example of this is shown in Figure 6.15 for Section 13W. Water appeared to be flowing through the slit-film geotextile along the interface between the base and the subgrade. During construction this slit-film geotextile was placed along the entire westbound lane and overlapped significantly into the eastbound lane (refer to Chapter 3). It did not appear that any of the geotextiles in the road were "daylighted". Meaning, water that infiltrated the pavement anywhere along the road was likely flowing through the geotextiles and pooling at low spots on top of the CH subgrade instead of draining out the edges of the pavement. Furthermore, while the ground was extremely dry in October 2010, the ditch on the south side of the road was filled with water on many site visits (refer to Figure 6.16). During particularly wet seasons, water would pool in the ditches all along the test sections, but would linger longer in the ditch south of the 6-in (15.2-cm) nominal sections.

In-situ moisture content samples were collected and weighed wet in the field for gravimetric moisture content measurements during the forensic excavation. These samples were collected every 2 inches (5.1 cm) throughout the base layer and every 2 inches (5.1 cm) for the first 6 inches (15.2 cm) of the subgrade. The moisture content values for these samples were determined at the University of Arkansas lab in accordance with ASTM D2216-09. While moisture content values were collected every 2 inches, all of the base moisture contents and all of the subgrade moisture contents have been averaged herein to obtain a single gravimetric moisture content for the base and subgrade in each section. The in-situ moisture content values of the base and subgrade are presented in Tables 6.2 and 6.3, respectively. The in-situ moisture
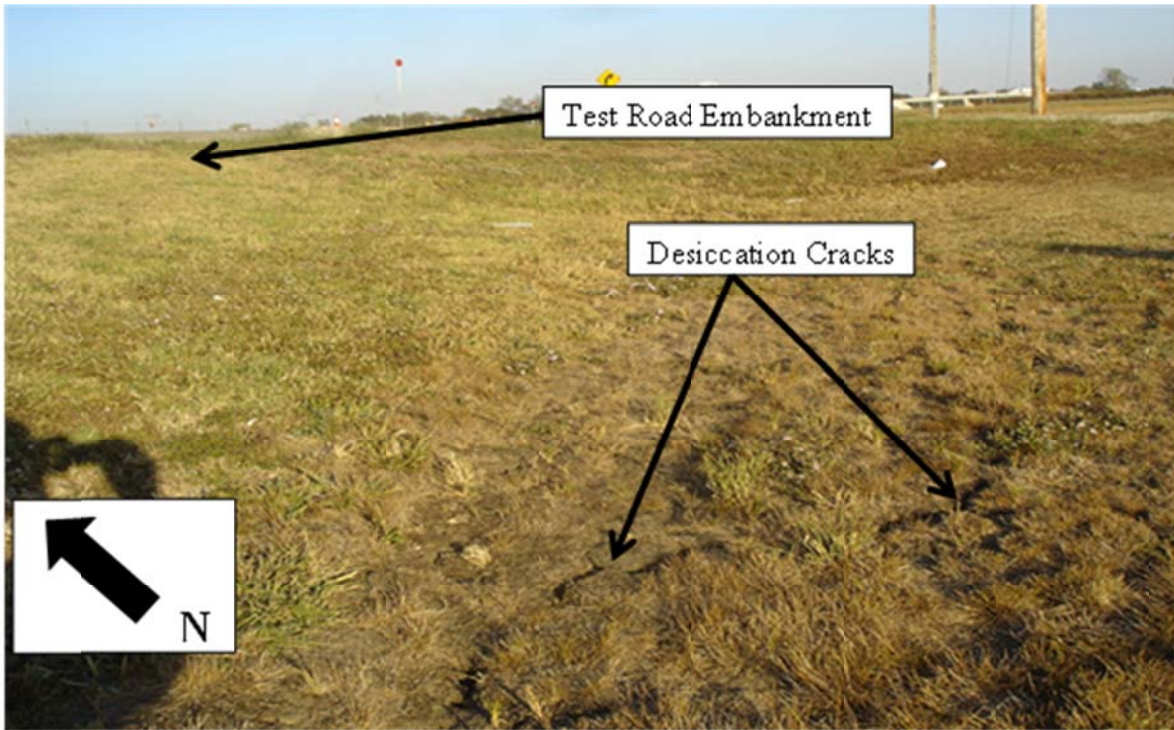
Figure 6.14. Desiccation cracks in ground south of test site in October 2010.

Figure 6.15. Pooling water on subgrade of Section 13W in October 2010.

Figure 6.16. Standing water south of Sections 8 through 13B in May 2011.

Table 6.2. Average in-situ gravimetric base moisture contents from the October 2010 site visit.

	Section	East Bound		West Bound	
		Water Content (%)	Rank	Water Content (%)	Rank*
10" Nominal Base Thickness	1B	3.82	16		
	1A	3.49	14		
	1	2.77	4		
	2	3.54	15		
	3	3.43	13		
	4	3.04	8		
	5	2.55	1		
	6	2.92	6		
Transition	7	-	-	-	-
6" Nominal Base Thickness	8	2.63	2		
	9	3.30	12		
	10	3.28	11		
	11	2.76	3		
	12	3.23	10		
	13	3.00	7	4.57	18
	13A	2.85	5		
	13B	3.16	9	3.66	16

* Represents potential rank if west bound lane was included in ranking
(East Bound rankings would change accordingly).

139
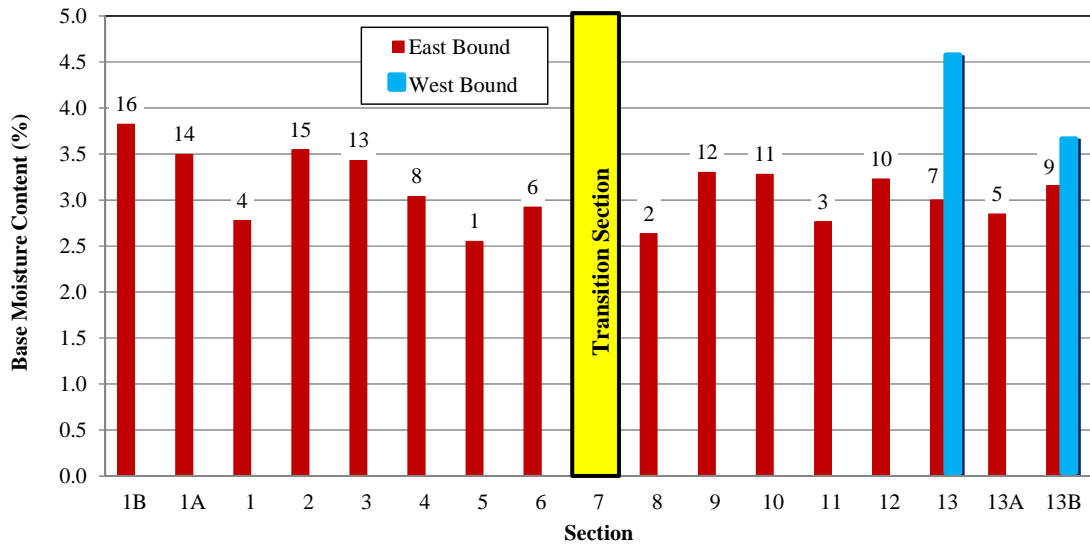
Figure 6.17. Average in-situ base gravimetric moisture contents from samples collected in October 2010.

Table 6.3. Average in-situ gravimetric subgrade moisture contents from the October 2010 site visit.

	Section	East Bound		West Bound	
		Water Content (%)	Rank	Water Content (%)	Rank*
10" Nominal Base Thickness	1B	15.47	1		
	1A	16.69	3		
	1	16.33	2		
	2	20.46	7		
	3	21.19	8		
	4	22.96	10		
	5	23.24	11		
	6	23.88	14		
Transition	7	-	-	-	-
6" Nominal Base Thickness	8	23.47	13		
	9	21.19	9		
	10	23.35	12		
	11	23.95	15		
	12	19.13	5		
	13	32.24	16	26.97	17
	13A	17.43	4		
	13B	20.43	6	22.47	10

* Represents potential rank if west bound lane was included in ranking
(East Bound rankings would change accordingly).

140
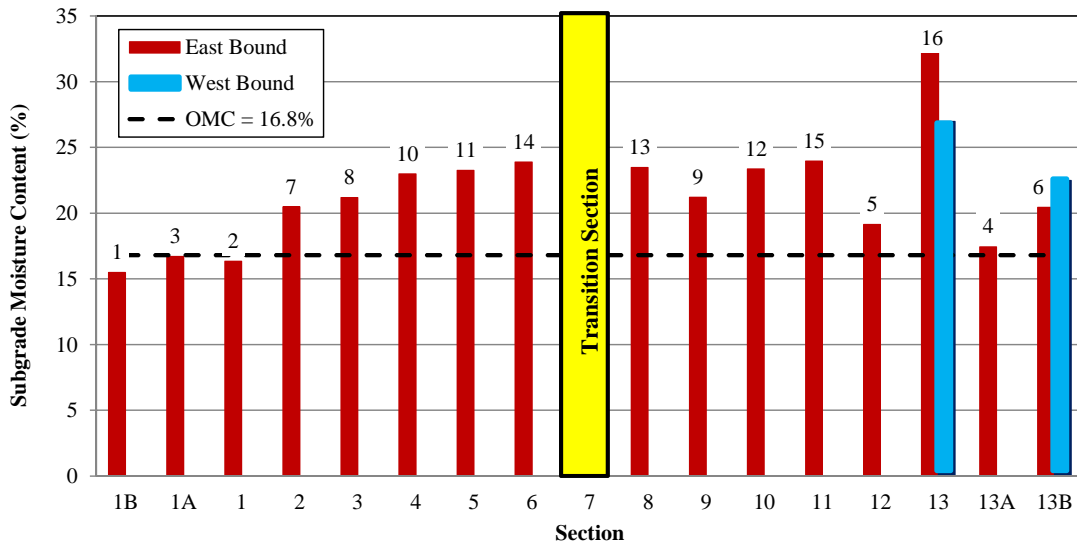
Figure 6.18. Average in-situ gravimetric subgrade moisture contents from samples collected in October 2010.

content values and ranks for the base and subgrade layers are also graphically displayed in Figures 6.17 and 6.18, respectively.

The average base moisture content values only range from approximately 2.6% - 3.8%, which are much lower than the optimum moisture content range of 6.5% - 8.2% reported in Howard (2006) (refer to Table 3.4). Therefore, on average, the base would be considered quite dry at the time of the forensic excavation with no significant differences between sections. According to Howard (2006), the optimum moisture content (OMC) of the compacted subgrade was 16.8% (refer to Chapter 3, Section 3.3.1). Note, from the in-situ moisture content data collected during October of 2010, only Sections 1B, 1A, 1, and 13A are within ± 2% of OMC. The average moisture contents from Sections 2 through 13B, excluding 13A, are wet of optimum and range from approximately 19.1% - 32.2%. However, the majority of the sections have a subgrade moisture content between 20% - 25%. Recalling that Sections 10, 12, 13W and 13BW had "failed" according to rutting, there does not appear to be a strong direct correlation between

141

subgrade in-situ moisture content and the pavement performance, especially considering that Section 13 had the highest subgrade moisture content and had not "failed" and Section 12 had the fifth lowest moisture content and had "failed". However, there could be a hidden, indirect link between the pavement performance and the combined effects of total section thickness and subgrade moisture content.

6.4.3 Plasticity Index

During the forensic excavation in October 2010, bag samples of the subgrade were collected every 2 inches (5.1 cm) down to a depth of 6 inches (15.2 cm) for plasticity index (PI) testing. The plasticity index testing was conducted per ASTM D4318 as documented in Boga (2011). The bag samples were oven dried then ground up and passed through a No. 40 sieve until enough material was obtained to conduct the liquid limit (LL) and plastic limit (PL) tests.

The plasticity index (PI) is the range of water content over which a soil behaves plastically, or the difference between the LL and the PL. PI values were calculated for three 2-in (5.1-cm) layers in the top 6 inches (15.2 cm) of subgrade soil by Boga (2011). These values were then averaged herein to obtain one overall PI value for each section. The average PI values and the associated rankings are presented in Table 6.4. The lowest PI value has the best ranking and so on. The PI values and ranks are graphically displayed in Figure 6.19.

The plasticity index values range from approximately 13 (Section 1A) to 41 (Section 13). Despite being unreinforced, with the highest average in-situ subgrade water content and the highest average subgrade PI, Section 13 is not one of the sections that has "failed" according to rutting data (refer to Figures 4.2 and 4.3). Furthermore, Section 12, which has "failed", has the second lowest PI. It does not appear that the subgrade PI values have a direct correlation to the pavement performance for the current data set.

142

Table 6.4. Average plasticity index (PI) values of subgrade soils at Marked Tree site.

| | Section | East Bound | | | | West Bound | | | |
		LL	PL	PI	Rank	LL	PL	PI	Rank*
10" Nominal Base Thickness	1B	36	17	19	3				
	1A	29	16	13	1				
	1	36	15	21	4				
	2	39	18	21	4				
	3	45	19	26	7				
	4	49	19	30	13				
	5	48	19	29	11				
	6	55	23	32	14				
Transition	7	-	-	-	-	-	-	-	-
6" Nominal Base Thickness	8	53	26	27	8				
	9	46	18	28	9				
	10	49	21	28	9				
	11	51	22	29	11				
	12	32	14	18	2				
	13	66	25	41	16	60	19	41	17
	13A	62	22	40	15				
	13B	40	16	24	6	47	19	28	11

* Represents potential rank if west bound lane was included in ranking (East Bound rankings would change accordingly).
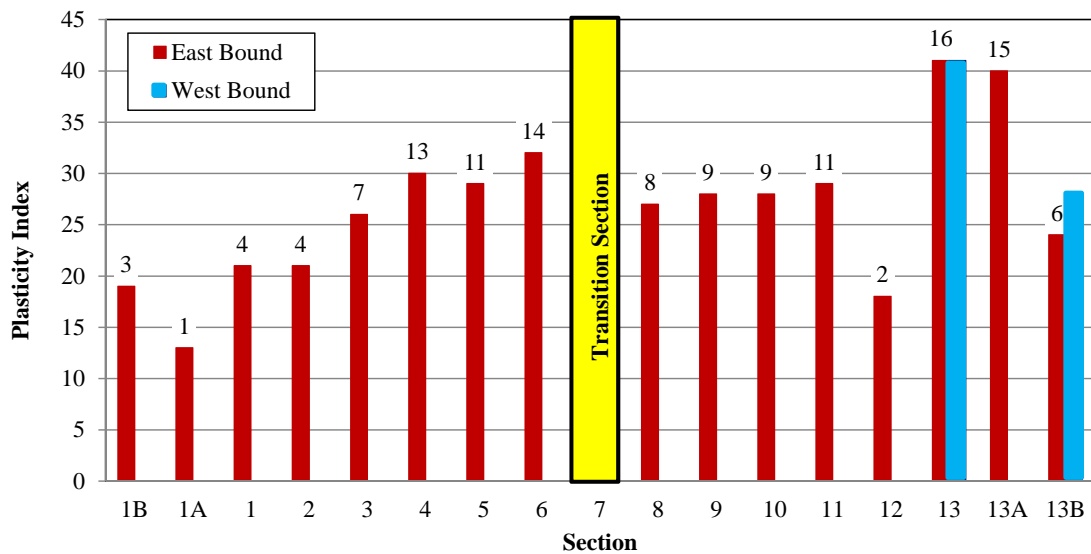
Figure 6.19. Average plasticity index (PI) values of subgrade soils at Marked Tree test site.

6.4.4 Dry Density

Estimates of in-situ dry density were calculated using two methods. The first method was based on nuclear density gage readings in each layer collected at 2-inch (5-cm) increments throughout the base and the first 6 inches (15.2 cm) of the subgrade. The total density values collected from the nuclear density gauge were used to calculate dry density using the gravimetric moisture contents discussed in Section 6.4.2. Meaning, the estimates of moisture content from the nuclear density gage were not used to calculate dry density because the gravimetric moisture contents were believed to be more accurate. Average dry densities for the base and subgrade calculated using total density values from the nuclear density gage and gravimetric water contents are provided in Table 6.5. The base dry density values are plotted in Figure 6.20 and range from 136.4 to 149.7 pcf (2265 – 2398 kg/m^3). The range of maximum base dry densities from modified proctor tests presented in Howard (2006) is approximately 142.2 to 144.0 pcf (2278 – 2307 kg/m^3), and the constructed dry densities measured with a nuclear gauge ranged from approximately 148.5 to 150.3 pcf (2379 – 2408 kg/m^3), which were believe to be too high (refer to Table 3.4). The base dry density values are randomly varying amongst the sections, yet the average variation of base dry density between sections is approximately 3.2 pcf (51.3 kg/m^3).

Note that of the sections that have "failed" (Section 10, 11, 12, 13W and 13BW) , only Section 13BW has a substantially lower in-situ base dry density [136.4 pcf (2185 kg/m^3)], which is only 6 pcf (96 kg/m^3) below the maximum dry density and still within 95% of modified proctor. Furthermore, Section 11 has the highest in-situ base dry density. Again, for this data set it does not appear that differences in the dry density of the base are closely correlated to pavement performance.

Table 6.5. Average in-situ dry density values of base and subgrade at the Marked Tree site obtained from nuclear gage total density and gravimetric water content.

| | | East Bound | | | | West Bound | | | |
| | | Base | | Subgrade | | Base | | Subgrade | |
	Section	Avg. Dry Density (pcf)	Rank	Avg. Dry Density (pcf)	Rank	Avg. Dry Density (pcf)	Rank*	Avg. Dry Density (pcf)	Rank*
10" Nominal Base Thickness	1B	147.1	10	112.6	1				
	1A	143.2	14	104.6	3				
	1	149.4	4	105.4	2				
	2	141.4	16	98.5	15				
	3	143.0	15	103.2	6				
	4	147.2	9	99.1	12				
	5	149.4	3	101.2	8				
	6	148.8	5	98.7	13				
Transition	7	-	-	-	-	-	-	-	-
6" Nominal Base Thickness	8	149.5	2	100.0	10				
	9	146.0	12	103.5	4				
	10	148.4	6	98.7	14				
	11	149.7	1	99.3	11				
	12	146.6	11	102.0	7				
	13	147.6	8	96.2	16	147.2	10	92.4	18
	13A	144.4	13	103.4	5				
	13B	147.9	7	100.8	9	136.4	18	98.8	13

* Represents potential rank if west bound lane was included in ranking (East Bound rankings would change accordingly).

Avg. dry density values were determined from total density readings from nuclear density gauge and in-situ moisture content.
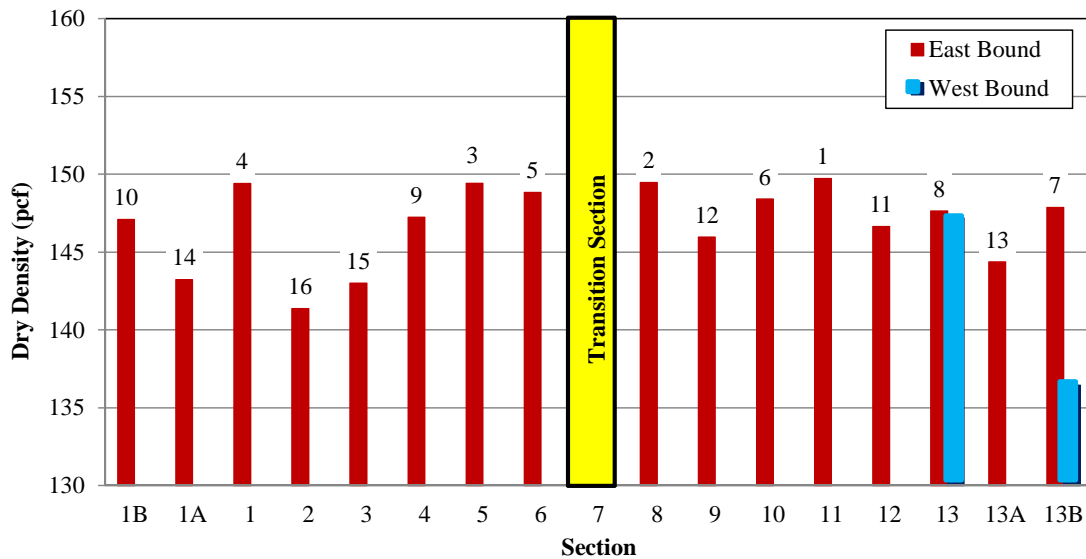
Figure 6.20. Base in-situ dry densities calculated from October 2010 site visit.

The other method only allows for the calculation of the subgrade dry density. This method utilized the Shelby tube samples from both resilient modulus (Mr) testing and unconsolidated undrained (UU) triaxial testing of intact subgrade specimens. A total density value was calculated for each Shelby tube sample. The height and diameter were calculated by averaging three measurements of each, for each sample, to use for the volume calculations. Then, the moist sample was weighed and divided by this volume, producing total density. Once the total density and water content values were calculated for each sample, the dry density values were easily obtained. The Shelby tube sample dry densities from Mr and UU testing are presented in Tables 6.6 and 6.7, respectively.

The subgrade dry density values from all three estimates were averaged together to account for variances in the multiple determination methods, as well as to have one number for comparison to pavement performance for each section. The average dry density values of the subgrade and the associated rankings are presented in Table 6.8 and Figure 6.21. The average subgrade dry density values range from 94.8 to 110.2 pcf (1519 – 1765 kg/m^3). The maximum proctor dry density determined in Howard (2006) was approximately 106 pcf (1698 kg/m^3). The initial compacted subgrade in October of 2004 did not achieve maximum dry density in any sections (refer to Figure 3.11). However, after reworking of the subgrade in June 2005 all sections exceeded maximum dry density.

The average dry density values obtained from the October 2010 forensic excavation agree more closely with the original dry densities from October 2004 construction. From observing Figure 6.21, it seems that the subgrade was compacted more in Sections 1B – 3 than any of the other sections, with dry densities ranging from approximately 105.1 to 110.2 pcf (1684 – 1765 kg/m^3).

Table 6.6. Subgrade dry densities from resilient modulus test samples.

	Section	East Bound		West Bound	
		Dry Density (pcf)	Rank	Dry Density (pcf)	Rank*
10" Nominal Base Thickness	1B	108.0	4		
	1A	107.8	5		
	1	111.1	1		
	2	108.4	2		
	3	108.2	3		
	4	100.9	13		
	5	101.1	12		
	6	101.3	10		
Transition	7	-	-	-	-
6" Nominal Base Thickness	8	101.2	11		
	9	99.7	14		
	10	104.3	7		
	11	102.7	9		
	12	105.4	6		
	13	103.4	8	91.6	17
	13A	91.1	16		
	13B	94.7	15	104.3	8

* Represents potential rank if west bound lane was included in ranking
(East Bound rankings would change accordingly).

Table 6.7. Subgrade dry densities from UU triaxial test samples.

	Section	East Bound		West Bound	
		Dry Density (pcf)	Rank	Dry Density (pcf)	Rank*
10" Nominal Base Thickness	1B	106.7	9		
	1A	112.3	3		
	1	114.1	2		
	2	108.4	4		
	3	114.2	1		
	4	99.5	14		
	5	102.0	13		
	6	103.4	10		
Transition	7	-	-	-	-
6" Nominal Base Thickness	8	107.1	8		
	9	103.3	11		
	10	103.1	12		
	11	107.5	6		
	12	95.2	15		
	13	84.9	16	103.4	12
	13A	107.8	5		
	13B	107.5	7	108.1	5

* Represents potential rank if west bound lane was included in ranking
(East Bound rankings would change accordingly).

Table 6.8. Average subgrade dry densities from three determination procedures.

		East Bound		West Bound	
	Section	Avg. Dry Density (pcf)	Rank	Avg. Dry Density (pcf)	Rank*
10" Nominal Base Thickness	1B	109.1	2		
	1A	108.2	4		
	1	110.2	1		
	2	105.1	5		
	3	108.6	3		
	4	99.8	15		
	5	101.4	10		
	6	101.1	11		
Transition	7	-	-	-	-
6" Nominal Base Thickness	8	102.8	7		
	9	102.1	8		
	10	102.0	9		
	11	103.2	6		
	12	100.9	13		
	13	94.8	16	95.8	17
	13A	100.7	14		
	13B	101.0	12	103.7	6

* Represents potential rank if west bound lane was included in ranking
(East Bound rankings would change accordingly).
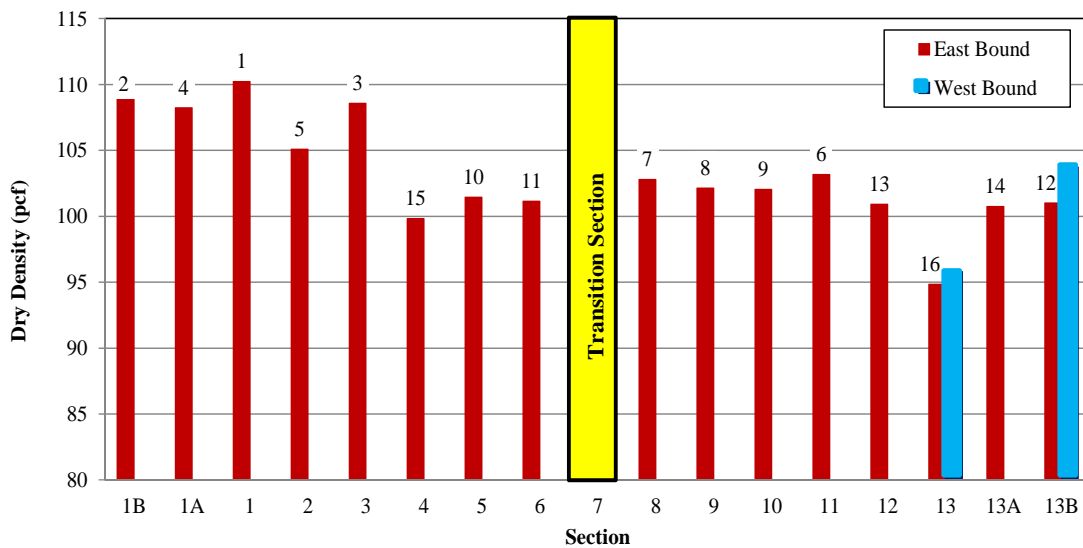
Figure 6.21. Average subgrade in-situ dry densities determined from three testing procedures.

The rest of the sections, excluding Section 13, have very similar average subgrade dry density values ranging from 99.8 to 102.8 pcf (1599 – 1647 kg/m^3), which are within the range of 94% to 97% of maximum proctor. The subgrade in Section 13 (unreinforced) has the lowest average in-situ dry density [94.8 pcf (1519 kg/m^3) or 89% of maximum proctor], highest in-situ water content, and highest PI, yet it has not "failed". However, the westbound lane at this exact location (Section 13W, reinforced with a slit-film geotextile) has almost identical properties and has "failed". The only observable difference is that Section 13 has approximately one more inch of combined asphalt and base than Section 13W. Again, for this data set it does not appear that differences in the dry density of the subgrade are closely correlated to pavement performance.

6.5 Strength/Stiffness Testing

During the October 2010 forensic excavation, in-situ strength/stiffness tests were conducted on site (DCP and CBR) and undisturbed samples were collected for laboratory testing of the subgrade (Mr and UU). The testing procedures, data analysis methods, and results from the strength/stiffness tests conducted on the base and subgrade soils are presented in the following sections.

6.5.1 Dynamic Cone Penetrometer (DCP)

The Dynamic Cone Penetrometer (DCP) test is a test method that measures the penetration rate of a cone through undisturbed soil, compacted materials, or both. The penetration rate may be related to in-situ strength (ASTM D6951-09), as well as strata thickness and bearing capacity. DCP is typically used in horizontal construction applications, such as pavements and shallow foundations. Normally the DCP is used to assess material properties to a depth of 30 inches (76.2 cm) below the surface, but with extensions, the drive rod can be advanced to 6 feet (1.8 m). The operator drives the DCP tip into the soil by lifting the sliding

hammer to the handle then releasing it. The total penetration for a given number of blows is measured and recorded in mm/blow (Kessler 2005). Hammer blows are applied to the drive rod until a specified depth of investigation is reached.

DCP tests were conducted at the Marked Tree site on two occasions: December 2009 and October 2010. The December 2009 DCP testing was conducted by drilling a hole through the asphalt in each test section to the assumed top of base. During the October 2010 site visit, the asphalt layer was removed from the base layer, so the DCP was placed directly on the base layer to perform the testing. For both test dates, the DCP was penetrated to a depth of approximately 48 inches (1200 mm) below the asphalt surface.

6.5.1.1 DCP Testing Procedure

All DCP testing was conducted with a Kessler Model 100 Dynamic Cone Penetrometer. A schematic of the DCP used for testing is presented in Figure 6.22. Each test was conducted with the 17.6 lb (8 kg) hammer, causing drop energy of approximately 33 lb-ft (45 N-m) per blow. Each test was conducted with at least two persons. One person was assigned to hold the DCP apparatus vertical while lifting and dropping the hammer, while the other person read the penetration from the vertical scale and recorded the reading at every blow. Each test was conducted with disposable cone tips with a 60 degree angle and a base diameter of approximately 0.8 in (20 mm) at the penetration end of the drive rod. The disposable tips were used to allow for easier extraction of the equipment from the soil when testing was completed.

The DCP equipment also included extension rods. When the original 30-in (76.2 cm) long drive rod was approximately 24 inches (600 mm) into the soil, a 24-in (60.9 cm) long extension rod was added for deeper exploration. The tests were concluded once the drive rod, with extension, had penetrated about 48 inches (1200 mm) below the base surface. To ensure
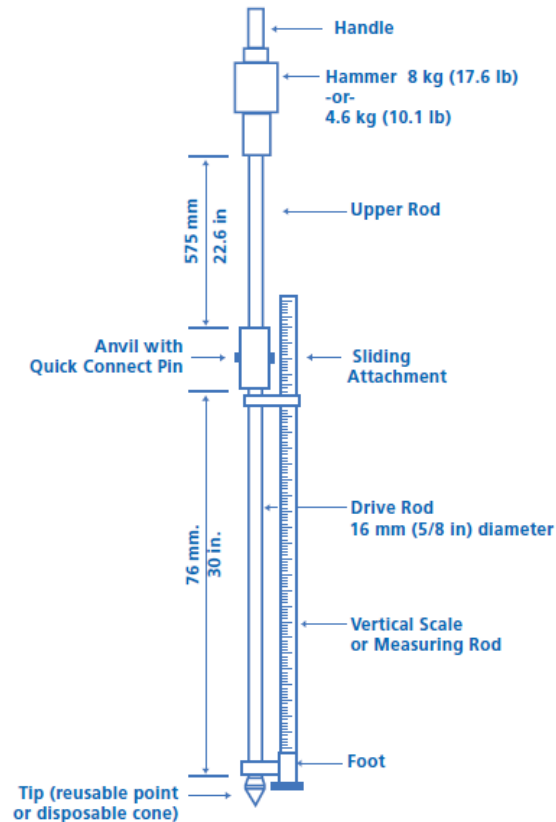
Figure 6.22. Schematic of Kessler K-100 DCP device (Kessler 2005).

reliable results, the DCP apparatus must remain vertical throughout the entire depth to which data will be analyzed. Pictures of the DCP testing being conducted at the Marked Tree are shown in Figure 6.23.

6.5.1.2 DCP Data Analysis

The data collected from the DCP testing consisted of the total penetration of the cone below the top of asphalt versus the number of blows of the drop hammer. Penetration curves were plotted using the penetration depth versus the blow count. Through observation of the penetration curves, each curve was divided up into three separate layers with distinct slopes. The slopes of the penetration curve (mm/blow) represent a stiffness value for each layer discernible

151

Figure 6.23. DCP testing at the Marked Tree site on December 2009 and October 2010, respectively.

in the data. Typical DCP results from a 10-in (25.4 cm) section and a 6-in (15.2 cm) section are provided in Figures 6.24 and 6.25, respectively. All penetration curves consisted of two distinct layers in the base course and one distinct layer at the top of the subgrade. The penetration data deeper in the subgrade was not considered as reliable since significant friction developed between the rod and the CH subgrade. During forensic excavation, the second slope in the base course was found to be caused by a 1 – 2 inch layer of base just above the subgrade interface with slightly higher moisture content. The interface between the base and subgrade layers was not assigned according to the measured layering in each section. However, the interface between the second layer (bottom of base) and the third layer (top of subgrade) always fell within a few millimeters of the base-subgrade interface determined from forensic excavation. The slight difference between the measured material interface and the DCP slope change could have occurred because the cone tip had to penetrate through the geosynthetics between layers.

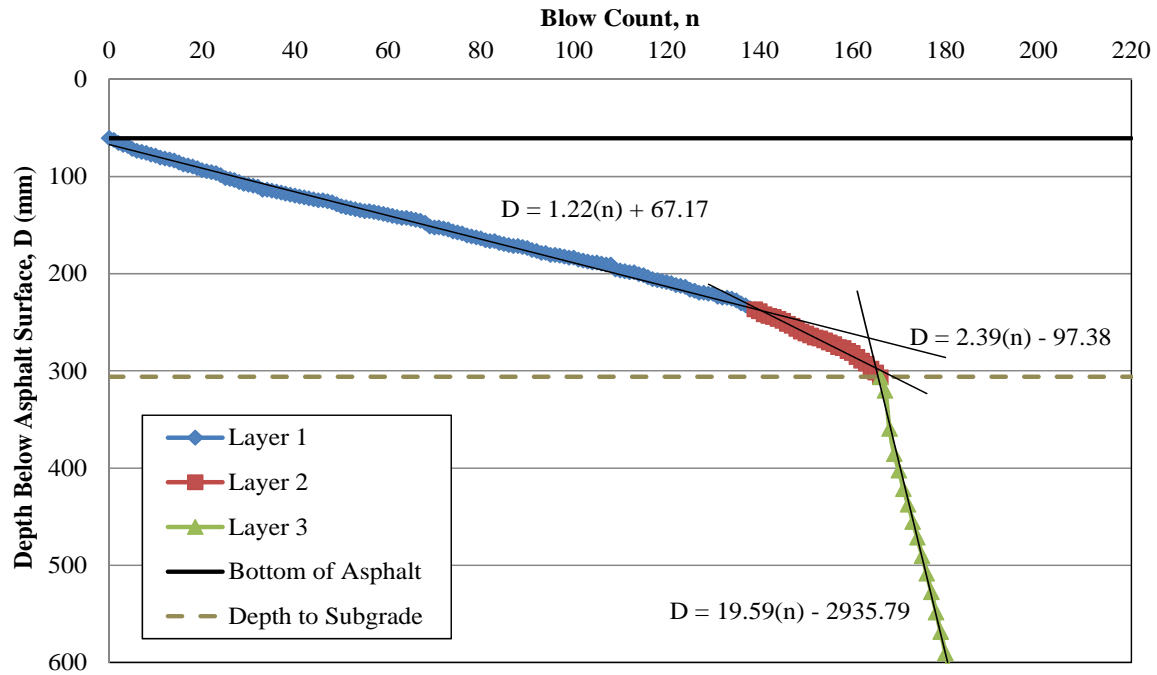Figure 6.24. Typical DCP penetration curve for a 10-in (25.3-cm) nominal base thickness section (Section 3) from October 2010 site visit.
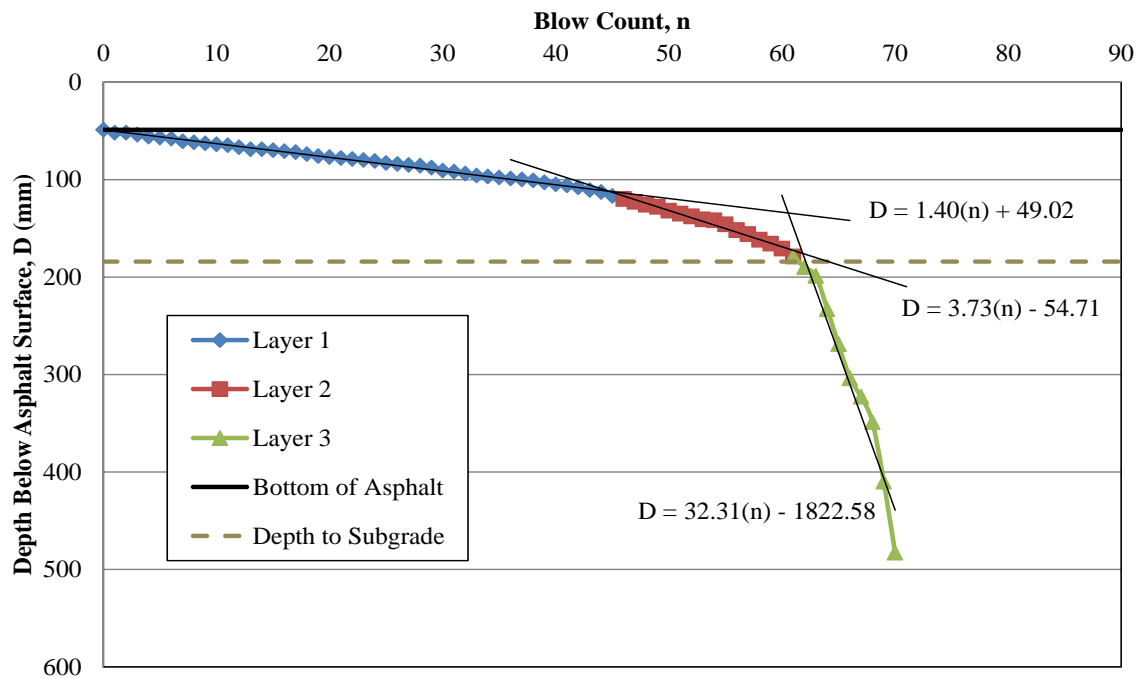
Figure 6.25. Typical DCP penetration curve for a 6-in (15.2 cm) nominal base thickness section (Section 13BW) from October 2010 site visit.

6.5.1.3 DCP Results

The results calculated from DCP testing conducted at the Marked Tree site on December 2009 and October 2010 are presented in this section. The results for each section on each date are quantified by the slopes of Layers 1 (top of base), 2 (bottom of base), and 3 (top of subgrade). The slopes represent the stiffness of each layer presented in millimeters of penetration per hammer blow (mm/blow). The slopes of the layers in each section were ranked by considering the lowest slope value (least penetration per blow) as the best and the highest slope value as the worst. The results calculated from December 2009 and October 2010 are presented in Tables 6.9 and 6.10, respectively. Graphical representations of these results are presented in Figures 6.26 through 6.31.

The Layer 1 (top of base) slopes determined from the DCP testing (refer to Figures 6.26 and 6.29) do not follow any distinct trend. However, the Layer 2 (bottom of base) slopes (refer to Figures 6.27 and 6.30) and the Layer 3 (top of subgrade) slopes follow a very similar trend to the measured rutting data (refer to Figures 4.2 and 4.3). Meaning, Sections 1B through Section 9 appear to be distinctly different/better in terms of both Layer 2 and Layer 3 slopes, as well as in terms of less rutting. Almost without exception these 10 sections consistently rank 1 through 10 in each of these categories. Furthermore, the Layer 2 and Layer 3 slopes from October 2011 both identify Section 10 as the worst section. However, the Layer 2 and Layer 3 DCP results do not strongly identify the other "failed" sections (Section 11, 12, 13W and 13BW) as the worst without exception.

In future composite rankings presented later in this chapter, the Layer 1 and Layer 2 slope rankings will be used in the composite base course rankings, while the Layer 3 slope rankings will be used in the composite subgrade rankings.

Table 6.9. DCP results from the December 2009 Marked Tree site visit.

	Section	Base Layer 1		BaseLayer 2		Subgrade Layer 3	
		Slope (mm/blow)	Rank	Slope (mm/blow)	Rank	Slope (mm/blow)	Rank
10" Nominal Base Thickness	1B	1.311	12	2.048	4	12.76	1
	1A	1.331	13	2.426	8	14.72	2
	1	0.735	4	1.495	1	15.55	4
	2	0.617	2	1.796	2	14.91	3
	3	1.104	10	2.287	6	15.91	5
	4	1.067	8	1.995	3	19.75	8
	5	0.755	5	2.445	9	16.74	6
	6	0.797	6	2.214	5	17.70	7
Transition	7	-	-	-	-	-	-
6" Nominal Base Thickness	8	0.573	1	2.337	7	19.96	9
	9	0.66	3	2.536	10	21.57	10
	10	1.639	14	4.461	14	30.55	12
	11	1.107	11	3.647	12	31.06	13
	12	0.877	7	3.698	13	29.06	11
	13	2.132	16	5.472	16	43.35	16
	13A	1.08	9	3.61	11	33.31	14
	13B	1.79	15	5.41	15	41.35	15

Figure 6.26. Layer 1 (top of base) slopes calculated from DCP testing during the December 2009 Marked Tree site visit.

155

Figure 6.27. Layer 2 (bottom of base) slopes calculated from DCP testing during the December 2009 Marked Tree site visit.

Figure 6.28. Layer 3 (top of subgrade) slopes calculated from DCP testing during the December 2009 Marked Tree site visit.

Table 6.10. DCP results from the October 2010 Marked Tree site visit.

	Section	Base Layer 1		Base Layer 2		Subgrade Layer 3	
		Slope (mm/blow)	Rank	Slope (mm/blow)	Rank	Slope (mm/blow)	Rank
10" Nominal Base Thickness	1B	0.844	2	2.057	1	17.349	3
	1A	1.235	10	2.499	4	16.735	2
	1	1.343	12	3.007	7	12.044	1
	2	1.430	14	3.342	10	20.786	7
	3	1.217	9	2.391	3	19.590	5
	4	1.059	5	2.848	6	22.506	8
	5	0.603	1	2.602	5	19.748	6
	6	0.935	4	2.257	2	18.251	4
Transition	7	-	-	-	-	-	-
6" Nominal Base Thickness	8	0.844	3	3.233	8	25.866	9
	9	1.438	15	4.324	13	27.654	10
	10	1.702	16	5.676	16	49.238	16
	11	1.098	7	3.297	9	34.682	13
	12	1.333	11	4.068	11	33.282	12
	13	1.132	8	4.418	14	43.250	15
	13A	1.081	6	4.861	15	38.633	14
	13B	1.414	13	4.304	12	29.654	11
	13W	1.738	18*	4.626	16*	47.929	17*
	13BW	1.404	13*	3.725	11*	32.309	11*

13W and 13BW are areas in the westbound lane adjacent to Sections 13 and 13B, respectively.

*Represents potential rank if westbound data was included in ranking (Eastbound ranks would change accordingly).
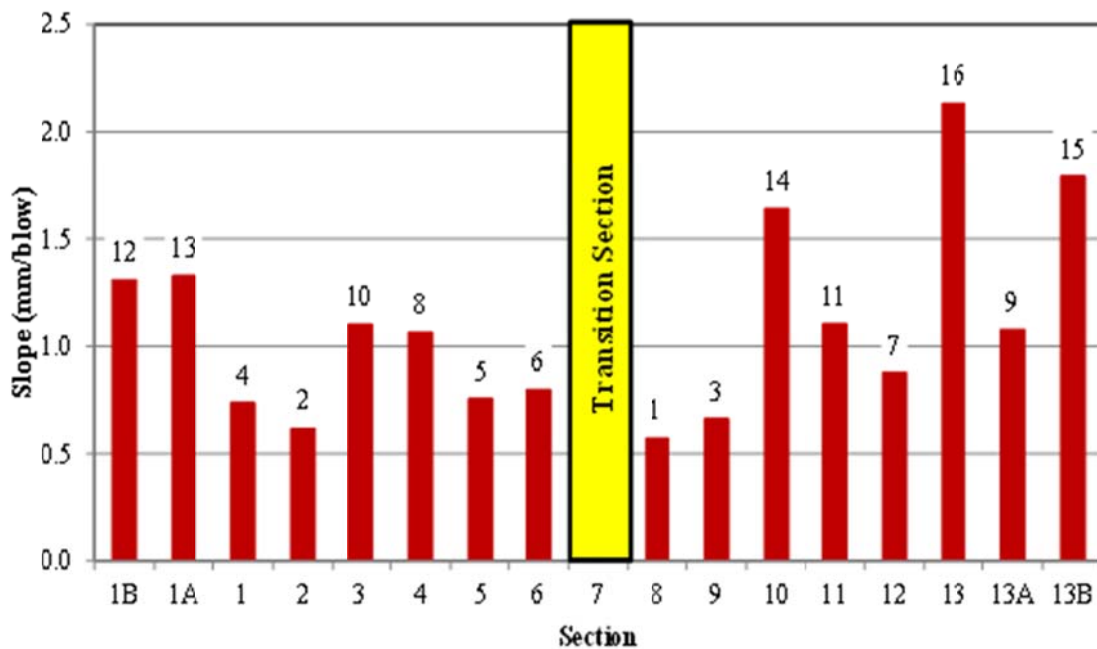

Figure 6.29. Layer 1 (top of base) slopes calculated from DCP testing during the October 2010 Marked Tree site visit.
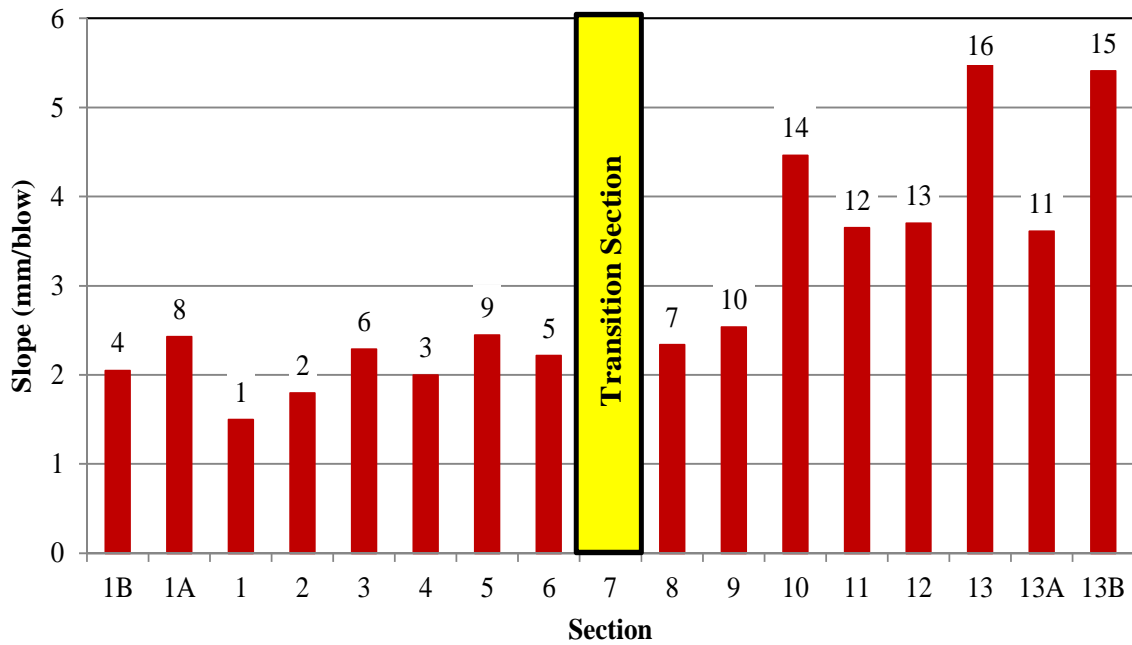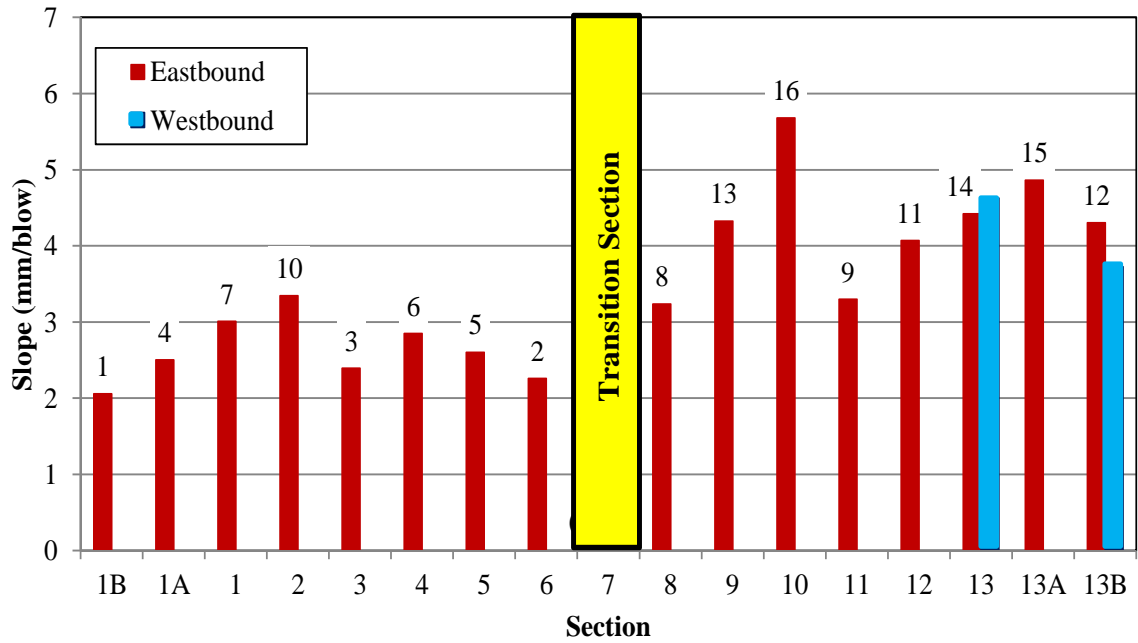
Figure 6.30. Layer 2 (bottom of base) slopes calculated from DCP testing during the October 2010 Marked Tree site visit.
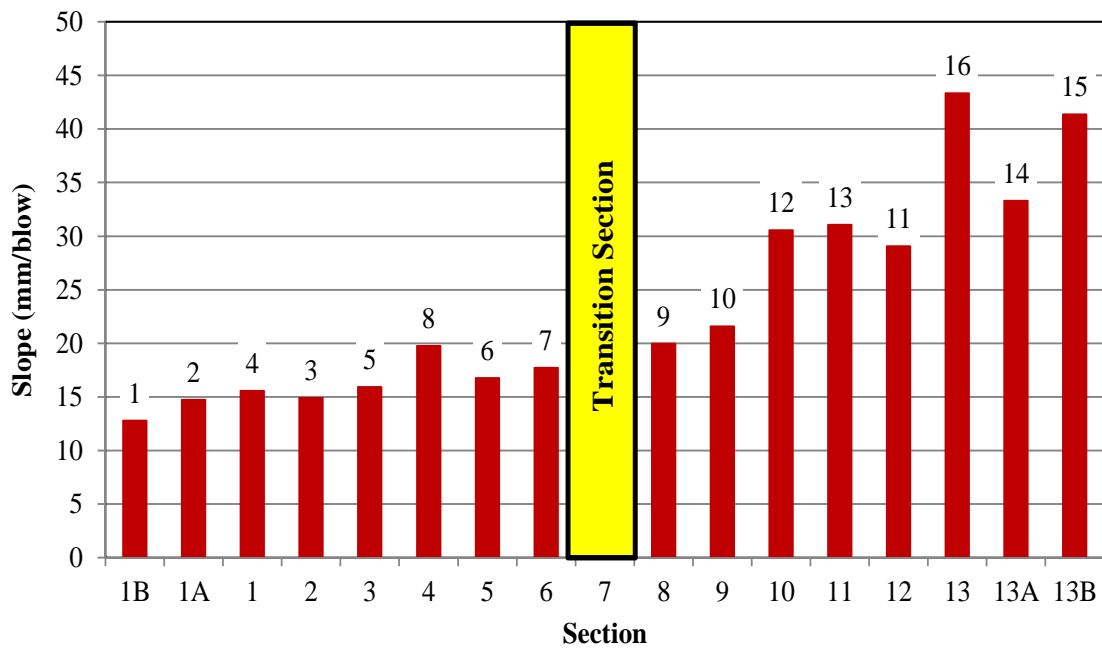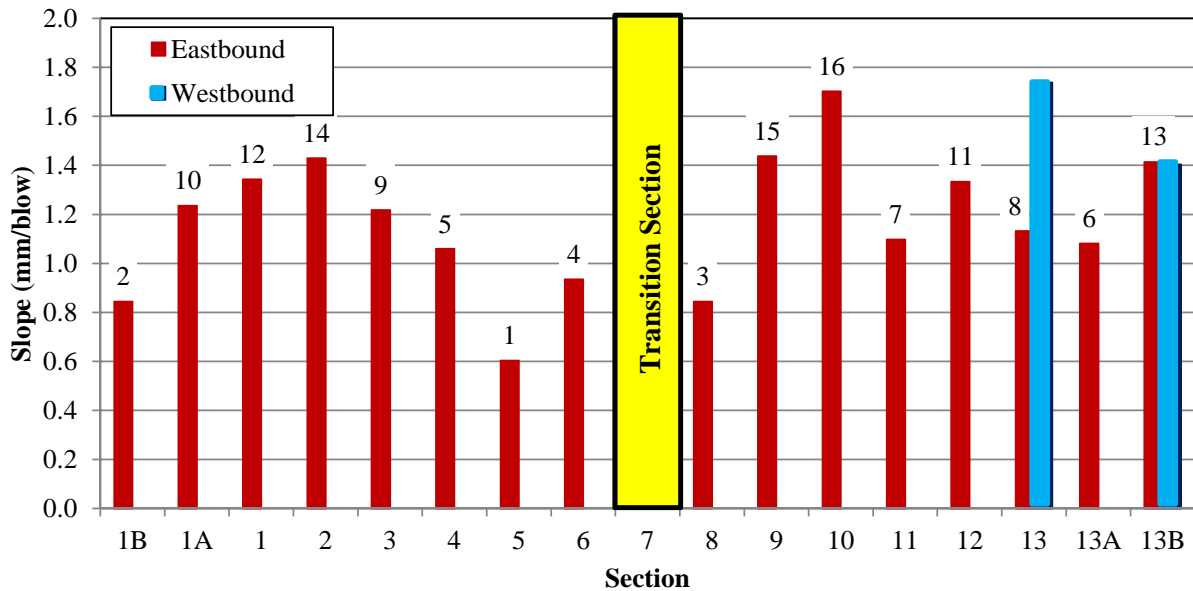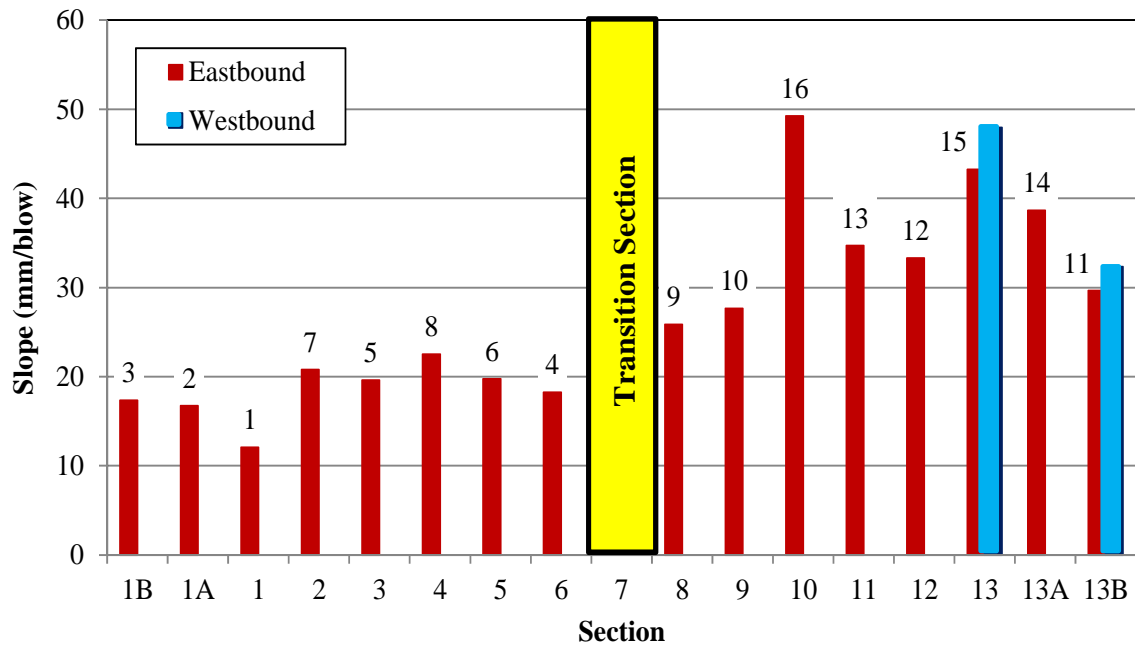

Figure 6.31. Layer 3 (top of subgrade) slopes calculated from DCP testing during the October 2010 Marked Tree site visit.

158

6.5.2 In-Situ California Bearing Ratio (CBR)

In-situ California Bearing Ratio (CBR) tests are used for evaluation and design of flexible pavement components such as base and subgrades by determining the relative strength of the soils in the condition at which they exist at the time of testing (ASTM D4429 – 2009a). CBR values are determined by observing the penetration of a 2-in (5.1-cm) diameter piston into the soil structure against the applied vertical pressure necessary to cause the penetration. For stiff soils, a nominal maximum CBR value of 100 is assigned to represent the soil has adequate construction strength.

CBR tests were conducted on all test sections, as well as the two westbound areas adjacent to Sections 13 and 13B (13W and 13BW), during the October 2010 site visit. These tests were conducted on both the base course and the subgrade at all areas. The CBR testing procedure, data reduction and analysis, and results from the October 2010 testing are presented in the following sections.

6.5.2.1 In-Situ CBR Testing Procedure

The in-situ CBR tests conducted at the Marked Tree site during the October 2010 site visit followed the testing procedures presented in ASTM D4429 – 2009a. The research group deviated from ASTM D4429 – 2009a by constructing an equivalent apparatus to the mechanical screw jack typically used for in-situ CBR testing. The research group employed an unconfined compression test jack to serve as the mechanical screw jack. The testing apparatus and setup is displayed in Figure 6.32. It was determined that the jack handle must go through one revolution every 12 seconds to ensure a penetration rate of 0.05 in (1.3 mm)/min would be achieved. The University of Arkansas's vibroseis truck was used as the reaction load by constructing a two-
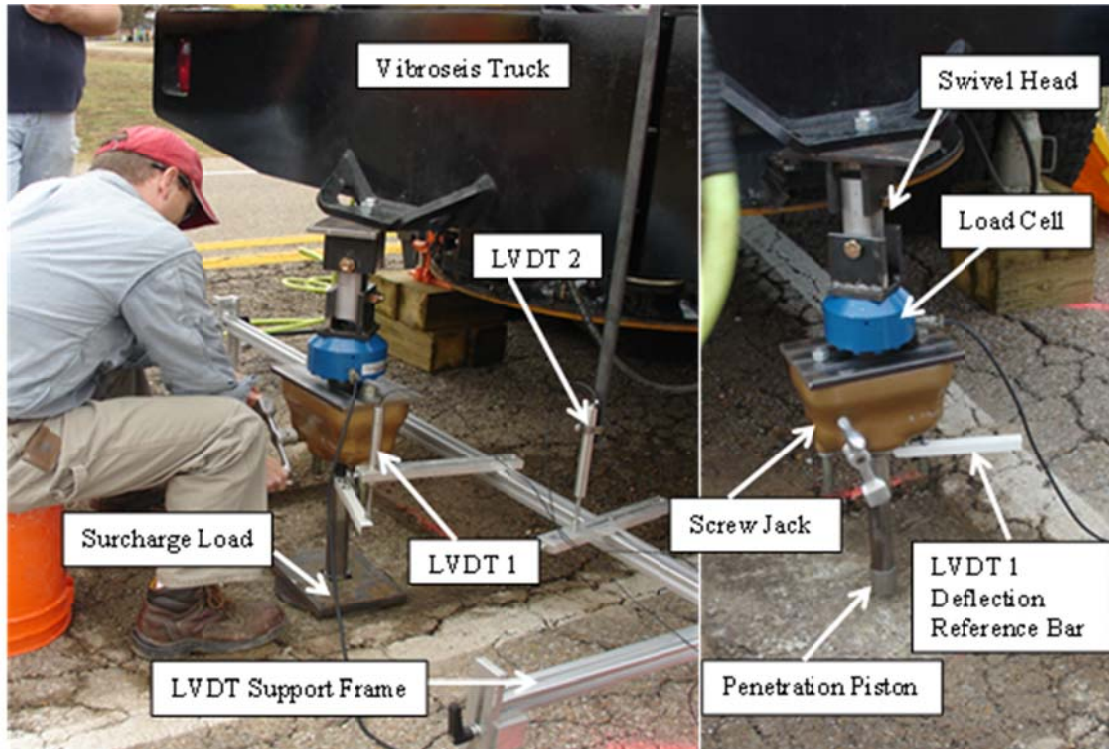
Figure 6.32. CBR testing setup and apparatus at Marked Tree site during October 2010 site visit.

dimensional swivel head that attached to the load cell that was bolted to the bumper of the vibroseis truck. The swivel head was constructed to ensure the piston was traveling vertically through the soil. The vibroseis truck was supported in the rear by blocks to prevent the wheels from rolling as the loading increased so vertical loading would be maintained. Two LVDTs were used to measure travel distances of both the penetration piston (LVDT 1; downward) and the vibroseis truck (LVDT 2; upward). The piston travel distance was observed by attaching a reference bar to the jack, at the top of the piston, which traveled with the piston. The truck uplift was measured by attaching an LVDT to the truck and using the stationary LVDT support frame as the reference point.

Prior to testing, surcharge loads were applied to the soil, surrounding the piston, to simulate the original overburden from the soil and/or asphalt removed from the testing surface.

160

The testing was conducted by turning the screw jack one revolution every 12 seconds for approximately 11 minutes to ensure at least 0.5 inches (1.3 cm) of penetration was achieved. However, while testing the base course, the truck was lifted much more than the piston penetrated into the soil. Only six of the sections had base course material soft enough for piston penetration and useful data collection.

6.5.2.2 In-Situ CBR Data Analysis

The data collected during the CBR testing consisted of deflection results from LVDTs 1 and 2, as well as the pressure being applied to the soil, recorded every 0.3125 seconds. LVDT 1 measured the penetration of the piston during testing, while LVDT 2 measured the uplift of the vibroseis truck. Total deflection values were calculated by subtracting the truck uplift values from the penetration values because the testing apparatus was rigidly connected to the vibroseis truck. The total deflection value represented only the penetration of the piston into the soil. The pressure values were plotted against the corresponding total deflection values to develop the stress-penetration curves used in data reduction. A typical stress-penetration curve for a subgrade section is presented in Figure 6.33. The CBR values were calculated in accordance with Section 7 of ASTM D4429 (2009). The pressure values corresponding to the penetration values of 0.1-in (0.25-cm) and 0.2-in (0.51-cm) were divided by the standard stresses of 1000 psi (6.9 MPa) and 1500 psi (10.3 MPa), respectively, and multiplied by 100. The CBR reported for the soil is typically from the bearing ratio at 0.1-in (0.25-cm) of penetration.

Penetration curves were developed for all sections; however, the base course was so stiff that only six sections rendered CBR test data that could be analyzed for the base course material. The typical stress-penetration curve for the subgrade presented in Figure 6.33 resembles the

161
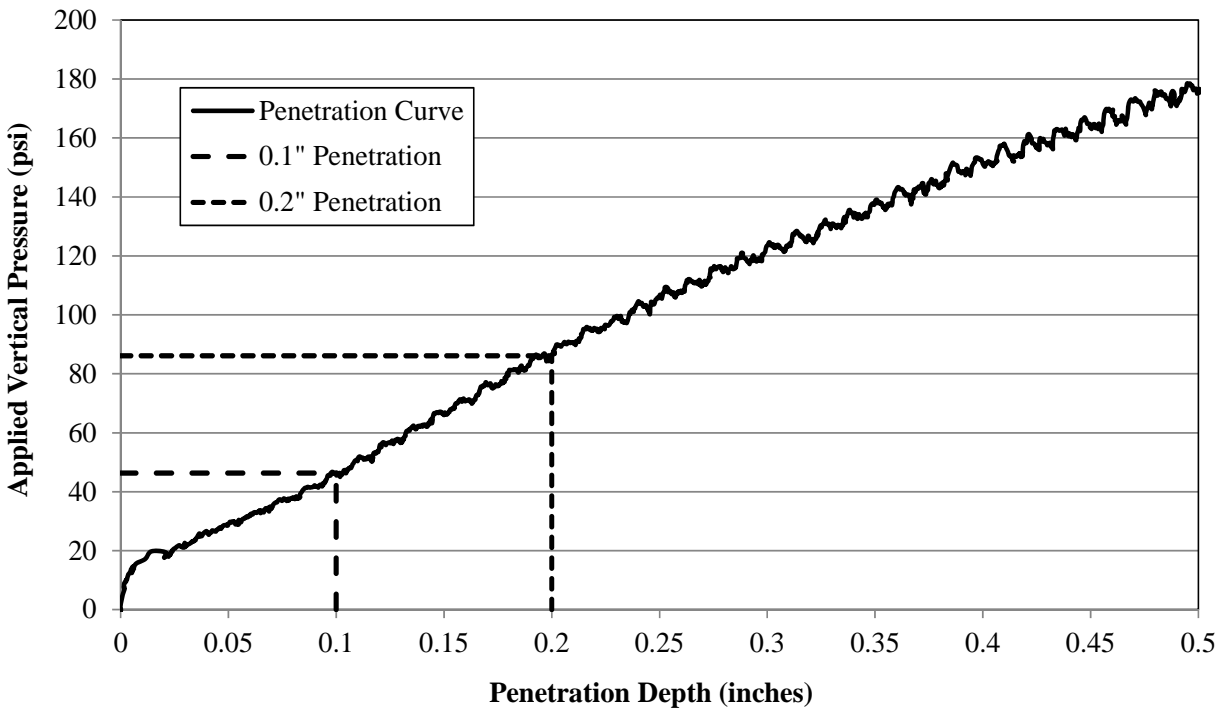
Figure 6.33. Typical subgrade stress-penetration curve developed from data collected at Marked Tree site during October 2010 site visit.

typical penetration curve that would be developed from the base course material with pressure values approximately one order of magnitude greater.

6.5.2.3 In-Situ CBR Results

The CBR calculations were performed in accordance with ASTM D4429 – 2009a. Only six sections had CBR test data on the base course that could be plotted as a decipherable stress-penetration curve. The other sections were all too stiff and the truck was simply lifted off the ground instead of penetrating the piston into the base. All base course sections that were not able to be analyzed were considered competent material with CBR values of at least 100. Of the six sections with calculated base course CBR values, only two sections had CBR values below 100. Section 10 had a calculated base course CBR of approximately 67, and Section 13W had a calculated base course CBR of approximately 80. Both of these sections were ones that had

"failed" based on rutting measurements. Since in-situ CBR values could only be obtained in two of the sections, these values will not be included in the final composite base course rankings. In-situ subgrade CBR values were obtained for all sections tested. The resulting subgrade CBR values and associated ranks are provided in Table 6.11. A graphical representation of these results is presented in Figure 6.34.

Subgrade soils with CBR values less than 6 are considered poor. Sections 1A and 13 are the only two sections with a subgrade CBR value greater than 6. These results are perplexing because, as stated previously, the subgrade in Section 13 ranked lowest of the 16 test sections in terms of in-situ water content, PI, dry density, and DCP slope (Layer 3). However, the in-situ CBR results do indicate that Section 10 is the worst of the 16 test sections. Other than that, the in-situ CBR values don't seem to correlate well with subgrade moisture content, subgrade dry density, or the observed trends in rutting.

It is possible that the CBR data in some sections may have a friction problem in the test results due to the small variation in diameter between the penetration rod and the inner diameter of the bottom surcharge plate. These dimensions are set by ASTM D4429, but the tolerances are so tight that the research team was often concerned that friction may have been developing between the rod and base plate in sections where the base plate did not sit extremely level on the subgrade. Even a small amount of friction could greatly affect the results when testing on such a soft soil.

Table 6.11. Subgrade in-situ CBR values from the Marked Tree site during October 2010 testing.

	Section	East Bound		West Bound	
		CBR Value	Rank	CBR Value	Rank*
10" Proposed Base Thickness	1B	5.25	9		
	1A	7.70	2		
	1	5.74	5		
	2	4.27	12		
	3	4.99	11		
	4	5.46	8		
	5	5.20	10		
	6	5.61	6		
Transition	7	-	-	-	-
6" Proposed Base Thickness	8	3.55	15		
	9	4.13	14		
	10	2.75	16		
	11	5.86	4		
	12	5.59	7		
	13	8.69	1	2.01	18
	13A	5.94	3		
	13B	4.14	13	4.41	12

* Represents potential rank if west bound lane was included
in ranking (East Bound rankings would change accordingly).
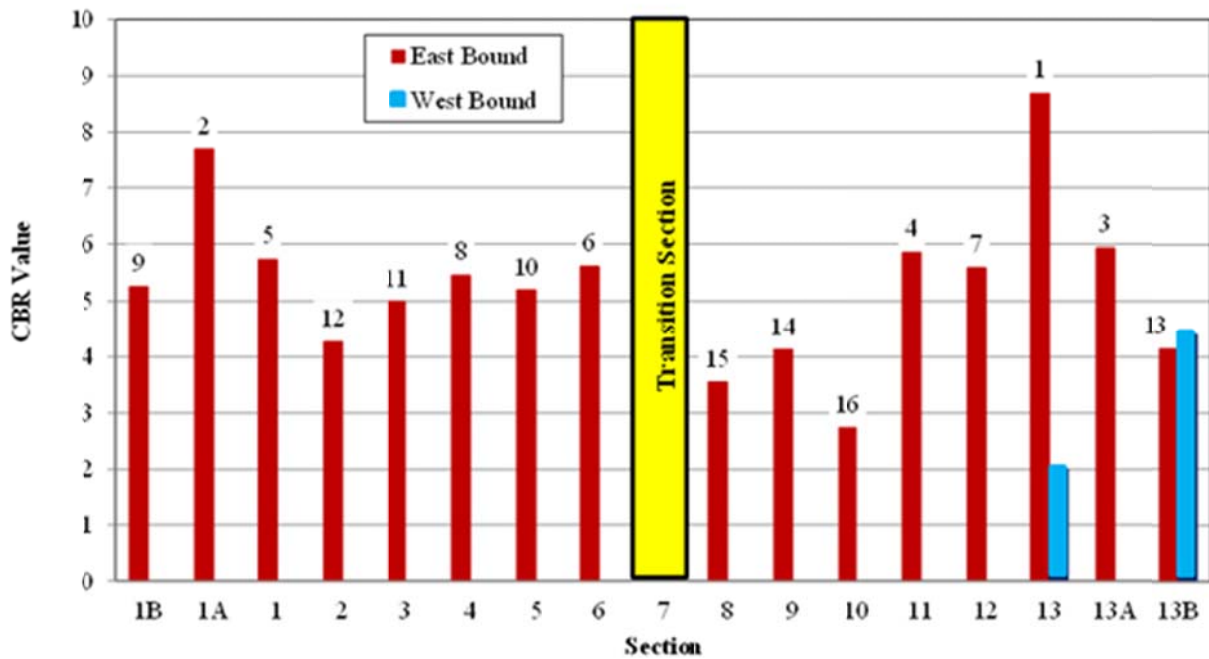
Figure 6.34. In-situ subgrade CBR values from the Marked Tree site during the October 2010 site visit.

6.5.3 Laboratory Resilient Modulus (M_R)

Resilient modulus testing is a laboratory procedure conducted on untreated subgrade soils under conditions representing a simulation of the physical conditions and stress states of materials beneath flexible pavements subjected to moving wheel loads. A test specimen is housed in a triaxial cell with predetermined, varying confining pressures applied to it, while continuous loading cycles of different axial loads are applied to the specimen. Stresses applied to the specimen at the different loading stages and specimen strains resulting from the applied loads are monitored throughout the test. The value of resilient modulus is a measure of the elastic modulus of untreated subgrade soils recognizing certain nonlinear characteristics (AASHTO T307 2007).

Resilient modulus (M_R) tests were conducted on Shelby tube samples collected during the October 2010 Marked Tree site visit. Two sets of Shelby tubes were pushed at every section, including the two areas referred to as 13W and 13BW in the westbound lane. The Shelby tubes were sealed with was immediately after extraction from the ground. Samples were collected in the northeast corner and the southwest corner of each 2-ft x 2-ft (0.61-m x 0.61-m) test area. Resilient modulus tests were conducted on the top six inches (15.2 cm) of the set of Shelby tube samples that were collected in the northeast corner to ensure testing consistency and to leave an entire set of undisturbed samples for later laboratory testing. However, after the first round of M_R testing the data from Sections 1B, 11, and 13 was not acceptable and samples from the second set of Shelby tubes were used to repeat the tests. The required specimen height of approximately 6 inches (15.2 cm) was determined to ensure a length to diameter ratio of at least 2:1, as described in AASHTO T307 (2007), because the Shelby tubes are manufactured with an interior diameter of approximately 2.87 inches (7.29 cm).

The testing procedure, data analysis method, and the results calculated from the resilient modulus testing for samples from the Marked Tree site are presented in the following sections.

6.5.3.1 Laboratory Resilient Modulus Testing Procedure

Resilient modulus tests were conducted on Shelby tube samples collected at the Marked Tree site during the October 2010 site visit. Before these tests could be conducted, however, the samples needed to be extracted from the tubes with minimal disturbance. Stages of the sample extraction process are displayed in Figure 6.35. The sample extraction process is described in the following steps:

1. The height of recovery determined in the field was used to find the top of the subgrade within the sealed Shelby tube.

2. The Shelby tube was placed in a horizontal band saw to cut out the appropriate section so only the top 6 inches (15.2 cm) were removed, Figure 6.35(a). (The remaining sample was re-capped at the open end and wrapped in cellophane and duct tape to ensure constant moisture content.)

3. The sample was then placed atop a bench vise and cut longitudinally down the thin-walled tube encasing the soil. The tube was first cut with a small angle grinder equipped with a metal cutting disc. When the tube wall along the cutting surface began getting very thin, the metal would begin bending under the pressure of the angle grinder. A small Dremel rotary tool was then used to finish cutting through the thin walled tube, Figure 6.35(b). Fortunately, because the Shelby

   tubes are constructed by welding ends of rolled steel together, they spring open once cut in the longitudinal direction.

4. After the tube was cut and sprung open, the sample was extracted from the tube by sliding the tube up and off the sample, leaving a free standing, minimally disturbed subgrade sample, Figure 6.35(c).

Once a sample was extracted from the Shelby tube, the ends of the sample were slightly trimmed to level the specimen in the vertical and horizontal directions to ensure bending loading was not applied to the specimen during testing. Digital calipers were used to collect three height measurements for an average original specimen height. A pi tape was used to measure the

(a)	(b)	(c)
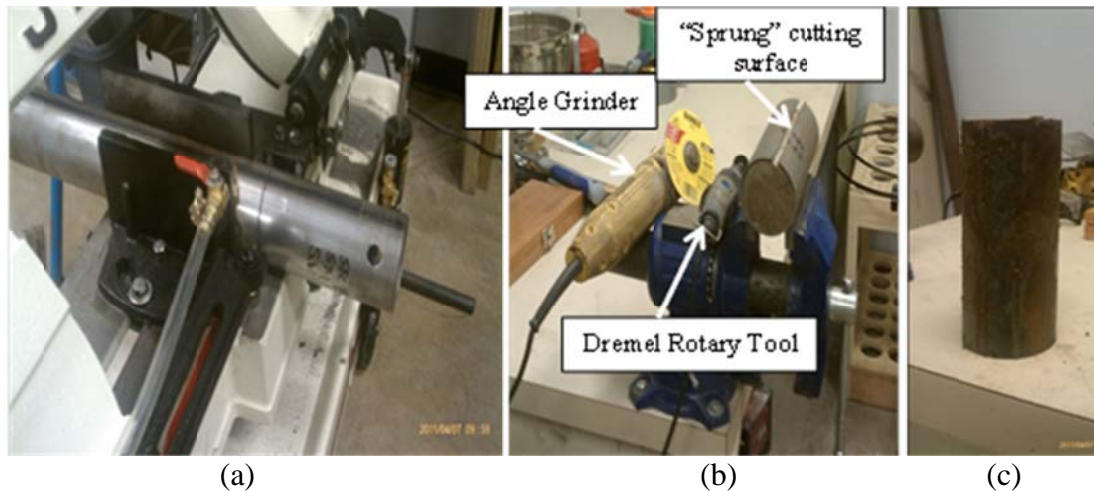
Figure 6.35. Resilient modulus sample extrusion process: (a) Step 2, (b) Step 3, (c) Step 4.

diameter of the sample in three locations for an original specimen diameter. The diameter, height and weight measurements were used in calculating a total subgrade density for each specimen for later determination of dry density, as described in Section 6.4.4.

After testing preparation was completed, the specimen was placed in the triaxial loading cell. The bottom surface of the sample was placed on top of the combination of the bottom loading surface, a porous stone, and filter paper, in order from the bottom of the triaxial cell up to the sample. Placed on top of the sample was another filter paper, followed by another porous stone, and finally the top cap with a ball bearing resting in an indention machined into the top cap. An example of this setup is presented in Figure 6.36. The ball bearing was utilized to transfer the load vertically to the sample from the loading piston rod which had a concave tip that rested atop the ball bearing. A thin-walled flexible membrane was placed around the specimen and was secured to the top and bottom cap by O-rings.

After the membrane and O-rings were in place, the triaxial confining cell was placed around the specimen setup and secured to the base plate. The loading piston rod was equipped
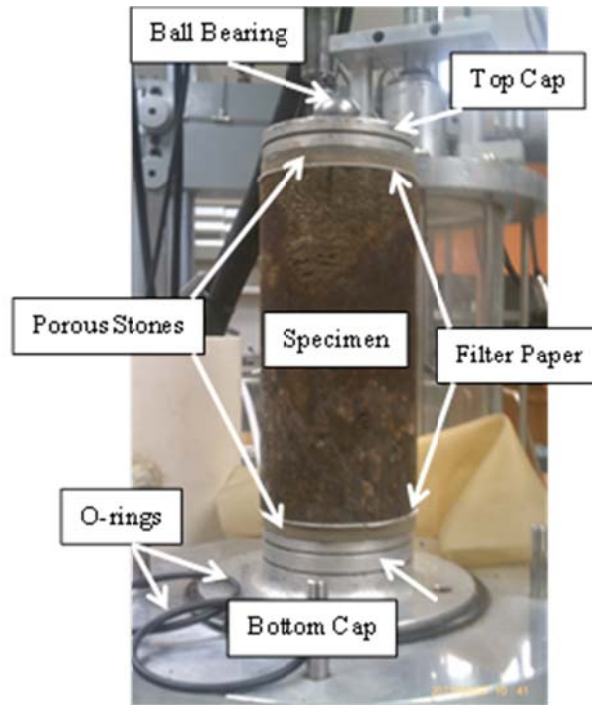
Figure 6.36. Resilient modulus specimen setup prior to placement of membrane and confining pressure cell.

with a solid bracket outside of the confining cell to secure two spring-loaded LVDTs utilized during testing to measure the specimen displacement. A hydraulically driven MTS loading frame was used for load application. A 1-kip (4.5 kN) load cell used to measure the actual applied loads during testing was rigidly attached to the load frame. The load cell had an extension rod extending from the bottom that rested atop another ball bearing that was seated atop the loading piston rod. Compressed air was supplied from an external source to the triaxial cell to serve as the confining fluid during testing. An air pressure gage was inserted into the vacuum inlet of the confining cell to ensure the correct amount of confining pressure was applied to the specimen. The vacuum inlet associated with the specimen was externally equipped with a small hose submerged in a water tub to verify that air was not leaking from the specimen. The final test setup is displayed in Figure 6.37.
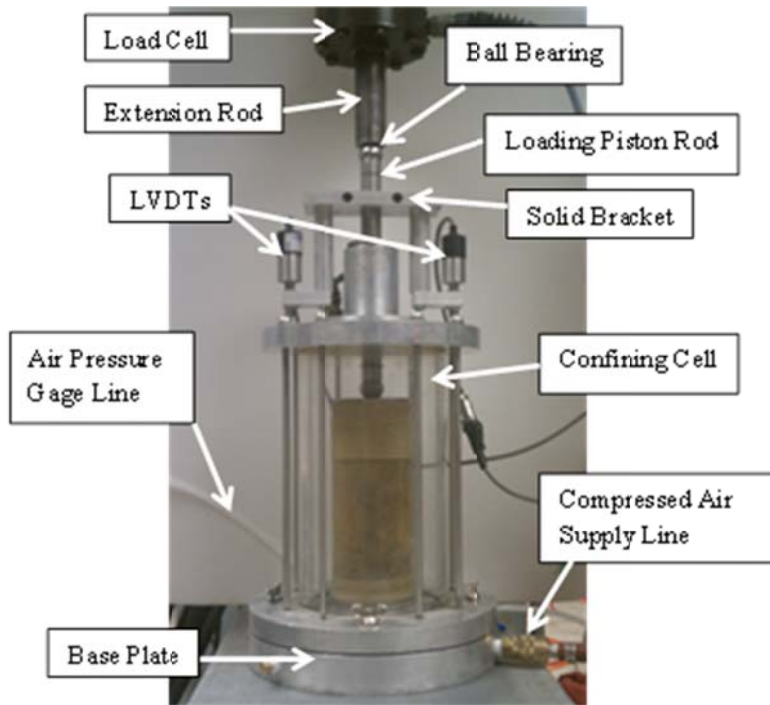
Figure 6.37. Resilient modulus testing configuration for Marked Tree subgrade samples.

Once the testing apparatus was completely setup, the resilient modulus testing was initiated. The resilient modulus testing procedure conducted for this project follows the procedure described in AASHTO T307 (2007). The loading process for this test is a cyclic loading procedure that produces a haversine-shaped loading pulse to the specimen every second. The load pulse is applied to the sample for a duration of 0.1 seconds and the remaining 0.9 seconds of the cycle is referred to a resting period.

The loading sequence displayed in Table 1 of AASHTO T307 (2007) was applied to the specimen during testing, except 2 psi (13.8 kPa) axial stress was applied during conditioning rather than 4 psi (27.6 kPa). The loading is presented in terms of stresses that should be applied to the specimen. To ensure the correct stresses were applied to the specimen, force calculations had to be performed because the MTS load frame applies specified forces. Piston uplift caused by the confining pressure was accounted for in the load calculations. The stress variation

supplied by the piston was determined by measuring the weight of all piston attachments below the load cell and dividing that load by the cross-sectional area of the piston. The difference in the downward stress applied by the piston weight and the confining pressure for each loading variation was determined to be the uplift force of the piston assembly. The total of the uplift stress and the required axial stress to be applied at each loading stage was divided by the initial specimen cross-sectional area to determine the forces necessary to apply the required stresses. The actual applied stress values varied slightly throughout testing due to the force values being calculated based on the initial specimen cross-sectional area while the specimen diameter changed throughout the test caused by permanent vertical deformation but no volume change.

At the completion of each resilient modulus test, the testing apparatus was taken down, and the flexible membrane was removed from the specimen. The entire specimen was used to determine moisture content. The moisture content values were used for calculating the dry density values for each sample, as presented in Section 6.4.4.

6.5.3.2 Laboratory Resilient Modulus Data Analysis

The data necessary for resilient modulus calculations are the minimum and maximum displacement and load values for each cycle of each load sequence. A resilient modulus value is calculated for all 15 loading sequences. The data from the last five cycles of any loading sequence was used for the resilient modulus calculations, per AASHTO T307 (2007). The equation used for resilient modulus (Equation 6.1) is as follows:

$$M_R = \frac{Applied\ Cyclic\ Stress}{Resilient\ Strain} \qquad (6.1)$$

Where: M_R = Resilient modulus, psi (kPa)

Applied Cyclic Stress = Max. Axial stress – Contact Stress, psi (kPa)

Resilient Strain = Avg. displacement / specimen height, in/in (mm/mm)

The applied cyclic stress is the difference in the maximum axial stress and the contact stress that remains on the specimen during the resting period of each cycle. The maximum axial stress was calculated by taking the average of the peak loads applied to the sample during the last five loading cycles and dividing it by the initial specimen cross-sectional area. The contact stress was calculated by averaging the minimum loads applied to the sample during the last five loading cycles and dividing it by the initial specimen cross-sectional area.

The resilient strain value is the resulting quotient from dividing the average displacement by the initial specimen height. The average displacement value was calculated by taking an average of the displacements caused by the last five loading cycles from both LVDTs. The displacement for each cycle was calculated by subtracting the minimum LVDT reading (resting portion of load cycle) from the maximum LVDT reading (load pulse portion of the load cycle).

Resilient modulus values were calculated for each load sequence for all tests. The five resilient moduli values were plotted against the nominal axial stress values for each confining pressure. A typical resilient modulus plot for the subgrade samples collected during the October 2010 Marked Tree site visit is presented in Figure 6.38. The in-situ resilient modulus value for each section was determined by observing the geometry of the resilient modulus plot and determining the appropriate confining pressure line to observe, which is based on the depth at which that sample was collected. The resilient modulus test samples were collected from the top six inches (15.2 cm) of the subgrade at the Marked Tree site. The estimated maximum overburden pressure over this depth range was approximately 1.2 psi (8.2 kPa), so the 2-psi (13.8-kPa) confining pressure line was selected for resilient modulus determination of each section for the Marked Tree site. The estimated overburden pressure was calculated based on a hot mix asphalt density of 145 pcf (2322 kg/m^3) and a maximum asphalt thickness for any
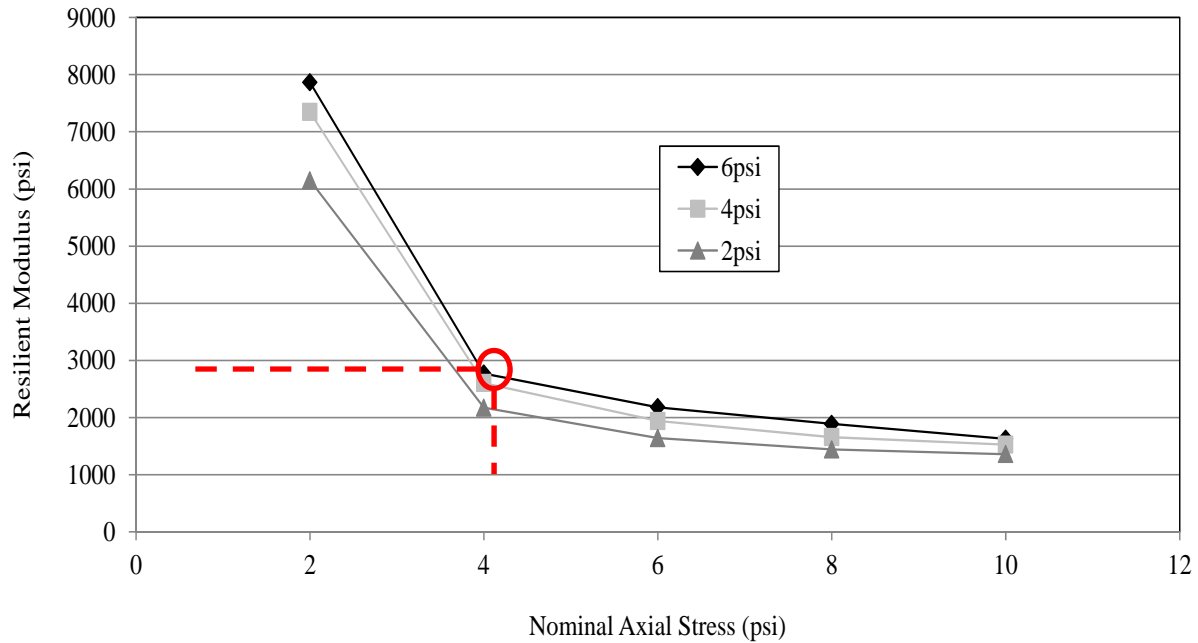
Figure 6.38. Typical resilient modulus plot for Marked Tree subgrade specimen.

section at the Marked Tree site of 2.65 in (6.73 cm), and a maximum base course dry density of

149 pcf (2387 kg/m^3) with the maximum base course thickness of any section at the Marked Tree

site of 11.33 in (28.78 cm).

Once the correct confining pressure line is selected, the geometry of the line is observed

to determine which axial load sequence the resilient modulus value should be selected from. The

confining pressure line will have an abrupt change from a steep slope to a more gradual slope.

The point where the two slopes transition is the resilient modulus value that should be used for

design, or in this case, the in-situ Mr for comparison purposes.

6.5.3.3 Laboratory Resilient Modulus Results

It was determined that the 2-psi (13.8 kPa) confining stress line should be used for

resilient modulus determination for all sections. Additionally, for every section tested, the

resilient modulus value was selected at the nominal axial stress of 4 psi (27.6 kPa). The resilient

modulus values and ranks are presented in Table 6.12. The results presented for Section 1 are based on a specimen that had a height to diameter ratio slightly less than 2:1. The resilient modulus values and ranks are graphically displayed in Figure 6.39. The minimum resilient modulus value was 1332 psi (9184 kPa), and the maximum resilient modulus value was 2777 psi (19147 kPa). The minimum value occurred at Section 5, while the maximum value occurred only 100 feet (30.5 m) east at Section 3.

The subgrade resilient modulus results do not seem to have any particular patterns or trends that correlate with the rutting data. All of the resilient modulus values are low, indicating soft subgrade soils. However, beyond this observation the Mr values may not be sensitive enough to distinguish subtle changes in the subgrade. The two highest rutting 10-in (25.4-cm) base sections (Sections 1 and 3) have the two highest resilient modulus values. Section 10, which has the largest average rut depth value out of all eastbound lanes, has the fourth highest resilient modulus value.

6.5.4 Unconsolidated Undrained (UU) Triaxial Test

The unconsolidated undrained (UU) triaxial test results are used to determine stress-strain relationship and undrained shear strength of a cylindrical specimen of either undisturbed or remolded cohesive soil. Specimens are subjected to a confining fluid pressure in a triaxial chamber. No drainage of the specimen is permitted during the test. The specimen is sheared in compression at a constant rate of axial deformation (ASTM D2850 – 2007). The results calculated from a UU test are total stress results, meaning the stresses are not corrected for pore-water pressure because the pore-water pressure within the soil specimen is not monitored throughout testing.

Table 6.12. Subgrade resilient modulus results at 2 psi (13.8 kPa) confining pressure.

	Section	East Bound		West Bound	
		M_R (psi)	Rank	M_R (psi)	Rank*
10" Nominal Base Thickness	1B	2173	6		
	1A	2172	7		
	1	2421	3		
	2	2030	9		
	3	2777	1		
	4	1510	15		
	5	1332	16		
	6	1899	11		
Transition	7	-	-	-	-
6" Nominal Base Thickness	8	1920	10		
	9	1649	14		
	10	2342	4		
	11	1780	13		
	12	2119	8		
	13	2432	2	1742	15
	13A	1871	12		
	13B	2314	15	1993	10

Note: Values were obtained through Resilient Modulus Testing
     in accordance with AASHTO T307 (2007).

Denotes H:D ratio < 2:1.

* Represents potential rank if west bound lane was included in
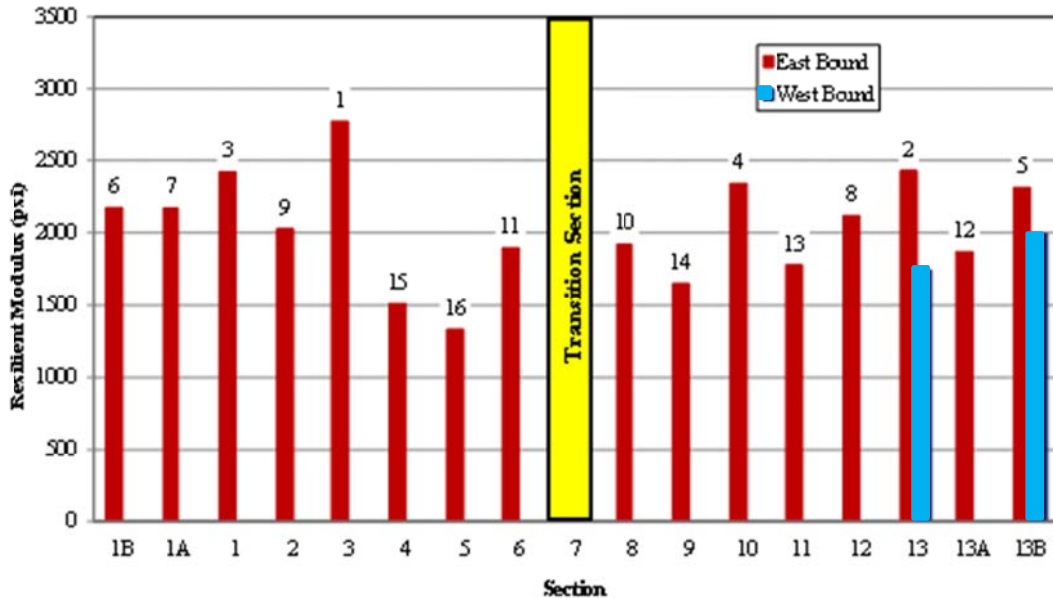ranking (East Bound rankings would change accordingly).

Figure 6.39. Subgrade resilient modulus results at 2 psi (13.8 kPa) confining pressure.

174

UU tests were conducted on Shelby tube samples collected during the October 2010 Marked Tree site visit. These tests were conducted on the Shelby tube samples collected in the southwest corner of the 2-ft x 2-ft (0.61 m x 0.61 m) testing areas. The UU tests were conducted on the top six inches (15.2 cm) of sample from each tube, except for Sections 1B, 11, and 13 which were tested at a subgrade depth of 6 to 12 inches (15.2 to 30.5 cm) since the top 6 inches of these tubes had been used in Mr testing.

The UU testing procedure, data analysis, and results are discussed below. Additional information about the UU testing procedure and data analysis is located in Boga (2011).

6.5.4.1 UU Testing Procedure

The UU tests were conducted on Shelby tube samples of the subgrade in each section at the Marked Tree site. The samples had to be cut to length and extracted from the Shelby tube prior to testing. The sample extraction and trimming processes discussed in Section 6.5.3.1 were followed by the research group from Boga (2011). The sample was placed in the triaxial testing cell once extracted from the tube and trimmed.

The triaxial testing cell used for the UU testing was manufactured by Trautwein Soil Testing Equipment Co., displayed in Figure 6.40. The Trautwein cell was equipped with a solid acrylic disc as the bottom loading cap because drainage ports are not needed for undrained conditions. The sample was placed directly onto the bottom loading cap with another solid acrylic cap placed on top of the specimen. The top acrylic cap was notched to allow for the loading piston to rest inside of it. Once the sample and top cap were in place, a thin-walled flexible membrane was placed around the specimen and the acrylic caps. The membrane was sealed off by placing O-rings around the portion of the membrane on the top and bottom acrylic caps. The confining cell was then connected to the base plate, and the entire apparatus was set in

place within the load frame to begin testing. The load frame, as well as the water pump supplying the confining pressure, the cell pressure transducer, and the software used during testing, is a Geotac product manufactured by Trautwein Soil Testing Equipment Co.

The testing procedure described in ASTM D2850 (2007) was followed for the UU testing. The soil was confined at a constant pressure of 4 psi (27.6 kPa). The confining fluid used during this testing was water supplied from a Geotac water pump. The confining pressure was monitored with a pressure transducer connected to a port at the top of the triaxial cell. Before the specimen loading began, the loading piston was raised slightly above the top cap, so the piston uplift could be accounted for with the first few recorded force values.

The UU test is a strain controlled test. It is stated in ASTM D2850 (2007) that an axial strain rate of approximately 1%/min should be applied for plastic materials. The force values collected during testing represent the amount of applied force necessary to keep that specimen deflecting at the specified strain rate. The UU test was conducted until the specimen reached approximately 15% strain.

6.5.4.2 UU Data Analysis

The data collected during the UU testing, using the equipment in the geotechnical testing lab at the University of Arkansas, is in terms of voltages. The collected data consisted of vertical displacement, vertical load, and cell pressure throughout the test. The data was first converted into engineering units. The displacement values were corrected by subtracting the initial recorded displacement from all displacement values. The corrected area and corrected strain values were calculated using the corrected displacement. The principal stress difference (PSD) was calculated by subtracting the constant friction load from the vertical loads and dividing the

176
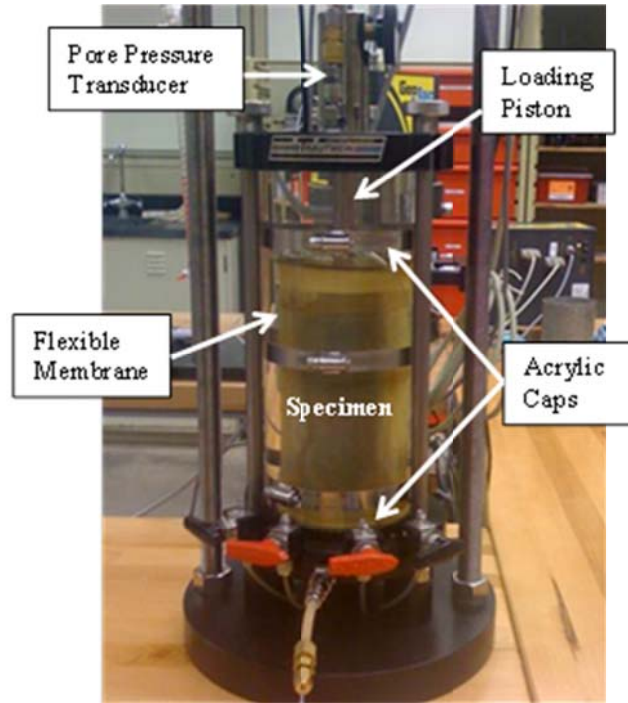
Figure 6.40. Trautwein triaxial cell setup with subgrade sample for UU testing.

difference by the corrected area. The corrected vertical stress (σ_v) was then calculating by adding

the PSD and the confining pressure (σ_h). Undrained shear strength (S_u) values were calculated for

the entire test by dividing the PSD by two. The peak S_u value, also known as the peak principal

stress difference (PPSD), was selected.

The S_u values were normalized by PPSD, which was referred to as the normalized stress

or PSD/PPSD. The PSD/PPSD values were plotted against the corrected strain values to observe

the shear strength behavior of all test specimens. The shear strength values were normalized so

the shape of the stress-strain curves of each specimen could be observed and compared on the

same scale. The stress-strain curves for a typical 10-in (25.4-cm) base section and a typical 6-in

(15.2-cm) base section are plotted in Figure 6.41. Note that the undrained shear strength values

(S_u) are denoted as q in Figure 6.41.

177

6.5.4.3 UU Results

UU tests were conducted on subgrade samples from all test sections, as well as the areas referred to as 13W and 13BW. The desired result from the UU tests was the maximum undrained shear strength (S_u) of each specimen. The shear stress on the soil was calculated throughout the entire test for each specimen. The maximum shear stress value the soil withstood before failing was selected as the undrained shear strength of the soil. The undrained shear strength (S_u) of the subgrade for each section, as well as the rank, is displayed in Table 6.13. Figure 6.42 is a graphical representation of the subgrade S_u values in each section. The undrained shear strength values range from approximately 0.71 to 2.11 ksf (34.0 to 101.0 kPa).

The S_u values exhibit no apparent trends compared to the average rut depth rankings presented in Table 4.4. Sections 6 and 8 have the two lowest average rut depth measurements, but the shear strength values at these two sections are ranked 6 and 7, respectively. Furthermore, Section 11 has "failed" yet has the third highest undrained shear strength.

6.6 Subsurface Layer Properties Composite Ranking

As most of the individual properties discussed above for the base and subgrade did not correlate well with pavement rutting measurements, the research group decided to compile two overall composite rankings of the subsurface (one for the base course properties and one for the subgrade properties) to investigate relative base and subgrade quality across the sections. It was hoped that these composite rankings, based on so many different in-situ and laboratory tests, might reveal trends in overall base and subgrade quality that might correlate better with pavement performance. The overall base course and subgrade layer rankings could then be compared with the average rut depth values in Table 4.4 and the composite deflection-based
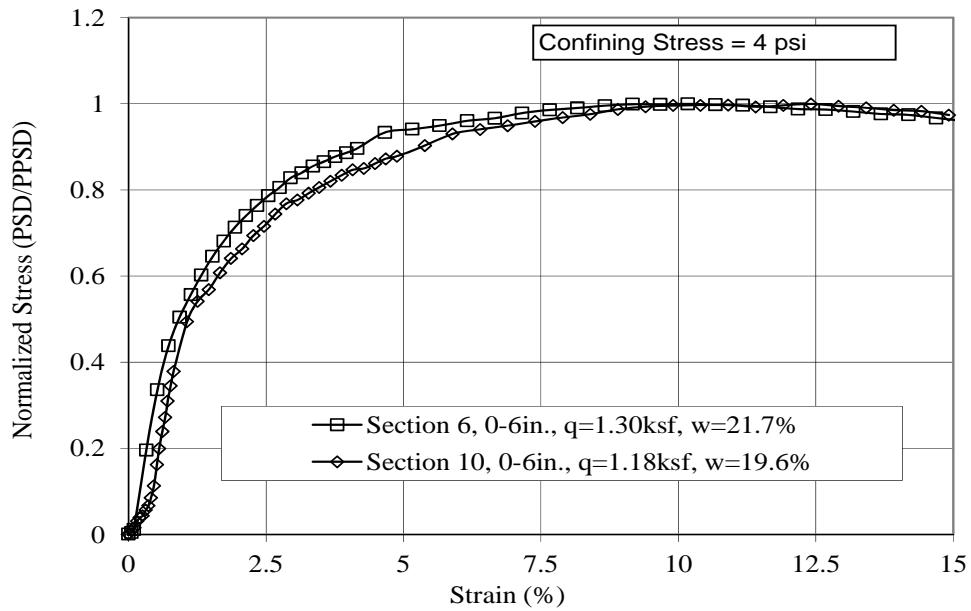
Figure 6.41. Normalized stress-strain curves of subgrade samples from Sections 6 and 10.

Table 6.13. Subgrade undrained shear strength (S_u) values calculated from UU testing.

	Section	East Bound		West Bound	
		S_u (ksf)	Rank	S_u (ksf)	Rank*
10" Nominal Base Thickness	1B	1.27	7		
	1A	2.06	2		
	1	2.11	1		
	2	1.26	9		
	3	1.60	4		
	4	1.20	10		
	5	1.02	13		
	6	1.30	6		
Transition	7	-	-	-	-
6" Nominal Base Thickness	8	1.27	7		
	9	1.39	5		
	10	1.18	11		
	11	1.85	3		
	12	0.71	16		
	13	0.73	15	1.11	13
	13A	1.11	12		
	13B	0.76	14	1.30	6

* Represents potential rank if west bound lane was included in
ranking (East Bound rankings would change accordingly).
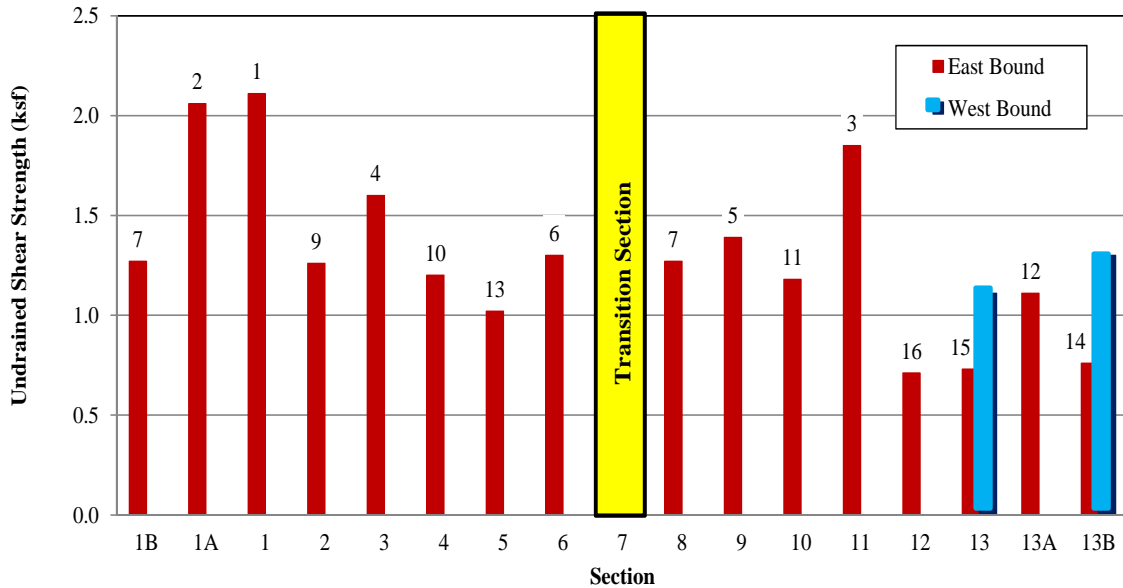
Figure 6.42. Subgrade undrained shear strength (S_u) values calculated from UU testing.

ranking in Section 5.8. The overall subgrade properties composite ranking consists of the rankings from all of the subgrade data previously presented in this chapter. The overall base properties composite ranking consists of the rankings from all of the base course data previously presented in this chapter. Note that the base layer thicknesses are not included in the overall base course properties rankings because thicker base course obvious correlates to better pavement performance and these values will be examined separately later in the chapter.

The subgrade composite ranking was compiled by adding all the rankings from individual subgrade tests previously presented in this chapter (in-situ moisture content, PI, dry density, DCP Layer 3 slope, in-situ CBR, lab M_R, and lab UU shear strength) and ranking the composite sums from lowest to highest. The subgrade composite rankings are presented in Table 6.14 and Figure 6.43. The base composite ranking was compiled by adding the rankings from the DCP base Layer 1 and Layer 2 slopes, the base in-situ moisture content values, and the base dry density values. The base composite rankings are presented in Table 6.15 and Figure 6.44.

It is noticed in Figure 6.43 that the composite subgrade layer properties definitely indicate much higher ranks for Sections 1B – 3 than the rest of the sections. Interestingly, these five sections are also the top five sections based on the composite PLT and ADD deflection-based test results. However, none of these five sections rank in the top five in terms of rutting. Furthermore, according to the subgrade composite rank, the subgrade soils in Sections 4 – 13B appear to be very similar, with no distinct difference in subgrade quality rankings for the "failed" sections (Sections 10, 11, 12, 13W and 13BW).The two unreinforced sections, Sections 1 and 13, have the best and the worst composite subgrade ranking, respectively, yet they have very similar rut depth values (refer to Figure 4.3). Oddly, Sections 6 and 8 had mid-range subgrade composite rankings (8 and 9, respectively) but had the two lowest amounts of average rut depth. The composite subgrade properties do not seem to correspond very well with the pattern of average rut depth and, therefore, the differences in subgrade properties are not believed to be significant enough to be controlling the observed differences in pavement performance.

The base course composite rankings are very scattered and do not trend toward either group of nominal base thickness (recalling that base thickness was not used in the composite base ranking). This seems reasonable since the individual tests performed on/in the base course did not reveal significant differences in the quality of the base course across the test sections. A clear pattern of base course quality does not exist that would either indicate the observed general trend for less rutting in Sections 1B-9, or "failure" in Sections 10, 11, 12, 13W and 13BW.

Table 6.14. Subgrade layer properties composite rank.

	Section	Composite	Rank
10" Nominal Base Thickness	1B	29	3
	1A	20	2
	1	19	1
	2	50	5
	3	38	4
	4	79	15
	5	78	14
	6	68	8
Transition	7	-	-
6" Nominal Base Thickness	8	69	10
	9	69	10
	10	75	13
	11	64	7
	12	62	6
	13	82	16
	13A	74	12
	13B	68	8

Note: composite values are composed of the summation of rankings from moisture content, plasticity index, dry density, DCP (subgrade layer 3), CBR, Mr, and UU measurements/testing.
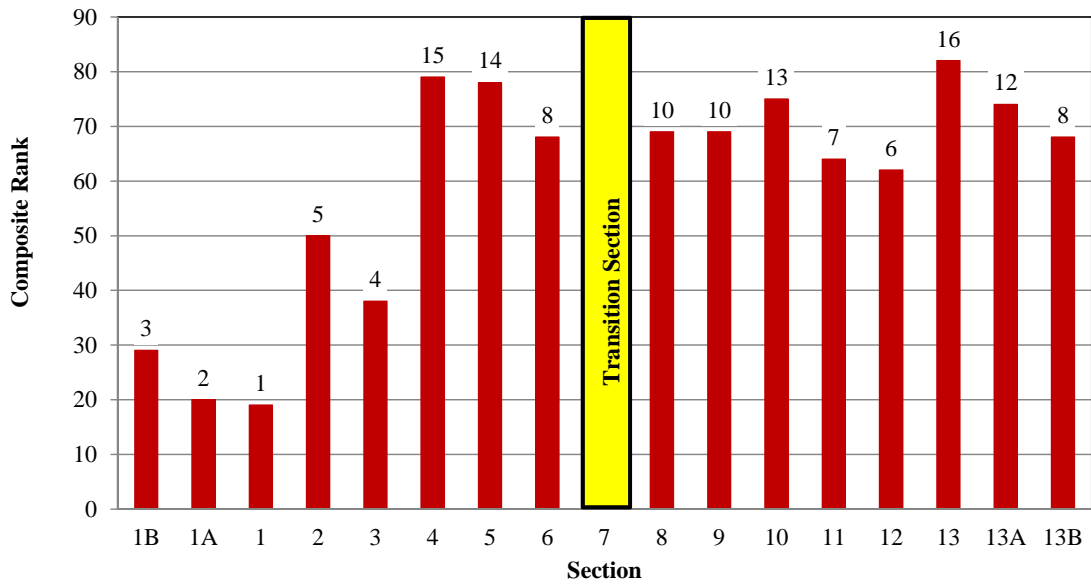
Figure 6.43. Subgrade layer properties composite rankings.

182

Table 6.15. Base course layer properties composite rank.

	Section	Composite	Rank
10" Nominal Base Thickness	1B	27	7
	1A	34	14
	1	11	1
	2	37	16
	3	32	11
	4	21	6
	5	12	2
	6	13	3
Transition	7	-	-
6" Nominal Base Thickness	8	13	3
	9	35	15
	10	32	11
	11	14	5
	12	33	13
	13	30	8
	13A	31	10
	13B	30	8

Note: composite values are composed of the summation of rankings from in-situ moisture content, dry density, and DCP (base Layers 1 & 2).
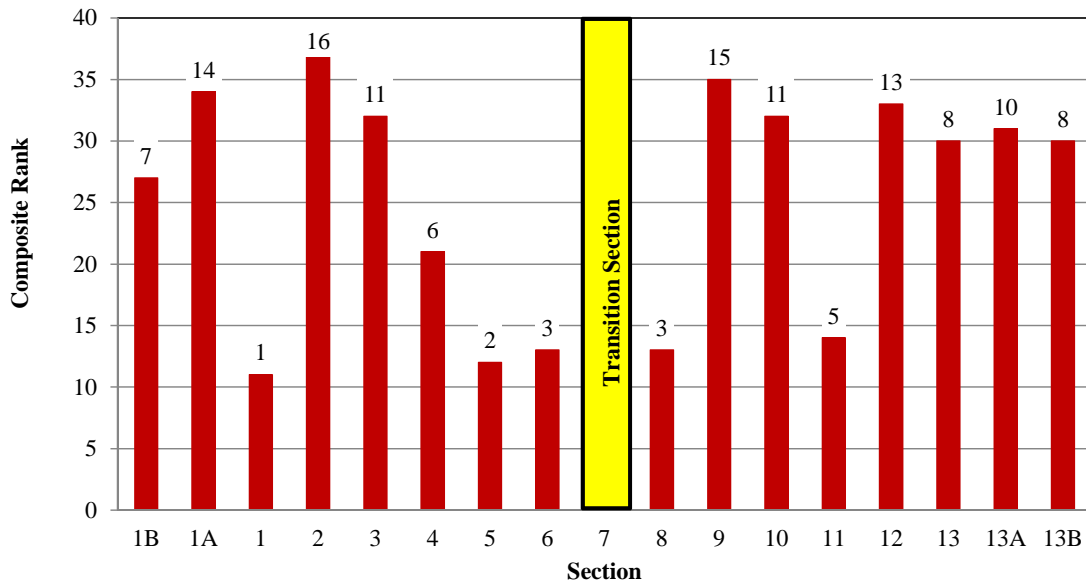
Figure 6.44. Base course layer properties composite rank.

183

6.7 Conclusions Drawn from Subsurface Layer Properties

Composite rankings for both the subgrade and base layer properties do not correlate well with the observed rut depth measurements presented in Table 4.4 and Figure 4.3. It appears that any differences in the strength/stiffness, density, moisture content, etc. of the base and subgrade are relatively minor and do not seem to be controlling the patterns in pavement performance. However, total pavement thickness (base plus asphalt thickness) seems to clearly govern failure more than any of the myriad of soil properties (or geosynthetic types) investigated in this chapter. Sections 10, 11, 12, 13W, and 13BW have all failed [rut depth > 0.5 in (1.3 cm)], with Sections 13B nearing failure. All of these sections are reinforced with various geosynthetics and appear to have relatively similar subgrade and base course properties. Remarkably, these six sections also have the six thinnest asphalt plus base course thicknesses (refer to Table 6.1 and Figure 6.13). This cannot be coincidental, since no other correlations appear to exist between rutting and any other property presented herein.

Referring back to Table 5.23 and Figure 5.29 for the composite PLT and ADD deflection-based test results, the 10-in (25.4-cm) nominal base sections generally performed better than the 6-in (15.2-cm) nominal base sections, only excluding Section 8. It is believed that the deflection-based test results (and the rutting) in Section 8 were positively influenced by the buttressing/confining effect of the abutting driveway. If this is the case, the total thickness values also follow a very similar trend as indicated by the composite ranking of the PLT and ADD tests. This makes sense, because the zone of influence for each of the deflection-based tests is constant no matter what section is being tested, so the sections with the thickest base course are expected to perform better, all other things being equal. Total pavement thickness (asphalt plus base) is

not the sole factor governing pavement performance at the Marked Tree site, but it seems to be the most influential single factor.

Chapter 7

7.0 Conclusions and Recommendations

7.1 Summary

In late 2004, the Arkansas Highway and Transportation Department (AHTD) began construction of a low-volume frontage road (Frontage Road 3) along US Highway 63 in the town of Marked Tree, Arkansas at the intersection of Arkansas Highway 75. An 850-ft (258-m) long segment of this frontage road was utilized for a research project (AHTD TRC-0406) aimed at determining the benefits, if any, of using geosynthetics to improve the performance of flexible pavements on state funded roadway projects where poor subgrade soils were encountered. This full-scale field study consisted of seventeen different 50-ft (15.2-m) long flexible pavement sections constructed over poor subgrade soils (CH or A-7-6). The test section configurations are depicted in Figures 3.1 and 3.2. Eight of the sections were constructed with a 10-in (25.4-cm) nominal base course thickness (Sections 1B – 6) and eight were constructed with a 6-in (15.2-cm) nominal base thickness (Sections 8 – 13B). The section in the middle (Section 7) served as a transition between the two sectors with different nominal base course thicknesses. Seven of the eight sections in each nominal base course sector were reinforced with various geosynthetics (woven and nonwoven geotextiles, and geogrids), which were all positioned at the base-subgrade interface of the roadway. One section in each nominal base course sector was left unreinforced (Section 1 and Section 13, respectively) to allow for monitoring of the relative performance between reinforced and unreinforced sections of like basal thicknesses.

The pavement test sections were instrumented with a wide array of earth pressure cells and strain gauges during construction. However, this instrumentation was only monitored for a

186

limited period of time (approximately 6 months) between September 2005 and March 2006 under normal and accelerated traffic loading. Limited conclusions were drawn from this monitoring (Howard 2006, Warren and Howard 2007a & 2007b) and the project was abandoned until July 2008. At this time, the Marked Tree project was re-started as research project AHTD TRC-0903, with the goal of continuing to monitor the instrumented sections. Unfortunately, all of the instrumentation, with exception of the asphalt strain gauges, had failed during the two-plus year gap in monitoring.

Since the original instrumentation was no longer functioning, the new research group decided to monitor the relative performance of the test sections through a combination of surficial and subsurface testing. The surficial testing techniques consisted primarily of deflection-based tests such as the Falling Weight Deflectometer (FWD), static Plate Load Test (PLT), Accelerated Dynamic Deflectometer (ADD), and Light Weight Deflectometer (LWD). Results from these tests have been used to infer relative pavement performance between test sections and conclusions drawn from them are summarized below.

Signs of serious pavement distress (primarily deep rutting with some alligator cracking) appeared in some of the test sections in the Spring of 2010, leading AHTD to document the pavement performance with manual distress surveys in June of 2010 and April of 2011. These distress surveys revealed that a few sections of the roadway, especially in the westbound lane, were performing poorly. All of the "failed" sections [defined herein as sections with average rut depths > 0.5 in (1.3 cm)] were located in the sector with 6-in (15.2-cm) nominal base thickness. The "failed" sections were Sections 10, 11 and 12 in the eastbound lane and Sections 13W and 13BW in the westbound lane. All of these sections were reinforced with various types of geosynthetics. Furthermore, traffic surveys conducted during this time frame indicated that the

10-in (25.4-cm) nominal base course sections had likely received more than twice the number of

ESALs over the life of the pavement than the 6-in nominal base course sections.

The research team was tasked with trying to figure out why certain 6-in nominal base

course sections had "failed", while others had not.. A subsurface forensic investigation was

completed on each test section during a site visit in October 2010. The subsurface investigation

was conducted so the research group could gather information concerning base and subgrade

properties (i.e., in-situ dry density, in-situ moisture content, plasticity index, etc.), as well as

subsurface strength/stiffness values (in-situ CBR, DCP penetration resistance, laboratory

resilient modulus and undrained shear strength), to determine what properties, or combinations

of properties, were causing some sections to fail while the rest of the sections performed

substantially better.

A ranking system (from 1 through 16) has been used throughout this work to distinguish

the "best" sections from the "worst" sections based on every test conducted at the site. The

surficial deflection-based tests and subsurface layer properties have been synthesized in terms of

these rankings to arrive at a final evaluation of the sections relative performance to one another

as well as absolute performance from pavement rutting measurements. While the data is not

perfect, and at times perplexing for any individual test, the one thing that seems to stand out is

that irrespective of geosynthetic reinforcement type (or lack thereof), all of the sections that have

"failed" via rutting are also the sections with the least combined total pavement thickness (i.e.,

asphalt plus base). Therefore, a clear benefit from utilizing geosynthetic reinforcements at the

Marked Tree site was not observed either through the deflection-based testing program or

through the observed pavement rutting. Specific conclusions derived from the rutting

measurements, surficial deflection-based tests, and subsurface investigations are synthesized below.

7.2 Conclusions

7.2.1 Rut Depth Measurements

Rut depth data from a distress surveys conducted by AHTD in June of 2010 and April of 2011 was used as the pavement performance standard (refer to Table 4.4 and Figures 4.2 and 4.3). This rut depth data represents the actual pavement performance, while the deflection-based test data may be used to infer relative performance, and the subsurface investigation data is used to explain relative performance. The following observations about the rut depth data allow for further comparisons to be made:

- Since September 2005, Sections 1B – 8 have been trafficked by approximately 39,600 ESALs (approximately 6,600 ESALs/year) while Sections 9-13B have been trafficked by approximately 19,200 ESALs (approximately 3,200 ESALs/year).

- It seems there is a distinct difference in the rutting pattern in the eastbound lane that begins between Sections 9 and 10. While not completely perfect, most of the 10-inch (25.4-cm) nominal base course sections, and Sections 8 and 9 from the nominal 6-inch (15.2-cm) base course sections, appear to have less rutting than the remaining 6-inch (15.2-cm) nominal base course sections. *Remembering, that Sections 1B – 8 have received, on average, more than twice as many ESAL's as Sections 9 – 13B.*

- Based on the most-recent April 2011 rutting data, Sections 10, 11, 12, 13W, and 13BW have clearly "failed" [i.e., approximately 0.5 inches (1.3 cm) or greater average rutting]. All of these sections are in the 6-inch (15.2-cm) nominal base course sections and are reinforced with various types of geosynthetics at the subgrade-base course interface (refer to Figure 3.2)

- The unreinforced section in the nominal 6-in (15.2-cm) base course zone (Section 13) has average rutting values that are less than 3-4 other eastbound reinforced test sections with the same nominal base course thickness and estimated ESAL's. Furthermore, it is directly adjacent to a portion of the westbound lane (Section 13W) that has failed that is reinforced with a slit-film geotextile.

- As of April 2011, no rutting failures had occurred in the 10-in (25.4-cm) nominal base sections, but the unreinforced section in the nominal 10-in (25.4-cm) base course sector

189

(Section 1) had average rutting depths that were the worst among the eastbound test sections with the same nominal base course thickness and ESAL's. Still, the average April 2011 rut depth difference between the best ranked section (Section 6) and the 11th ranked section (Section 1) is only approximately 0.19 in (0.48 cm) and due to the method for collecting the average rut depth values they can only be considered accurate within approximately +/- 0.125 in (0.318 cm).

- Section 8 has rutted less than any other nominal 6-in (15.2-cm) base section. This is interesting for at least three reasons: (a) Section 8 has received approximately twice as many ESAL's as the other 6-in sections; (b) The traffic flow in and out of the nursing home (refer to Figure 4.1) splits Section 8 in half, with much of the traffic crossing perpendicular across the middle of the section, and; (c) The nursing home driveway certainly helps to keep dynamic deflections and rutting lower than anticipated by buttressing Section 8. This buttressing effect is revealed in the deflection-based test results presented in Chapter 5.

- The rutting data does not appear to be of sufficient quality to draw conclusions about which specific types of geosynthetics outperform others within a given nominal base course thickness and similar ESAL's. Furthermore, no distinct pattern is discernible and it is highly likely that other factors (e.g., base or subgrade density, base or subgrade moisture content, base thickness, etc.) are influencing the varied pavement performance more than the specific type of geosynthetic.

7.2.2 Deflection-Based Tests to Infer Relative Performance

It was noted above that no clear pattern could be discerned from the rutting measurements within either nominal base course thickness regarding which type of reinforcement, or lack thereof, was "best". However, it was clear that certain 6-inch (15-cm) nominal base course sections had "failed" (Sections 10, 11, 12, 13W, and 13BW) despite having less than half the estimated ESAL's of the 10-inch nominal base course sections. Furthermore, it appeared that in general the rutting was less in Sections 1B – 9 than in Sections 10 – 13B, possibly as a result of weaker/different subsurface conditions or differences in pavement thickness. The results from the deflection-based testing methods presented in Chapter 5 (i.e., FWD, PLT, ADD, LWD, and RDD) were used as a means to determine if these tests could have predicted, or inferred, the observed pattern in rutting prior to "failure". In particular, these test results were also investigated as a means to determine which test(s) and associated method(s) of

data analysis might be most useful to infer relative pavement performance. The following

conclusions were drawn from analysis of the deflection-based tests:

- The results from the PLT and ADD deflection-based tests correlated more closely with the observed pavement rutting than the results from the FWD, LWD, or RDD testing. Therefore, the rankings from the PLT and ADD tests were used to determine a composite rank for each section in the eastbound lane (note that two of the "failed" sections were in the westbound lane but the PLT tests and most of the ADD tests were not conducted in the westbound lane).

- The composite ranks from the PLT and ADD tests are provided in Figure 5.29. These composite ranks clearly identified Sections 10, 11 and 12 as the worst sections in the eastbound lane, which were the same sections that had "failed" based on rut depth measurements. Therefore, one may conclude that these tests were successful at inferring relative pavement performance in terms of identifying sections that had, or were about to, rut to the point of "failure".

- The composite PLT and ADD deflection-based tests also clearly indicated the general rutting trend of better performance in Sections 1B – 9 and poorer performance in Sections 10 – 13B. However, the correlation between the composite PLT and ADD rankings and the average rut depth measurements was not perfect, as indicated by the superior performance of Section 1 in terms of deflection-based ranking despite having the greatest rutting out of all 10-in (25-cm) sections.

- Trends indicating distinct benefits from the addition of geosynthetics are hard to observe in either the rutting measurements or the results from the deflection-based tests. Among the deflection-based tests analyzed herein, the PLT and ADD test agreed best with the average rut depth values and these tests should be further studied to determine if they can be used to detect more subtle differences in relative pavement performance. Some sort of data normalization based on absolute base course thickness or pavement stiffness may be required to detect these subtle differences. No doubt others will seek to analyze and interpret this data in a different manner in the future.

7.2.3 Subsurface Layer Properties

A forensic excavation of the site was conducted in October 2010 in an effort to discern

what subsurface properties of the base and/or subgrade were most influencing pavement

performance and failure of the test sections. The following subsurface layer properties in each

section were investigated either in-situ, or in the laboratory shortly thereafter: asphalt and base

thickness, in-situ moisture content of the base and subgrade, in-situ dry density of the base and

subgrade, in-situ DCP penetration resistance of the base and subgrade, in-situ CBR of the base and subgrade, PI of the subgrade, and resilient modulus (M_R) and UU triaxial shear strength of subgrade from "undisturbed" Shelby tube specimens. The forensic excavation and testing results are detailed in Chapter 6. Additionally, Boga (2011) analyzed other data collected during the forensic excavation such as permeability of the base course and fines migration from the subgrade into the base course in may sections. The following conclusions were drawn from the subsurface forensic investigations:

- The combined asphalt plus base layer thicknesses were found to correlate very well with the observed rutting measurements (refer to Figure 4.3 and Figure 6.13). In particular, Sections 10, 11, 12, 13W and 13BW had "failed" based on average rut depth measurements, with Section 13B nearing "failure" [defined herein as an average rut depth > 0.5 in (1.3 cm)]. Coincidentally (or perhaps not), these six sections also had the six thinnest combined asphalt and base course thicknesses.

- The three sections with the worst rutting (Sections 10, 13W and 13BW) all had combined asphalt and base thicknesses that were less than 8-in (20.3-cm) thick.

- Section 8, which was the best performing 6-in (15.2-cm) nominal base course section in terms of both rutting and deflection-based results, has the thickest combined asphalt and base. This fact, combined with the buttressing/confining effect of the nursing home driveway, likely has a positive impact on the observed performance.

- None of the other individual base course or subgrade layer properties (other than combined asphalt and base thickness) were found to correlate well with the observed pavement rutting (likely because significant enough differences in subgrade and base properties did not exist across the site). These individual results are too numerous to discuss in this brief conclusions section, but the reader is referred to Chapter 6 to make specific comparisons with the rutting data presented in Chapter 4.

- All of the tests conducted on the base and subgrade during the forensic excavation (with the exception of asphalt and base thickness) were combined to form a composite rank of the base and subgrade across the site. It was hoped that while no individual test result seemed to correlate well with observed performance, that when combined to form a composite rank some trend might appear. The composite rankings for the subgrade and base layers are presented in Figures 6.43 and 6.44, respectively. It is observed from these figures that subgrade and base beneath the "failed" sections is not ranked among the worst along the site.

- Composite rankings for the subgrade and base layer properties do not directly correlate well with the observed average rut depth measurements. It appears that any differences in the strength/stiffness, density, moisture content, etc. of the base and subgrade are relatively minor and do not seem to be controlling the patterns in pavement performance.

- All of the "failed" sections are reinforced with various geosynthetics and appear to have relatively similar subgrade and base course properties. However, remarkably, these sections also have the thinnest total thickness values of asphalt plus base course. This cannot be coincidental, since no other correlation is as evident between rutting and any other property presented herein. Total pavement thickness (asphalt plus base) is not the sole factor governing pavement performance at the Marked Tree site, but it seems to be the most influential single factor governing failure.

- A clear trend of better performance in relation to specific geosynthetic types or manufacturers was not clearly observed from the average rut depth values, the deflection-based test results, or the subsurface soil properties.

7.3 Recommendation for Future Work

It is suspected that the results from this study will be met with both positive and negative feedback. It is obvious that thicker asphalt and base course layers over the top of poor subgrade soils will result in better performance. However, inclusion of various geosynthetics as reinforcement/separators in flexible pavements is believed by many to help offset the need for thicker asphalt and base layers while still maintaining equal or better performance. The trends from this study were not perfect in every case, but the most obvious conclusion after reviewing a plethora of data was that the sections that had "failed" through rutting after 5-6 years of trafficking all had the thinnest combination of asphalt plus base course. The differences in combined asphalt and base thickness between sections that had and had not failed was not great [less than 1 inch (2.54 cm) in many cases], and it is possible that other indiscernible factors also were contributing to failure. Future studies of the stress and strain distribution beneath the surface may be beneficial to see if a critical threshold of combined asphalt and base thickness exists for the loading and subsurface properties documented herein.

It has also been documented herein that all geosynthetic reinforcement, regardless of type/function, was placed at the subgrade-base interface during construction. This configuration is clearly not the most beneficial for geogrid reinforcement, but the conclusions from this study are based on the pavement test sections as built. Furthermore, while obvious to many, it will be reiterated that geosynthetics which have the capacity to conduct water should be "daylighted" to formal edge drains, or at least to the edge of the embankment, if they are expected to benefit the pavement. Otherwise, they may in fact simply channel water to low spots in the pavement (particularly when place on top of low permeability subgrade) and worsen the performance of the pavement in those areas. Boga (2011) reports on an elevation survey at the Marked Tree site that was conducted during the October 2010 forensic excavation. The results from that elevation survey should be examined in light of the conclusion derived herein to see if any links exist, despite the fact that no distinct correlations between average base or subgrade moisture content and pavement rutting were observed.

Many of the base and subgrade properties such as PI, moisture content, and dry density were averaged as a function of depth within each section. This was done as a means to see if any gross differences existed between sections. While the depths of averaging were minimal [i.e., less than 6-12 inches (15.2-30.5 cm)] for any given property, it is possible that thin layers, for example, with higher than average moisture content or greater than average PI may have influenced relative pavement performance. This may warrant further study.

The PLT and ADD deflection-based test results were found to correlate most clearly with observed pavement rutting. However, even these tests did not have a direct correlation with pavement performance. It is possible that when normalized to a constant base course thickness or stiffness, or perhaps a common number of ESALs, that a better correlation with rutting may be

194

achieved. This would be desirable since an in-situ test has not been clearly identified that can reveal subtle differences in performance in geosynthetic-reinforced pavements. While the ADD test requires specialized equipment (i.e., a vibroseis truck), the PLT test is easy to conduct. Furthermore, if PLT tests were conducted sequentially with various sized plates to stress different layers, potentially combined with static/residual deflection basin readings like the ADD, they might be even more useful.

Clearly, more research is needed to quantify the contribution of geosynthetics to pavement performance and to reach a consensus on how to design geosynthetic-reinforced pavements for a desired level of performance. Hopefully this future research will lead to clear cost-benefit studies that will help transportation agencies make rational decisions regarding when (under what trafficking and soil conditions) and how (what configurations and materials) to use geosynthetics to improve pavement performance.

Chapter 8

8.0 References

Al-Qadi, I. L., Brandon, T. L., Valentine, R. J., Lacina, B. A. and Smith, T. E. (1994). "Laboratory Evaluation of Geosynthetic Reinforced Pavement Sections," Transportation Research Record 1439, TRB, National Research Council, Washington DC, pp. 25-31.

American Association of State Highway and Transportation Officials (2007). "Standard Method of Test for Determining the Resilient Modulus of Soils and Aggregate Materials." AASHTO Designation T 307-99.

American Society for Testing and Materials (2009) "Standard Test Method for Repetitive Static Plate Load Tests of Soils and Flexible Pavement Components, for Use in Evaluation and Design of Airport and highway Pavements" Annual Book of ASTM Standards, Designation D 1195M, ASTM International, West Conshohocken, PA.

American Society for Testing and Materials (2009). "Standard Test Method for Unconsolidated-Undrained Triaxial Compression Test on Cohesive Soils" Annual Book of ASTM Standards, Designation D 2850, ASTM International, West Conshohocken, PA.

American Society for Testing and Materials (2009a). "Standard Test Method for CBR (California Bearing Ratio) of Soils in Place" Annual Book of ASTM Standards, Designation D 4429, ASTM International, West Conshohocken, PA.

American Society for Testing and Materials (2009). "Standard Test Method for Use of the Dynamic Cone Penetrometer in Shallow Pavement Applications" Annual Book of ASTM Standards, Designation D 6951, ASTM International, West Conshohocken, PA.

American Society for Testing and Materials (2007). "Standard Test Method for Measuring Deflections with a Light Weight Deflectometer (LWD)" Annual Book of ASTM Standards, Designation E 2583, ASTM International, West Conshohocken, PA.

Archer, S. (2008). "Subgrade Improvement for Paved and Unpaved Surfaces Using Geogrids." Professional Development Advertising Section – CONTECH Construction Products Inc., Professional Development Series, pp. 3-11.

Barksdale, R. D., Brown, S. F. and Chan, F. (1989). "Potential Benefits of Geosynthetics in Flexible Pavement Systems." National Cooperative Highway Research Program Report No. 315, Transportation Research Board, National Research Council, Washington, DC.

Bay, J. A. and Stokoe, K. H. (1998). "Development of a Rolling Dynamic Deflectometer for Continuous Deflection Testing of Pavements." Project Summary Report 1422-3 F. Center

for Transportation Research. Bureau of Engineering Research, University of Texas at Austin.

Bay, J. A., Stokoe, K. H. and Jackson, J. D. (2005). "Development and Preliminary Investigation of Rolling Dynamic Deflectometer." Transportation Research Record 1473, TRB, National Council, Washington DC, pp. 43-54.

Berg, R., Christopher, B. and Perkins, S. (2000). "Geosynthetic Reinforcement of the Aggregate Base Course of Flexible Pavement Structures." GMA White Paper II, Geosynthetic Materials Association, Roseville, MN, USA, 130p.

Boga, A. A. (2011). "Efficacy of Geosynthetics Seperators: an Evaluation of Test Sections in Marked Tree, Arkansass." Master's Thesis, Dept. of Civil Eng., University of Arkansas, Fayetteville, AR.

Brandon, T. L., Al-Qadi, I. L., Lacina, B. A. and Bhutta, S. A. (1996). "Construction and Instrumentation of Geosynthetically Stabilized Secondary Road Test Sections." Transportation Research Record 1534, TRB, National Council, Washington DC, pp. 50-57.

Brooks, J. A. (2009). "Strain Gage Installation and Survivability on Geosynthetics used in Flexible Pavements." Master's Thesis, Dept. of Civil Eng., University of Arkansas, Fayetteville, AR.

Coduto, D. P. (2001) "Foundation Design, Principles and Practices, Second Edition" Prentice-Hall, Inc. Upper Saddle River, New Jersey.

Cox, B. R., McCartney, J. S. and Trowler, C. N. (2010). "Accelerated Characterization of Full-Scale Flexible Pavements Using a Vibroseis." Department of Transportation, University Transportation Centers Program, MBTC 3013.

Cox, B. R., McCartney, J. S., Wood, C. M. and Curry, B. (2010b). "Performance Evaluation of Full-Scale Geosynthetic-Reinforced Flexible Pavements Using Field Cyclic Plate Load Tests." TRB 2010 Annual Meeting, Transportation Research Board, Washington, DC.

Cuelho, E. and Perkins, S. (2009). "Field investigation of Geosynthetic Used for Subgrade Stabilization." Performed for the State of Montana, Department of Transportation, NAUE GmbH & Co. KG, in cooperation with the U.S. Department of Transportation, Federal Highway Administration.

Cuelho, E. V., Perkins, S. W. and Maubeuge, K. v. (2011). "Full-Scale Field Study of Geosynthetics Used as Subgrade Stabilization." Proceedings of Geo-Frontiers Conference 2011, Dallas, Texas, USA, pp. 4703-4712.

Das, B. M. (2006). "Principles of Geotechnical Engineering, Sixth Edition" Cengage Learning, Stamford, CT. 634 pp.

Fannin, R. J. and Sigurdsson, O. (1996). "Field Observations on Stabilization of Unpaved Roads with Geosynthetics." Journal of Geotechnical Engineering, ASCE, 122, No. 7, pp. 544-553.

Federal Highway Administration (2006). "Guidelines for Review and Evaluation of Backcalculation Results." Publication No. FHWA-HRT-05-152, Final Report.

Garber, N. J. and Hoel, L. A. (2001). "Traffic and Highway Engineering, Third Edition." Brooks/Cole, Pacific Grove, CA.

Giroud, J. P. and Han, J. (2004). "Design Method for Geogrid-Reinforced Unpaved Roads. I. Development of Design Method." Journal of Geotechnical and Geoenvironmental Engineering, Vol. 130, No. 8, pp. 775-786.

Giroud, J. P. and Noiray, L. (1981). "Geotextile Reinforced Unpaved Road Design." Journal of Geotechnical Engineering Division. ASCE, Vol. 107, No. GT9, pp. 1233-1254.

Haas, R., Wall, J., and Carroll, R. G. (1988). "Geogrid Reinforcement of Granular Bases in Flexible Pavements." Transportation Research Record 1188, TRB, National Research Council, Washington, DC, USA, pp. 19-27.

Hatami, K., Wang, Z., Mahmood, T., Ghabchi, R. and Zaman, M. M. (2011). "In-Aggregate Testing of Unitized and Woven Geogrids for Base Reinforcement Applications." Proceedings of Geo-Frontiers Conference 2011, Dallas, Texas, USA, pp. 4635-4644.

Henry, K. S., Clapp, J, Davids, W. G. and Barna, L. (2011). "Back-calculated Pavement Layer Modulus Values of Geogrid Reinforced Test Sections." Proceedings of Geo-Frontiers Conference 2011, Dallas, Texas, USA, pp. 4673-4682.

Howard, I. L., (2006). "Full-Scale Field Study and Finite Element Modeling of a Flexible Pavement Containing Geosynthetics", Doctoral Dissertation, Dept. of Civil Eng., University of Arkansas, Fayetteville AR.

Hufenus, R., Ruegger, R., Banjac, R., Mayor, P., Springman, S. M. and Bronnimann, R. (2006). "Full-scale Field Tests on Geosynthetics Reinforced Unpaved Roads on Soft Subgrades." Geotextiles and Geomembranes 24/1, pp. 21-37.

Joshi, R. V. and Zornberg, J. G. (2011). "Use of Falling Weight Deflectometer Data to Quantify the Relative Performance of Reinforced Pavements Sections." Proceedings of Geo-Frontiers Conference 2011, Dallas, Texas, USA, pp. 4713-4722.

Kessler DCP (2005). Kessler Dynamic Cone Penetrometer-Model 100 with Quick Release Pin User's Manual.

Kinney, T. C., Stone, D. K. and Schuler, J. (1998). "Using Geogrids for Base Reinforcement as Measured by Falling Weight Deflectometer in Full-Scale Laboratory Study." Journal of the Transportation Research Board, TRB Record 1611, pp. 70-77.

Koerner, R. M. (2000). "Emerging and Future Developments of Selected Geosynthetic Applications." Journal of Geotechnical and Geoenvironmental Engineering, Vol. 126, Issue 4, pp. 293-306.

Ling, H. and Liu, Z. (2001). "Performance of Geosynthetic Reinforced Asphalt Pavements." Journal of Geotechnical and Geoenvironmental Engineering. 127(2), pp. 177-184.

Maubeuge, K. v. and Klompmaker, J. (2011). "New Developments for Geogrid Reinforced Base Courses." Proceedings of Geo-Frontiers Conference 2011, Dallas, Texas, USA, pp. 4624-4634.

McCartney, J. S., Khosravi, A., Cox, B. R., Trowler, C., and Wood, C. M. (2011). "Seasonal Effects on the Dynamic Deformation of Geosynthetic-Reinforced Pavements." Proceedings of Geo-Frontiers Conference 2011, Dallas, Texas, USA.

Montanelli, F., Zhao, A. and Rimoldi, P. (1997). "Geosynthetic-Reinforced Pavement System: Testing and Design." Proceedings of the Conference Geosynthetics '97, Long Beach, CA, USA, Vol. 2, pp. 619-632.

Perkins, S. W. and Cortez, E. (2005). "Evaluation of Base-Reinforced Pavements using a Heavy Vehicle Simulator." Geosynthetics International. 12(2), pp. 87-98.

Perkins, S. W., Bowders, J. J., Christopher, B. R. and Berg, R. R. (2005). "Geosynthetic Reinforcement for Pavement Systems: US Perspectives." GSP 141 International Perspectives on Soil Reinforcement Applications.

TenCate Geosynthetics North America (2010). "Geosynthetic Reinforcement of the Aggregate Base/Subbase Courses of Pavement Structures." Technical Note, TenCate Geosynthetics North America, Pendegrass, GA, USA.

Tingle, J. and Jersey, S. (2005). "Cyclic Plate Load Testing of Geosynthetic-Reinforced Unbound Aggregate Roads." Transportation Research Record: Journal of the Transportation Research Board, No. 1936, Transportation Research Board of the National Academies, Washington, DC, 2005, pp. 60-69.

Warren, K. A. and Howard, I. L. (2007a). "Sensor selection, installation, and survivability in a geosynthetic-reinforced flexible pavement." Geosynthetics International, Vol. 14, No. 5, pp. 298-315.

Warren, K. A. and Howard, I. L. (2007b). "Low Volume Flexible Pavement Roads Reinforced with Geosynthetics." Final Report: AHTD TRC-0406.

Warren, K., Christopher, B. and Howard, I. (2008). "Techniques Used to Measure Strain on Geosynthetics in Dynamic Applications." ASCE Conference Proceedings for GeoCongress 2008.

Webster, S. L. (1993). "Geogrid Reinforced Base Courses for Flexible Pavements for Light Aircraft, Test Construction, Behavior Under Traffic, Laboratory Tests and Design Criteria. Technical Report GL-93-6, USAE Waterways Experiment Station, Vicksberg, MS, USA, 86p.

White, D. J., Vennapusa, P. K. R., Gieselman, H. H., Douglas, S. C., Zhang, J. and Wayne, M. H. (2011). "In-Ground Dynamic Stress Measurements for Geosynthetic Reinforced Subgrade/Subbase." Proceedings of Geo-Frontiers Conference 2011, Dallas, Texas, USA, pp. 4663-4672.